NTNU

Norwegian University of
Science and Technology

Evaluation of Robustness in Volumetric Modulated Arc Therapy (VMAT) plans for Head and Neck Cancer Patients

Marit Funderud

Master of Science in Physics and Mathematics
Submission date: June 2017
Supervisor: Kathrine Røe Redalen, IFY
Co-supervisor: Veronika Kristine Tømmerås, Universitetssykehuset Nord-Norge
Jorunn Andrea Skjelvareid, Universitetssykehuset Nord-Norge

Norwegian University of Science and Technology
Department of Physics

Abstract

Purpose: To investigate the robustness of volumetric modulated arc therapy (VMAT) plans for head and neck (H&N) cancer patients.

Methods and materials: The patient population consisted of 15 patients with H&N cancer having received VMAT radiotherapy at the University Hospital of North Norway (UNN). Original treatment plans were compared to alternative plans where a virtual bolus was applied during optimization. Perturbed uncertainty plans were generated for various isocenter shifts in three directions, and the widths of the uncertainty plots were calculated. In addition, the original plan was compared to three other plans where different optimization strategies were used; the simultaneous, sequential and intermediate plan. Comparison was done in terms of various dose-volume parameters, the conformity index (CI), homogeneity index (HI) and newly proposed robustness index (RI). Verification of all plans was performed using a Delta^4 phantom. The global γ index was found, where a pass-fail criteria of 2% dose difference (DD) and 2 mm distance to agreement (DTA) was used. The difference between including, or not including, the fixation mask in the body contour for dose calculation was determined. Wilcoxon signed rank test was applied to determine whether there was a statistically significant difference in the mentioned parameters.

Results: Comparing the original plan with the plan optimized with bolus, the dose to 98% (D_{98}) of the planning target volume (PTV) to which 52 Gy had been prescribed, PTV52, was significantly higher in the original plan. That was the case for the maximum dose ($D_{\max}$) to the spinal cord as well. D_{98} of PTV64 and the mean dose (D_{mean}) of both parotid glands and both submandibular glands were significantly higher in the plan which was optimized with bolus. The γ index and RI were determined to be significantly superior in the plan which was optimized with bolus. The widths of the uncertainty plots were determined to be significantly narrower in the original plan for $D_{\max}$ of spinal cord and spinal cord planning organ at risk (PRV). The simultaneous plan performed the best in terms of dose coverage to target volumes, as D_{98} of ITV52, ITV64, PTV52, PTV64 and PTV68/70 all were significantly higher than in the original plan. The HI was also determined to be significantly superior in the simultaneous plan for PTV52, PTV64 and PTV68/70. The intermediate plan, followed by the sequential plan, was determined to have significantly better γ indices than the original plan, in addition to having the best the robustness indices. Small, but significant differences were found between including, or not including the fixation mask in dose calculation.

Conclusion: The results in the comparison between the original plan and the plan which was optimized with bolus were ambiguous and none of the plans were proven to be superior to the other. The intermediate plan, followed by the sequential plan, had the best γ and robustness

indices, suggesting they can be further investigated as a method to improve practice. Also, the simultaneous plan was better than the original plan, implying that taking the time to optimize and calculate dose several times after a plan has met the tolerance criteria, is worth the while. It was concluded that the fixation mask should always be included in the body contour for dose calculation.

Sammendrag

Hensikt: Å undersøke robusthet i volumetric modulated arc therapy (VMAT) planer for øre-nese-hals kreftpasienter.

Material og metode: Pasientpopulasjonen besto av femten øre-nese-hals kreftpasienter tidligere behandlet med VMAT. Den originale planen ble sammenlignet med en alternativ plan der en virtuell bolus ble påført under optimalisering. Perturberte usikkerhetsplaner ble generert for flere isosenterforflytninger i tre retninger, og bredden til usikkerhetsplottene ble regnet ut. I tillegg ble originalplanen sammenlignet med tre andre planer der ulike optimaliseringstrategier ble benyttet: simultan-, sekvensiell- og intermediate planer. Sammenligning ble gjennomført ved flere dose-volum parametre, og utregning av konformitetesindeks (CI), homogenitetsindeks (HI) og robusthetsindeks (RI). Verifisering av alle planer ble utført med et Delta^4-fantom. Den globale γ-indeksen ble funnet, der kriteriet for å få godkjent verifiseringen var 2% dose forskjell (DD) og 2 mm avstand til overenstemmelse (DTA). Forskjellen på å inkludere fikseringsmasken i kroppskonturen under doseberegningen eller ikke, ble bestemt. Wilcoxon signed rank test ble anvendt for å bestemme om det var statistisk signifikant forskjell i de nevnte parameterne.

Resultat: Sammenligning av original plan og plan optimalisert med bolus viste signifikant høyere dose til 98% av volumet (D_{98}) til det planning target volume (PTV) der 52 Gy ble rekvirert, PTV52. I tillegg var maksimal dose ($D_{\max}$) til medulla spinalis lavere i den originale planen. På den andre siden var D_{98} til PTV64, gjennomsnittsdosen (D_{mean}) til både høyre og venstre glandula parotis og glandula submandibularis signifikant høyere for planen som var optimalisert med bolus. Både γ-indeksen og robusthetsindeksen ble funnet til å være signifikant bedre i planen som var optimalisert med bolus. Bredden til usikkerhetsplottene var signifikant smalere i den originale planen for $D_{\max}$ til medulla spinalis og medulla spinalis planning organ at risk (PRV). Den simultane planen viste gode resultater når det gjelder dekning til målvolum, ved at D_{98} til ITV52, ITV64, PTV52, PTV64 og PTV68/70 var signifikant høyere enn i den originale planen. HI ble også funnet til å være signifikant bedre i den simultane planen for PTV52, PTV64 og PTV68/70. Intermediate planen, etterfulgt av den sekvensielle planen, hadde en signifikant bedre γ-indeks enn den originale planen, i tillegg til å ha best robusthetsindeks. Det ble funnet små, men signifikante forskjeller mellom å inkludere fikseringsmasken i kroppskonturen eller ikke.

Konklusjon: Resultatene av sammenligningen mellom den originale planen og planen som ble optimalisert med bolus er tvetydige. Begge planene er klinisk akseptable, men ingen av dem utmerker seg. Intermediate planene, etterfulgt av de sekvensielle planene, hadde best γ-og robusthetsindeks, og det kan derfor anbefales å undersøke bruk av disse klinisk. Den simul-

tane planen var også bedre enn den originale, som tyder på at det lønner seg å optimalisere og beregne dose flere ganger, selv etter at toleransekravene er møtt. Til slutt, fikseringsmasken bør alltid inkluderes i kroppskonturen ved doseplanlegging.

Preface

This master's thesis was written in cooperation with the radiotherapy department at the University Hospital of North Norway. Sections 2.2, 2.4 and 3.7.2 are based on the corresponding sections in my project thesis, written in the fall semester of 2016.

First of all, I would like to give a big thank you to my supervisors at UNN, medical physicists Veronika K. Tømmerås and Jorunn A. Skjelvareid, for their continuing help and guidance both in the experimental and writing part of this thesis! Further, I would like to thank my supervisor at the department of physics, associate professor Kathrine Røe Redalen, for answering all my questions and for valuable feedback in the writing process. Also, I would like to thank medical physicists Brede Dille Pedersen and Camilla Hægeland for staying after working hours and verifying plans with me. Lastly, I would like to thank Paul for his support and great company as this thesis was written.

Marit Funderud
Trondheim, June 2017

Table of Contents

Abbreviations

3D	Three-dimensional
AAA	Anisotropic analytical algorithm
AP	Anterior-posterior
CC	Cranio-caudal
CI	Conformity index
CP	Control point
CPE	Charged particle equilibrium
CT	Computed tomography
CTV	Clinical target volume
DAHANCA	Danish head and neck cancer group
DD	Dose difference
DMLC	Dynamic multileaf collimator
DTA	Distance to agreement
DVH	Dose-volume histogram
FFF	Flattening filter free
GTV	Gross tumor volume
Gy	Gray
HI	Homogeneity index
H&N	Head and neck
IM	Internal margin
IMRT	Intensity modulated radiotherapy
ITV	Internal target volume
Linac	Linear accelerator
LF	Local failure
keV	Kilo electron volt
K-N	Klein-Nishina
MeV	Mega electron volt
ML	Medial-lateral
MLC	Multileaf collimator
MRDC	Multi-resolution dose calculation
MU	Monitor unit
OAR	Organs at risk
PET	Positron emission tomography

PMMA	Polymethylmethacrylate
PRO	Progressive resolution optimizer
PRV	Planning organ at risk
PTV	Planning target volume
QA	Quality assurance
RI	Robustness index
SABR	Stereotactic ablative radiation therapy
SM	Setup margin
Std	Standard deviation
TCPE	Transient charged particle equilibrium
TM	Trademark
TMN	Primary tumor (T), distant metastasis (M), regional lymph nodes (N)
TPS	Treatment planning system
TV	Target volume
UNN	University hospital of North Norway
VMAT	Volumetric modulated arc therapy

1 Introduction

The total number of new cases of cancer in Norway was 32592 in 2015[1], out of these, 774 were head and neck (H&N) cancers. There were 505 males and 269 females, reflecting the trend in which more males than females are diagnosed with cancer in the H&N area. The 10-year relative survival proportion[2] for H&N cancer was 54.0% for males and 64.2% for females [2].

Volumetric modulated arc therapy (VMAT) is a technique in which the linear accelerator gantry continuously rotates around the patient while treatment is given. It is the preferred radiotherapy treatment delivery technique for H&N cancer patients in Norway, today. This is due to faster delivery times, reduction of monitor units (MUs) and increased sparing of the normal tissue and organs at risk (OAR) [3, 4, 5, 6, 7].

When a patient receives radiotherapy treatment, the dose distribution is planned in a treatment planning system (TPS). The primary goal in treatment planning is to make sure that the tumor(s) receives the full prescribed dose, and for the surrounding tissue and OAR to receive as low dose as possible. This is done by first contouring the tumor(s) with margins and the relevant OAR. Afterwards, the dose distribution is optimized by the TPS[3] and finally the dose plan is calculated. This plan is used by the linear accelerator treatment machine to deliver the planned treatment.

The principal aim of this thesis was to investigate the robustness of H&N VMAT plans delivered at University Hospital of North Norway (UNN).

The experimental part of this thesis included comparing the original plans, used to treat the patients, to plans that were optimized with a so-called virtual bolus. Further, as a method of comparing the robustness of these two plans against uncertainties in positioning, a total of 18 so-called uncertainty plans were made. These plans were made in the TPS by simulating that the patient was moved ± 1, ± 2 and ± 5 mm in the three principal directions. In addition, the original plan was compared to three other plans in which different strategies of optimization were used, called the intermediate, simultaneous and sequential plan. Statistical analysis was performed, comparing the original plan to the other plans. This was done in terms of dose coverage to the target volumes, dose to the OAR and by calculation of conformity and homogeneity indices. Further, the robustness index (RI) proposed by Hægeland [8], was calculated and compared for all the plans. At UNN, dosimetric quality assurance for VMAT plans is done using a Delta^4 phantom. From this verification, the γ index was found and compared for all the plans. This index is a measure of whether the dose plan calculated

[1] 17498 were male and 15094 were female.

[2] Which is the percentage of survival from the cancer, when taking into account the deaths that was not caused by the cancer. It has been defined as the observed survival proportion divided by the expected survival proportion for a comparable group in the general population [2].

[3] This is for VMAT. In conventional radiotherapy, the optimization may be done manually.

by the TPS and the dose which was measured by the phantom, coincides sufficiently.

2 Theory

2.1 Photon Interactions with Matter

2.1.1 Photon Interactions and Interaction Cross-Sections

X-ray photons and γ-ray photons interact with matter in five different ways, by the photoelectric effect, the Compton scattering effect, pair production, Rayleigh (coherent[4]) scattering and photonuclear interactions. However, the first three of these are the most important and will be presented further. Note that Compton scattering is the main effect in radiation therapy, amongst others due to the applied energy range of between 6 and 20 mega electron volt (MeV).

The probability of a photon interaction with for example atomic electrons, nuclei, atoms or molecules is usually described in terms of interaction cross-sections σ. This probability, given by σ, is equal to the cross-sectional area of one of these targets normal to the incident photon direction, divided by the unit area. The total interaction cross-section is a sum of the cross-sections for the individual processes. Atomic cross-section ${}_a\sigma$ means cross-section per atom, and electronic cross-section ${}_e\sigma$ means cross-section per electron. They are related in the following way:

$$ {}_a\sigma = Z \cdot {}_e\sigma. \tag{1} $$

A third quantity is the mass attenuation coefficient, given by

$$ \frac{\sigma}{\rho} = \frac{N_A Z}{A} \cdot {}_e\sigma, \tag{2} $$

where N_A is Avogadro's number, Z is the atomic number and A is the number of grams per mole of a material.

In an interaction process, photons are either absorbed or scattered. Following a full absorption process, meaning all the photon energy is transferred to the target, secondary particles are emitted. They further interact with the electrons of the outer shells of the atoms they pass by and excite or ionize them. However, in a scattering process, the direction of motion, energy and momentum of the scattered photon may be changed, but no secondary particles are produced.

2.1.2 The Photoelectric Effect

The photoelectric effect happens when an incoming photon interacts with an orbital electron of the attenuator which is tightly bound, the photon is absorbed and the orbital electron is

[4]When scattering occurs without energy loss.

ejected from the atom with an kinetic energy

$$E_{\mathrm{K}} = h\nu - E_{\mathrm{B}}. \tag{3}$$

Here, $h\nu$ is the energy of the incident photon and E_{B} is the binding energy of the electron. The incident photon energy $h\nu$ must be above the binding energy, otherwise the photon cannot undergo photoelectric effect. The energy range in which this process dominates is about 10-25 kilo electron volt (keV) for soft tissue and in the range of a few hundred keV for contrast media, lead and materials used in e.g. films and screens. The atomic interaction cross-section for photoelectric absorption is given by

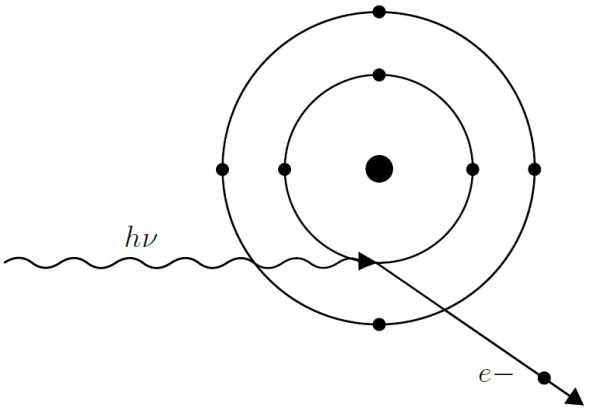

Figure 1: The photoelectric effect is illustrated. A photon of energy $h\nu$ is incident and an orbital electron is ejected.

$$_{a}\sigma \cong \frac{Z^4}{(h\nu)^3}. \tag{4}$$

Clearly, this absorption cross-section strongly increases with decreasing photon energy $h\nu$ and increasing attenuator atomic number Z. The mass attenuation coefficient is proportional to Z^3, according to equation (1). Explaining why the photoelectric effect is the most prominent in diagnostic imaging, as the x-ray beam is much more strongly attenuated by bones than by soft tissue. This is because bones have a higher Z material than soft tissue. Further, the vacancy which is left in the atomic shell is filled with an electron from an outer shell. Energy is released either as a photon, called characteristic x-ray, or as an so-called Auger electron [9, 10, 11, 12].

2.1.3 Compton scattering

Compton scattering is when a photon interacts with an electron which is assumed to be free and at rest, i.e. the binding energy is much smaller than the incident photon energy $h\nu$. Parts of the photon energy will be lost to the electron, which is ejected with a kinetic energy $E_{\mathrm{K}} = h\nu - h\nu'$ at an angle ϕ. The rest of the energy is scattered, at an angle θ, as a photon with energy

$$h\nu' = \frac{h\nu}{1 + \alpha\,(1 - \cos\theta)}. \tag{5}$$

Here $\alpha = h\nu/m_0c^2$ and m_0 is the electron rest mass. The electron energy will be deposited within the electron range, close to the point of interaction, but the scattered photon may

travel much further, and may undergo additional interactions. With increasing energy, photons are increasingly scattered in the forward direction and an increasing fraction of the energy is transferred to the electron. For example, at 1.7 MeV, 50% of the energy is transferred to the electron.

The Klein-Nishina (K-N) electronic cross-section ${}_e\sigma$ is independent of Z, as only electrons which are assumed to be free are considered. Further, the K-N atomic cross-section ${}_a\sigma$ depends linearly on the attenuator atomic number Z, according to equation (1). The mass attenuation coefficient σ/ρ, is practically independent of Z, according to equation (2). The fraction Z/A is for most materials around 0.5, except for hydrogen, which has a Z/A of 1. As a consequence, materials with a high hydrogen content, e.g. water and soft tissue, will have more electrons per gram.

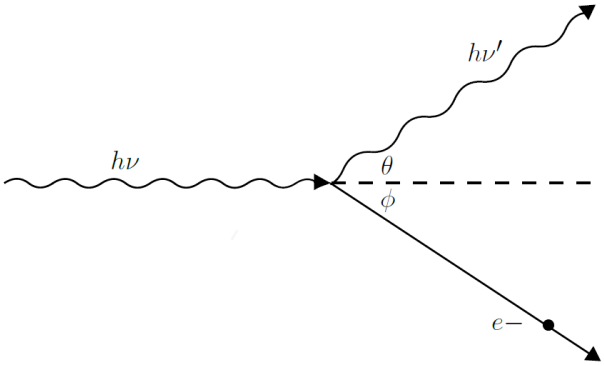

Figure 2: Compton scattering is illustrated. A photon of energy $h\nu$ is incident and a photon of energy $h\nu'$ and an electron is ejected.

If an image is taken with photons in the energy range for which the Compton effect dominates ($\sim$ 25 keV-25 MeV), there will be very little contrast between soft tissue and bone, this is because of the atomic number independence. Compton scattering is the main effect in radiation therapy, due to the applied energy range (6-20 MeV), as well as the fact that human tissue is a low Z material [9, 10, 11, 12, 13].

2.1.4 Pair Production

Pair production is when a photon is absorbed in the Coulomb field of a nucleus and a electron-positron pair is emitted with combined kinetic energy of $h\nu - 2m_0c^2$. The energy of the incident photon needs to be at least $2m_0c^2 = 1.02$ MeV for this process to happen. The pair production process dominates in the the energy range of more than 25 MeV.

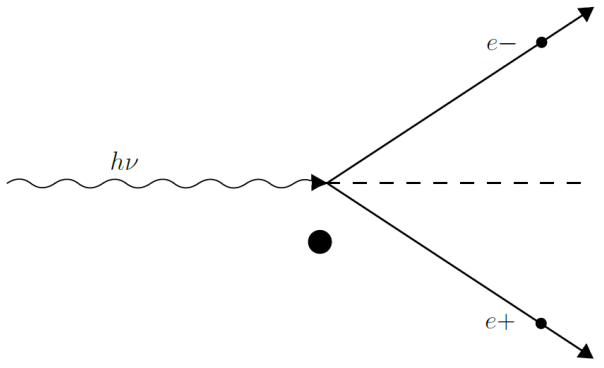

Figure 3: Pair production is illustrated. A photon of energy $h\nu$ is incident and a electron and a positron is ejected, in the presence of a nucleus.

The atomic attenuation coefficient is proportional to Z^2 and the mass attenuation coefficient is proportional to Z, according to equation (2). Afterwards, there is annihilation of the positron with an electron assumed to be free and at rest, and two annihilation quanta, typically with energies of 0.511 MeV, are emitted

180° from each other. Triplet production, where pair production happen in the electric field of an atomic electron and three electrons emerge, is also possible. However, it is less important for elements of higher atomic number than hydrogen. The energy threshold for triplet production is $4m_0c^2 = 2.04$ MeV [9, 10, 11, 12].

2.1.5 Photon Beam Attenuation

Photon beam attenuation is described as the change in intensity, $I(x)$, of a narrow monoenergetic photon beam which is passing through an attenuator of thickness x. It is given by

$$I(x) = I(0)e^{\mu(h\nu,Z)x}, \tag{6}$$

where $I(0)$ is the intensity of the beam before it was attenuated and $\mu(h\nu, Z)$ is the linear attenuation coefficient. Note that the linear attenuation coefficient, μ, is dependent on the photon energy $h\nu$ and the atomic number Z of the attenuator, and it represents the probability for interaction per unit length [9, 10, 11, 12].

2.1.6 Particle and Energy Fluence

Particle fluence is given by

$$\Phi = \frac{\mathrm{d}N}{\mathrm{d}A}, \tag{7}$$

and energy fluence is given by

$$\Psi = \frac{\mathrm{d}E}{\mathrm{d}A}. \tag{8}$$

Here, N is the expectation value of the number of particles, and E is the expectation value of the total energy carried by the N particles, striking an infinitesimal sphere of cross sectional area $\mathrm{d}A$ [10].

2.1.7 Kerma

The energy of the photons in a treatment beam is transferred to matter in two steps, first the photons transfers energy to secondary electrons through photon interaction processes like the photo electric effect, Compton scattering and pair production. Secondly, these secondary electrons transfer energy to the medium though excitations and ionizations. Kerma stands for kinetic energy released per unit mass and it representes energy transferred from photons to electrons via collision interactions, described by collision kerma K_{col}, and radiative interactions, described by radiative kerma K_{rad}. Collision kerma, from both hard and soft collisions, represent the production of electrons that dissipate their energy as ionizations a the medium. It is defined as the expectation value of energy transferred to charged particles per unit mass.

Note that radiative energy loss and energy transferred from one charged particle to another is not included. Radiative kerma represent bremsstrahlung and electron-positron annihilation [10].

2.1.8 Bremsstrahlung

When electrons are decelerated in the strong Coulomb field of a nucleus, parts of the electron energy is lost as bremsstrahlung photons, also called radiative loss. A continuous spectrum of photons, with kinetic energies from zero to the energy of the incident electron, is generated. This deceleration of electrons is proportional to Z/m, where m is the mass of the electron. These radiative losses will be significantly larger than the collision losses. In the mega voltage range of the linear accelerator treatment beam, there will be almost exclusively bremsstrahlung photons, which have been created in the target [9, 10].

2.1.9 Charged Particle Equilibrium

Charged particle equilibrium (CPE) is reached if all charged particles of a given type and energy leaving a certain volume is replaced by identical particles entering the volume [9]. As a result of the finite range of secondary electrons, the energy transferred from the photon beam at a certain location is not absorbed at that exact location. Normally, the radiative/bremsstrahlung photons escape the volume of interest, and therefore, absorbed dose is commonly associated with collision kerma, K_{col}. When a high energy photon beam penetrates a medium, photon fluence and therefore K_{col}, is greatest at the surface of the medium. The charged particle fluence, and thus the absorbed dose, increases with depth until the depth of maximum dose is reached, this is visualized in figure 4.

At CPE conditions, see figure 4 (a), production of secondary electrons is considered, but not attenuation of the photon beam or scattering in the medium, in this case, absorbed dose is equal to K_{col}. At the more realistic transient charged particle equilibrium (TCPE), see figure 4 (b), there is a constant relation between K_{col} and absorbed dose. Here, photon attenuation and scattering in the medium is taken into account. The build-up of absorbed dose is responsible for the skin sparing effect in high energy photon beams. The surface dose is small in practice, but does not equal zero. The contribution originate from electron contamination in the beam, which is due to photon interactions in the media upstream from the phantom, or due to charged particles generated in the treatment head and beam modifying devices [10]. This will be discussed further in later sections.

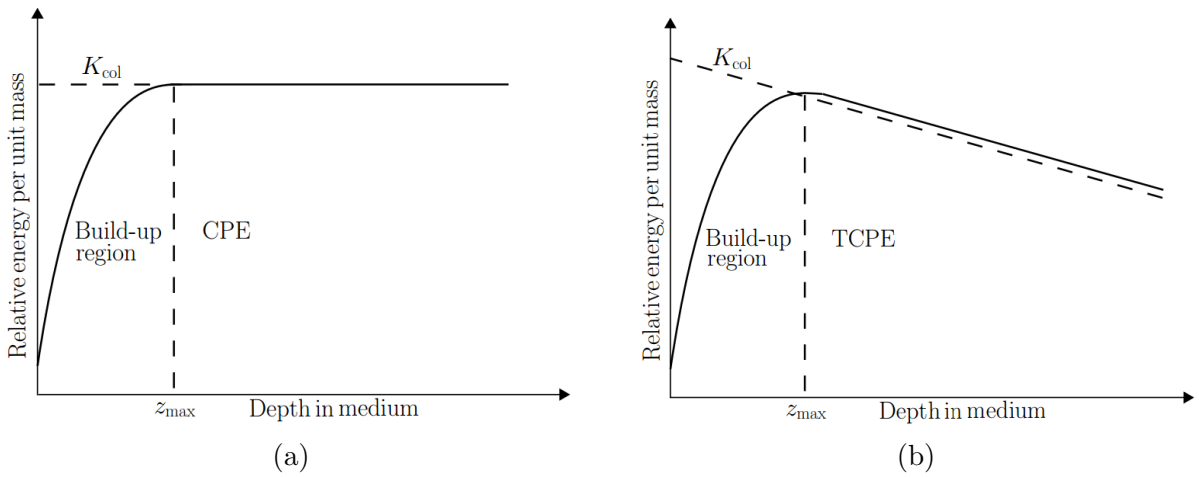

Figure 4: Absorbed dose as a function of depth is shown. Charged particles equilibrium is illustrated in (a) and transient charged particle equilibrium is illustrated in (b). The depth at maximum dose is represented by z_{max} The figures are inspired by figures in [10].

2.2 Definition of Volumes in Radiotherapy

The gross tumor volume (GTV) is an anatomical volume, which can be described as the gross palpable or radiologically visible tumor, or in other words, the demonstrable extent and location of the tumor. It can be a primary tumor, regional lymph nodes, distant metastasis or local recurrence [14, 15, 16]. The primary tumor is denoted, GTV-T, and for lymph node involvement, GTV-N is used [17].

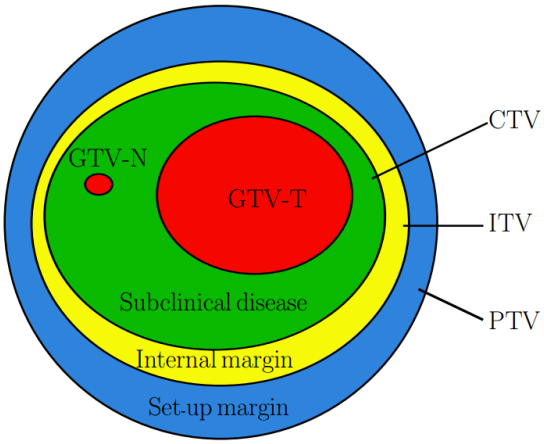

Figure 5: Volumes and margins. The figure is inspired by a figure in [14].

The clinical target volume (CTV) contains GTV and/or subclinical microscopic malignant disease with a certain probability of occurence considered relevant for therapy. Subclinical disease includes microscopic tumor spread at the boundary of the GTV. Thus it cannot be palpated nor visualized in diagnostic imaging [15].

The internal target volume (ITV) is a margin based volume which contains the CTV in addition to an internal margin (IM) taking into account uncertainties in size, shape and position of the CTV within the patient. Also, there can be variations in delineation of the target volumes by different physicians which is also taken into account [15, 16].

The planning target volume (PTV) is also a margin based volume, and it is a geometrical volume introduced to ensure that the prescribed dose will be delivered to all parts of the

CTV with a clinically acceptable probability. This volume contains the total margin, which in turn include both the internal margin (IM) and the set-up margin (SM). The SM take patient positioning and alignment of therapeutic beams in all the treatment sessions into account, in addition to the uncertainties of the imaging system. Normally, the total margin is established based on population data on systematic and random uncertainties (which occur both in the IM and SM) [15, 16].

2.3 Dose-Volume Parameters

When treatment plans are being evaluated in radiotherapy, several parameters are used to determine whether a treatment plan give good enough dose coverage to the tumor and good enough sparing of the OAR. Some of these parameters can be found in a dose-volume histogram (DVH). The D_{98}, also called the near minimum dose, is the dose level that 98% of the volume of interest receives. The D_2, which is also called the near maximum dose, is the dose level that 2% of the target volume receives. This value is considered to be less sensitive to the resolution of the dose matrix, and therefore more clinically relevant. Further, the mean dose, D_{mean}, is the arithmetic mean dose of a volume. Lastly, the median dose D_{median}, also denoted D_{50}, is the middle value when all dose values are sorted by size, i.e. the dose value where equal volume get lower and higher dose [16].

2.4 Anatomical Terms for Directions

The medial-lateral (ML) direction means the direction from the center to the outer limit of the body in the left-right direction of a body. The cranio-caudal (CC) direction is the direction from feet to head of a body and anterior-posterior (AP) is the direction from the front to the back of a body.

2.5 Head and Neck Cancer

2.5.1 Biology and Anatomy

Most cancers of the H&N area are so-called squamous cell carcinomas. Squamous cells are flat cells that make up the surface of the skin and the mucous membranes, which are moist tissues lining body cavities, e.g. the mouth, nose, throat and the intestines [18, 19]. The most common regions in which H&N cancers originate are the oral cavity, pharynx (throat) which is subdivided into the nasopharynx, oropharynx and the hypopharynx, larynx (voicebox), paranasal sinuses, nasal cavity, and finally the salivary glands, these correspond to diagnosis codes C00-C14 and C30-C32. Note that the oropharynx include the tonsils,

base of tongue and soft palate (in the back of the mouth). Further, cancer of the larynx include the supraglottis, glottis (vocal cord) and subglottis. These H&N cancer regions are illustrated in figure 6 [19, 20].

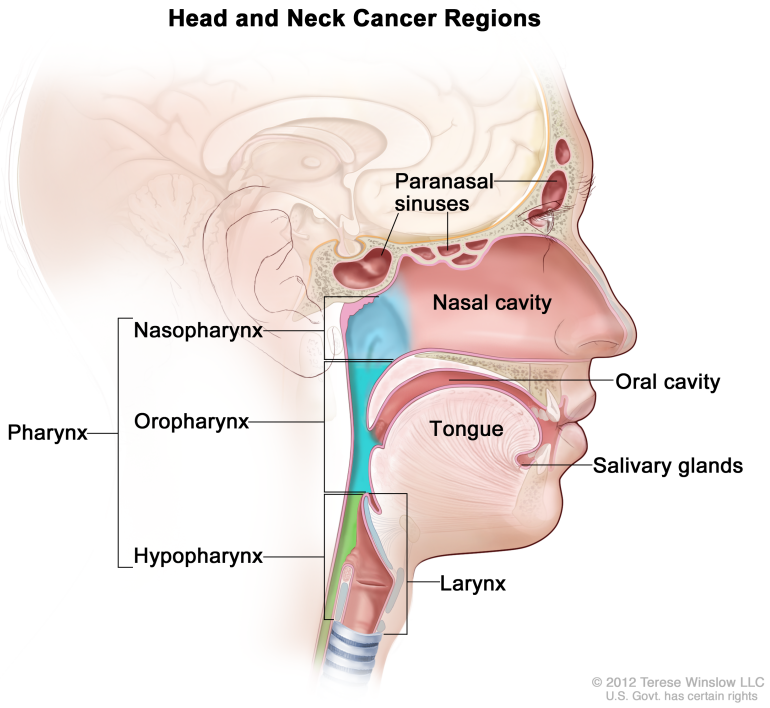

Figure 6: For the National Cancer Institute © 2012 Terese Winslow LLC, U.S. Govt. has certain rights. Reproduced with permission from Terese Winslow.

2.5.2 Treatment Methods

The main treatment options for H&N cancer patients are surgery, radiotherapy and chemotherapy, often in a combination of these. Patients with tumors in the oropharynx or small tumors in the hypopharynx are seldomly treated with surgery, and often treated with radiotherapy to large parts of the neck. Large tumors of the hypopharynx are considered for surgery [20]. Large tumors of the larynx are primarily treated with radiotherapy. In the case of recurrence or very advanced tumor, the entire larynx is removed [21].

2.5.3 TMN Staging for Head and Neck Cancers According to National Comprehensive Cancer Network [1]

Primary tumor (T):

TX Primary tumor cannot be assessed.

T0 No evidence of primary tumor.

T1 Tumor $\leq$ 2 cm in the greatest dimension.

T2 Tumor $\geq$ 2 cm, $\leq$ 4 cm in the greatest dimension.

T3 Tumor $\geq$ 4 cm in the greatest dimension.

T4a Moderately advanced local disease.

T4b Very advanced local disease.

Regional Lymph Nodes (N):

NX Regional lymph nodes cannot be assessed.

N0 No regional lymph node metastasis

N1 Metastasis in a single ipsilateral lymph node, $\leq$ 3 cm in greatest dimension.

N2 Metastasis in a single ipsilateral lymph node, $\geq$ 3 cm, $\leq$ 6 cm in greatest dimension or in bilateral or contralateral lymph nodes, all of which $\leq$ 6 cm.

N2a Metastasis in single ipsilateral lymph node, $\geq$ 3 cm, $\leq$ 6 cm in greatest dimension.

N2b Metastasis in multiple ipsilateral lymph nodes, all $\leq$ 6 cm.

N2c Metastasis in bilateral or contralateral lymph nodes, all $\leq$ 6 cm.

Distant Metastasis (M):

M0 No distant metastasis.

M1 Distant metastasis.

Note that bilateral means that both sides (of the neck) are affected, contralateral refers to the opposite side of where the tumor is located and ipsilateral meaning on the same side that the tumor is situated.

2.5.4 Material Heterogeneities

A problem which often appears in the treatment planning of H&N patients[5] is that the CTV is situated so close to the skin that the PTV reaches out to the body contour, or even extend beyond. If this is the case, the optimization system will increase the weights of the beamlets in this area, i.e. increase the fluence to this area outside of the skin to reach the dose-volume objectives that are set for the PTV. This is discussed further in section 2.10. Increasing the fluence is unwanted, firstly because it is unnecessary and secondly because the dose to skin will also increase. Further, there will always be small geometric uncertainties involved in radiation therapy. If there is a high fluence in the air just outside the skin, and the PTV were to move into this region; both the PTV and the skin would get highly overdosed [22, 23, 24, 25, 26].

[5]This is also the case in other patient groups, such as in breast cancer patients and in lung cancer patients.

2.6 Organs at Risk

There are two groups of OAR, the serial OAR, e.g. the chiasm, optic nerve and spinal cord, and the parallel OAR, like the lungs, parotid glands and kidneys. The difference between the two is that the functionality of serial OAR is compromised even if only a small volume receives a dose above a certain tolerance level. However, it is acceptable for a parallel OAR to receive a dose above a given tolerance level, to a small volume of the organ. It should be noted that the greater the volume with dose above the tolerance level is, the greater will the probability of loss of functionality be. For serial OAR, $D_{2\text{cm}^3}$ or an absolute volume is often set as limiting to the dose, this is because higher doses in a smaller volume than that, is clinically irrelevant. For parallel OAR, often the mean value is used as dose limitation. In reality, many OAR are not completely serial, or completely parallel, but somewhere in between. Serial OAR are often prioritized before target volumes, which are, in turn prioritized before parallel OAR or less critical OAR.

OAR which are often of interest, and therefore contoured, for H&N cancer patients are the spinal cord, the parotid glands and the submandibular glands, see figure 7. Depending on the tumor location, the lenses, retina, brain stem, chiasm, optic nerve, larynx and pituitary gland could also be contoured and evaluated [17, 27, 28].

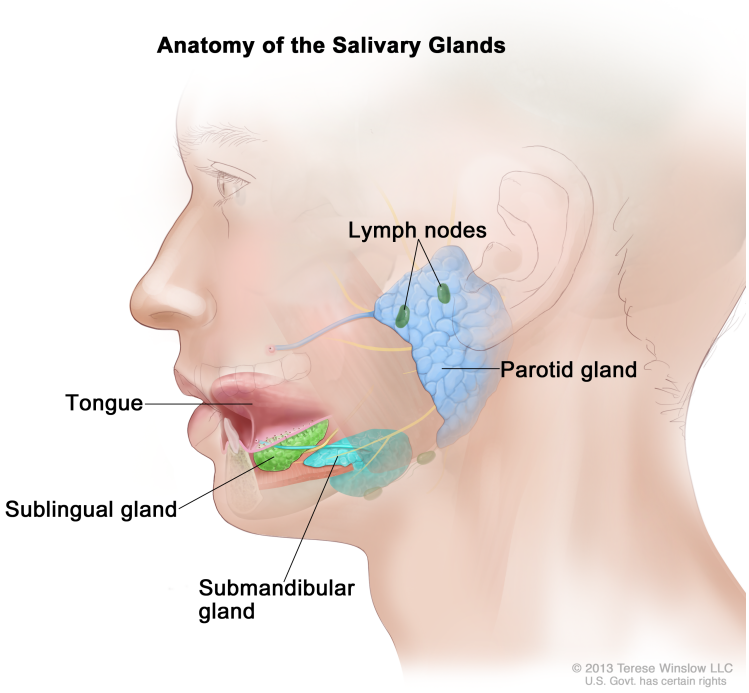

Figure 7: For the National Cancer Institute © 2013 Terese Winslow LLC, U.S. Govt. has certain rights. Reproduced with permission from Terese Winslow.

2.7 The Linear Accelerator

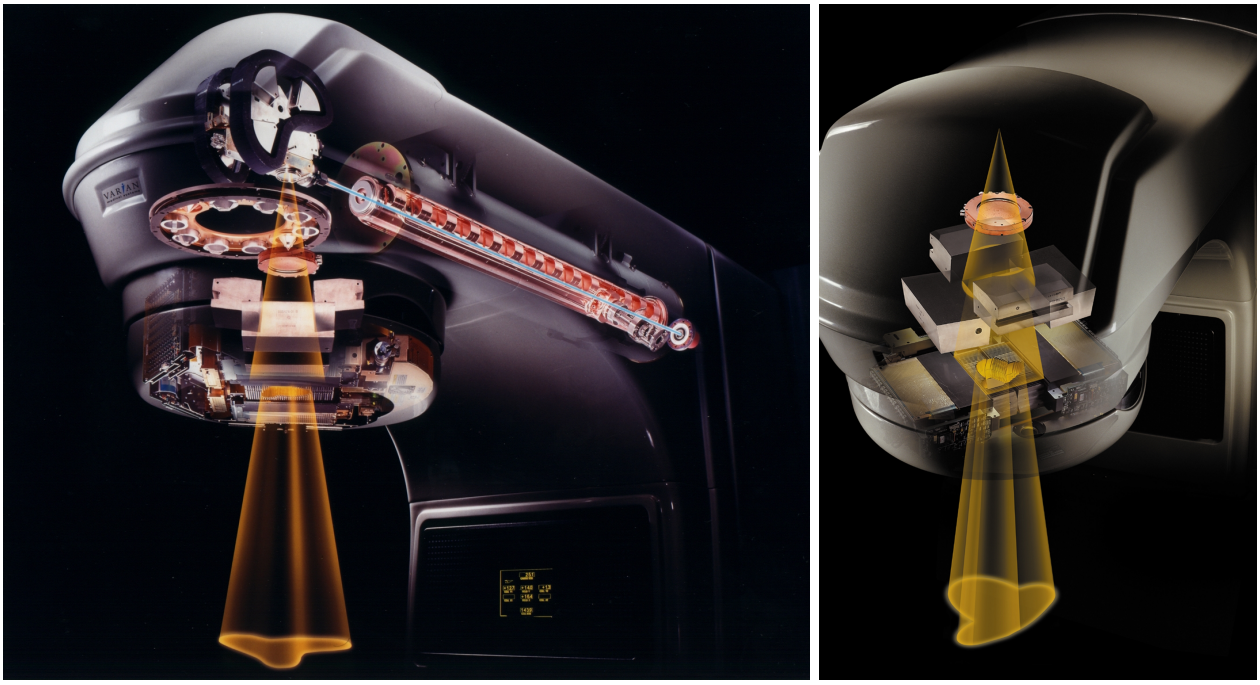

(a) (b)

Figure 8: The inside of a Varian linear accelerator in (a) and dose shaping of the treatment beam in (b). From the right in (a), the accelerating waveguide, the bending of the electron beam on top of the figure, further, from the top, the target(s), flattening filter and secondary jaws. From the top in (b), flattening filter, secondary collimators and the MLC leaf banks. Note a Clinac® linear accelerator is displayed, but the principles are the same as for a TrueBeam™. The figures are retrieved from [29].

2.7.1 Beam Generation

The linear accelerator (linac) is used for radiotherapy of cancer patients. In the linac, electrons interact with a synchronized radio-frequency electromagnetic field and from this, gain energy. A long cylindrical tube containing circular baffles is called the accelerating waveguide, shown in figure 8 (a). In the first part of the tube, these baffles are constructed such that the microwave propagation can reach speeds of close to the speed of light. Bunches of electrons from the electron gun are introduced into the waveguide synchronized with pulsed microwave radiation. These electron bunches are then carried down the waveguide in a similar way as a surfer is riding the crest of a wave. This high energy electron beam is used directly for treatment of some groups of patients, but this will not be discussed further in this study. The electron beam is bent 270° by a magnetic field[6], such that the electrons are

[6]The Varian linear accelerator has a 270° three sector system and the Elekta linear accelerator uses a 112.5° double focusing system.

focused against a thick so-called target. This is made up of a high atomic number material, usually tungsten. The energy loss of the electrons is converted into bremsstrahlung radiation, as described in section 2.1.8. At energies relevant for radiation therapy, the dominating direction of the bremsstrahlung emission is the forward direction. Therefore, a flattening filter is used to even out the beam intensities radially out from the central axis, making the beam profile uniform.

2.7.2 Collimation

The linac also includes various collimators which constrains the beam to where the patient is treated. Note that only characteristics for the Varian linac will be presented, because of relevancy to this thesis. First, a primary collimator is situated close to the target. Then, two pairs of secondary collimators/jaws made of blocks of lead are placed such that they are aligned with the diverging edge of the beam, 90° to each other. This can be seen in figure 8 (b). The X-jaws are located closest to the target and the Y-jaws are situated closest to the patient. Above the primary collimator, there is a ionization chamber which controls the dose delivery, e.g. beam uniformity and dose rate. Moving from conventional treatment methods with rectangular fields, to more advanced techniques, multileaf collimators (MLCs) were introduced. These are much more flexible, up to 80 pairs of leaves can move independently, making up the desired beam shape [9]. These MLC leaves are mounted on leaf banks, as seen in figure 8 (b). Illustrations of such MLCs and the tongue-and-groove design of the Varian MLCs can be seen in figure 9.

2.7.3 Isocenter

The isocenter is ideally a fixed point defined by the intersection of the central axis of the treatment beam and the gantry rotation axis. The distance between the x-ray target and the isocenter is set to be 100 cm [9]. Lasers in the treatment room are set up to intersect the isocenter from left, right and above the treatment machine. These lasers are used for patient positioning to ensure that the patients lie in the same position at each treatment session, as when the planning computed tomography (CT) was taken. The isocenter is also used as a reference point by the TPS [9].

2.7.4 Monitor Units

The ionization chamber measurement of the beam is proportional to the delivered dose. The term quantifying this is called monitor units (MUs). The linac is usually calibrated such that 100 MUs correspond to 1 Gy, at isocenter [9].

2.8 Volumetric Modulated Arc Therapy

VMAT is a radiotherapy treatment delivery technique in which gantry speed, MLC leaf positions and dose rate is varying continuously as the gantry rotates around the patient. This technique is a distinct type of the wider concept intensity-modulated radiation therapy (IMRT), but in conventional IMRT the treatment is given at fixed gantry angles. This means that the gantry stops at each of these angles and delivers the planned segment, before rotating to the next gantry angle. Both delivery techniques are widely used, but VMAT is now getting increasingly more popular due to fast delivery time and reduction of MUs. Compared to IMRT, VMAT has more flexibility, as dose can be delivered from all 360° of a full gantry rotation, and the beam aperture is modulated continuously [3]. In a treatment session, the gantry most commonly rotates around the patient one or two times, but additional rotations are also possible for more complicated cases. For Varian linacs, it is customary for 178 control points (CPs) to be created in one such 360° arc. For each of these points, a fluence profile is iteratively generated, and the following parameters are defined: gantry angle, collimator angle, collimator position, MLC leaf position and cumulative MUs delivered at that point. The CPs which are situated adjacently are grouped together, and the fluence profile is approximated within one such group. Further, the dose is calculated and the motion between two CPs is calculated using a number of interpolated dose calculation points. The linac delivery control system moves the gantry, collimators and MLC leaves dynamically between the control point positions and the dose rate is chosen so that the right number of MUs is delivered at every control point. There is a feedback system that monitors and adjusts the motion and dose rate when needed [4].

2.9 Fluence Delivery Modeling Algorithms

Generation of MLC leaf sequences involves an algorithm which tries to define the MLC leaf shapes that are needed to make a fluence distribution as similar as possible to the fluence distribution made by the optimizer, see next section. To be able to deliver a predictable dose distribution, there are several refinements needed to make the MLC leaf-setting sequence as accurate as possible. The Eclipse^{TM}(Varian Medical Systems Inc., Palo Alto, CA, USA) TPS is used at UNN, and is therefore the TPS in focus in this thesis. The fluence delivery modeling algorithms in Eclipse^{TM} take into account leaf transmission, dosimetric leaf gap and tongue-and-groove modeling. MLCs always transmit a small amount of radiation through the leaves. A transmission factor is configured for all available energies and for each treatment unit, and it is used in all fluence calculations. The ends of the MLC leaves are rounded to produce better off-axis dosimetric characteristics. Consequently, even when a pair of leaves

is closed, some radiation goes through, this is called the rounded leaf end transmission. This effect is handled by the so-called dosimetric leaf gap configuration parameter. The leaf edges are modeled as sharp by the algorithms, but in the actual fluence calculation they are pulled back by half the value of the dosimetric leaf gap parameter, such that the gap between a fully closed leaf pair is equal to the dosimetric leaf gap parameter, seen in figure 9 (a). The Varian MLC models have a so-called tongue-and-groove design which minimizes leakage between the leaves, visualized in figure 9 (b). The tongue blocks some radiation[7], thereby modifying the fluence delivery. The amount of radiation blocked is proportional to the ratio between the tongue and the leaf widths [30].

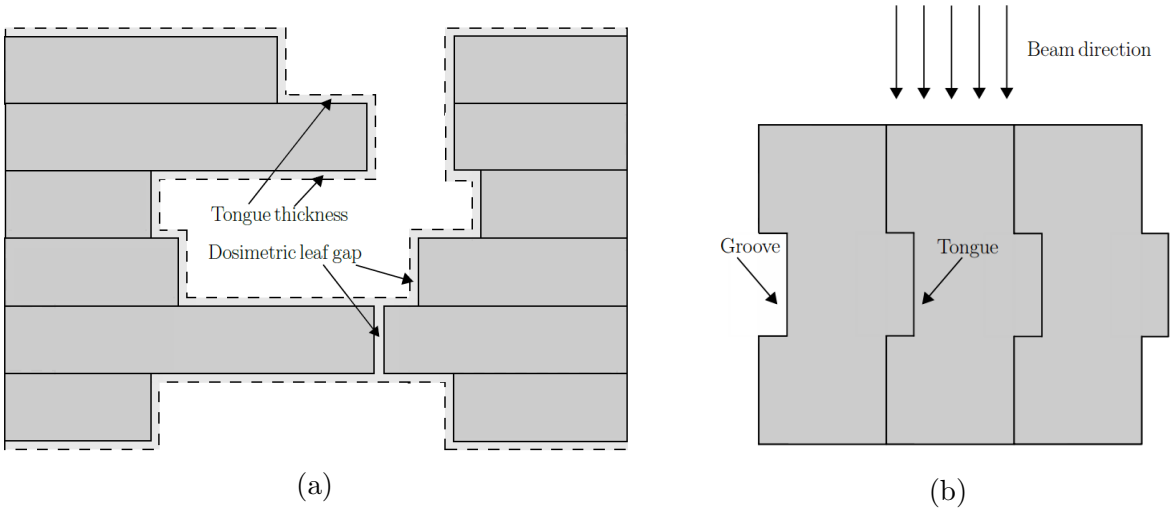

Figure 9: Tongue thickness and dosimetric leaf gap are shown in (a) and the Varian tongue-and-groove design is visualized in (b). The arrows indicate the direction of the beam in relation to the MLC leaves.

2.10 Inverse Optimization

As opposed to forward treatment planning used in conventional radiotherapy, IMRT and VMAT requires a completely different treatment planning strategy, called inverse treatment planning. In inverse planning, the main focus is the final dose distribution, and not how this dose distributions is accomplished. The goals or objectives are specified in the optimization system by the user and the beam parameters are then determined and adjusted iteratively by the optimization algorithm to achieve the desired dose distribution.

As response of the tumor and normal tissue is a function of both the radiation dose and the volume receiving each dose level, dose-volume objectives are used in most optimization systems [31]. The upper dose-volume objective is typically used to limit the dose for a given

[7]The groove effect is smaller and is not modelled in the algorithm.

structure, for example, 0% of the spinal cord may receive more than 46 Gy. The lower objective is used to get a certain level of dose to a given structure. For example, 100% of the ITV52 should get at least 52 Gy. The two objectives are also often combined. A weighted quadratic cost is added to the total objective function if these dose-volume objectives are not met. For the upper objective, the cost is applied to the fraction of the doses that is above the requested dose and volume level. For the lower objective, the cost is applied to the fraction of the doses that is below the requested dose and volume level [30].

Optimization algorithms in general work by tracing only the beamlets passing through the target volume and setting the weights of all other beamlets to zero. Dose is calculated for a 3D description of the patient which is divided into small voxels, with a given set of beamlet weights [31]. In the common gradient based optimization algorithm, first a direction is selected, and then search is performed along this direction to find a good point to start the next iteration [32]. This dose distribution is used to calculate the total objective function. If changing the beamlet weights would mean improving the value of the objective function, than such a change is accepted, otherwise, it is not. Further, this process is repeated for all the beamlets, and when this is finished, an iteration has been made, and the treatment plan has slightly improved. The resulting beamlet intensities are then used to calculate another dose distribution and a new value for the objective function. The iteration process continues until further improvements cannot be made, and the presumed optimal plan has been made. If multiple extrema exist, the optimization will lead to the nearest one, which might be a local minima and therefore not be the optimal plan. However, this has not been reported to be a large obstacle in achieving good solutions [31].

For VMAT optimization in the Eclipse^{TM} TPS, MLC leaf position and MU weights are used as optimization parameters. MLC leaf positions or MU weights are constrained such that the aperture shapes and MU values are possible to achieve in practice. Overlapping of opposing leaves or negative MU are examples of weights that are impossible, and therefore rejected. For each iteration of the optimization, random available gantry samples are chosen, then either the MU weight or a MLC leaf position is changed. If such a change is allowed, the dose distribution and cost function is calculated. If the cost is reduced, the change is accepted, otherwise, not. In the beginning of the VMAT optimization, a quite coarse sampling of gantry sectors is used, distributed evenly over an entire arc. After a number of iterations including MLC and/or MU weight changes, a new sample is added midway between to existing samples. The MLC positions for this new sample are linearly interpolated from the MLC positions of the adjacent samples. The MU weight of the new sample is a function of the MU weight of the adjacent samples. The VMAT algorithm optimizes both the previous beam samples and the newly added sample. After a full gantry range has been resampled, the process continues

by returning to start again, this continues until a desired sampling frequency is obtained. The VMAT optimization is not so much restricted by efficiency constraints in the beginning, but become more restricted as new samples are added. Naturally, as new samples are introduced, the accuracy of the optimized plan with regards to the delivered plan is improving. In the beginning, the number of iterations between each sample addition is relatively large, and there are exponentially fewer iterations between each new sample as the number of samples increases [33].

2.11 Photon Beam Source Model

The photon beam source model describes the output radiation from the linac and it is used by the anisotropic analytical algorithm (AAA) which is implemented in the Eclipse$^{\text{TM}}$ TPS. The parameters of each clinical beam is specified and a customized phase-space is constructed. The photon beam source model consists of the primary photon source, the extra-focal source and the electron contamination source. The full clinical beam is separated into beamlets, for which the size is a function of the grid size which is used for calculation [30, 34, 35].

2.11.1 The Primary Source

The primary source is a point source situated at the target plane in the treatment unit head, as described in section 2.7 and seen in figure 10. Here, the bremsstrahlung photons created in the metal target and which have not interacted before reaching the patient surface, are being modeled. Further, the beam will consist of relatively more high energy photons after passing the flattening filter, as low energy photons are attenuated more easily, a phenomena called beam hardening [36]. The thickness of the flattening filter varies with the radial distance from the central axis. As a result, the beam hardening effect is modeled by individually attenuating the energy components of the initial photon energy spectrum $S(E)$, for each radial distance. Below the flattening filter, the primary photon spectrum is given by

$$S(E, r) = S(E)e^{-\frac{\mu d(r)}{\rho(E)}}, \tag{9}$$

where $\frac{\mu}{\rho(E)}$ is the linear attenuation coefficient of the flattening filter material, for a given energy E [37].

The primary energy fluence, ψ, take into account the modulating functions of the MLCs, as well as the modulating functions of the tops and bottoms of the X- and Y-jaws. In addition, the intensity profile curve, $I(r)$, accounts for the fact that the energy fluence distribution of photons below the flattening filter might not be completely uniform [30, 34, 35].

2.11.2 The Extra-Focal Source

The extra focal source is a finite-sized virtual source in which photons resulting from interactions in the treatment unit head, other than in the target, are being modeled. This secondary source is situated at the bottom plane of the flattening filter and the intensity distribution is assumed to be Gaussian. The photons modeled will mainly originate from the flattening filter, primary collimators and secondary jaws. These are called the extra-focal components. As a consequence, for flattening filter free (FFF) beams, this extra-focal source modeling is not used. As this source is situated below the target, the energy fluence distribution will be wider than the one from the primary source, and is therefore most notable outside the beam from the primary source.

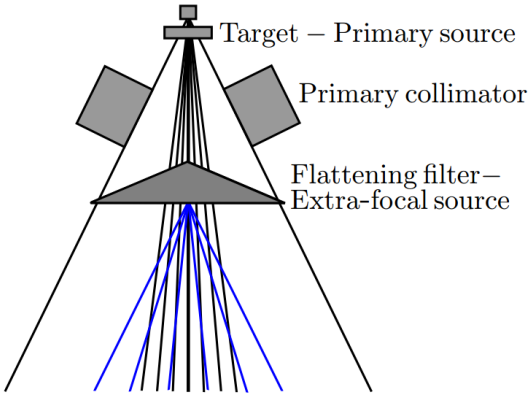

Figure 10: Schematic illustration of the treatment unit head, with the target, primary collimators and flattening filter.

The energy fluence from the extra focal source at a given plane is obtained by adding the contributions from of the each source components, for each pixel in the destination fluence array. If a given ray hits the X- or Y-jaws, or the MLC leaves, the contribution will be zero[8]. Further, the contributions are scaled with the inverse square of the distance from the source component to the destination element, with the Gaussian weight of the source component and with the cosine of the ray angle relative the central axis. The extra focal photon energy spectrum is only modeled on the central axis. It is empirically derived, and the energy axis is scaled to obtain mean energies $\bar{E}_{\text{ef}}$ [30, 34, 35].

2.11.3 Electron Contamination

The primary photon beam is contaminated with electrons originating from the flattening filter, collimator jaws and from the air, this contamination depends strongly on beam energy and field size. Further, the photons that are created in electron interactions are also taken into account. Modeling is performed using a (radiological) depth dependent curve describing the dose from electron contamination at a certain depth [30].

[8]Or, the contribution is equal to a MLC transmission value, set by the user.

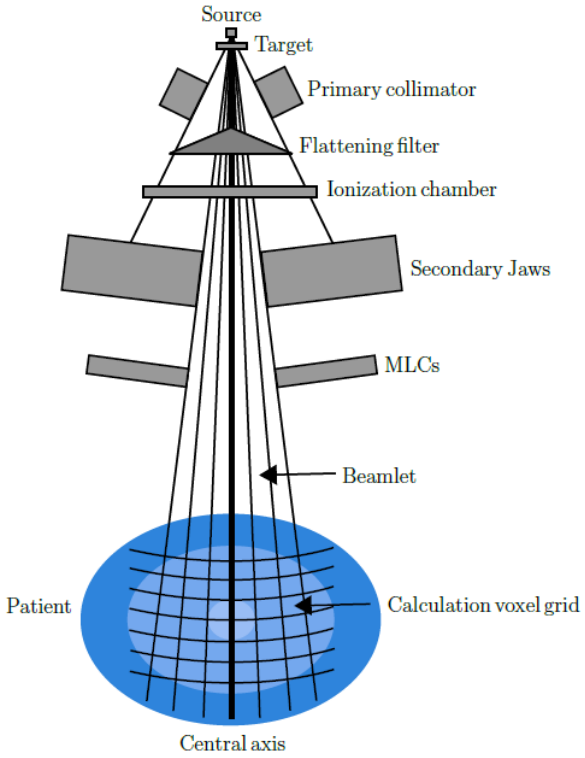

Figure 11: Schematic illustration of the linear accelerator components. This figure is inspired by a figure in [30].

2.12 Photon Dose Calculation in the Anisotropic Analytical Algorithm

Accurate dose calculation is essential for the patient to receive the planned dose level at the precise location where it was planned. The task of dose calculation can be divided into two parts: modeling the output radiation from the linear accelerator, called source modeling (described earlier in section 2.11) and based on that, calculating the dose deposited in the patient. Tillikainen *et al*. have developed a multiple-source model, where the parameters were derived from an automatic optimization procedure from water-phantom measurements. This model is used by the AAA algorithm in the Eclipse^{TM} TPS.

AAA is a three-dimensional pencil beam convolution/superposition algorithm. Primary photons, extra-focal photons and contaminating electrons are modeled separately using Monte Carlo derived scatter kernels. The dose deposited laterally is modeled using six exponential functions. Further, by the use of convolution, the computation time is greatly reduced. Tissue heterogeneity is taken account for anisotropically in the three-dimensional neighborhood of an interaction site. This is done using photon scatter kernels in multiple lateral directions.

The developers of the original AAA algorithm were Ulmer *et al*. [38, 39, 40], however,

exponential functions have replaced the Gaussian functions used originally, to improve the modeling of scatter near lateral heterogeneities. The treatment beam is divided into small beamlets β, and the patient body is divided into a 3D matrix of divergent calculation voxels along the direction of the beamlets.

The primary and extra-focal source calculation is very similar, and will therefore be derived simultaneously. For energies E between 0.25 and 25 MeV, mono-energetic Monte Carlo-simulated pencil beam kernels $h_{\mathrm{E}}(z,r)$ $\left[\frac{\mathrm{J}}{\mathrm{MeV\,m^3}}\right]$ were simulated. Here, z refer to the distance from the surface and r, the orthogonal distance from the central axis. The kernel $h_\beta(z,r)$ is calculated as a superposition of the mono-energetic kernels $h_{\mathrm{E}}(z,r)$ and weighted with the primary (or extra-focal) photon energy spectrum $S_\beta(E)$,

$$h_\beta(z,r) = \frac{\int h_{\mathrm{E}}(z,r) S_\beta(E) \mathrm{d}E}{\int S_\beta(E) \mathrm{d}E} \tag{10}$$

[30, 34, 35].

2.12.1 Exponential Modeling

The energy deposition is divided into two components; along the fanlines in the depth-direction and perpendicular to the fanlines in the lateral direction. The depth-dependent energy deposition I_β, which accounts for the total energy deposited in a horizontal layer p_z, is given by

$$I_\beta(p_z) = \psi_\beta \int\int h_\beta(t,\nu,p_z)\,\mathrm{d}t\,\mathrm{d}\nu \ \left[\frac{\mathrm{J}}{\mathrm{m^2}}\right]. \tag{11}$$

Here, ψ_β is the primary (or extra-focal) photon fluence of a beamlet β, and is assumed to be uniform over the beamlet cross-section. For each depth p_z and angle θ, the fraction of energy, $f_\beta(\theta,\lambda,p_z)$, deposited into an infinitesimal angular section at a distance λ from the central axis, is given by

$$f_\beta(\theta,\lambda,p_z) = \frac{\lambda h_\beta(p_x+\lambda\cos\theta, p_y+\lambda\sin\theta, p_z)}{I_\beta(p_z)}. \tag{12}$$

The coordinates of a point p within the beamlet is represented by (p_x,p_y,p_z) in the diverging coordinate system. Note that f_β is calculated from Monte-Carlo derived data. Further, it is necessary to divide with $I_\beta(p_z)$ to normalize the f_β-integral over each calculation plane.

The lateral energy deposition k_β is modeled as a superposition of six radial exponential functions on the form

$$k_\beta(\theta,\lambda,p_z) = \sum_{i=1}^{6} \frac{c_i(\theta,p_{z)}}{\lambda} \cdot e^{-\mu_i\lambda} \ \left[\frac{1}{\mathrm{m}}\right]. \tag{13}$$

For each calculation plane p_z, the weight parameters c_i are adapted such that k_β and f_β becomes as equal as possible. The linear attenuation coefficients are chosen such that the effective ranges, $1/\mu_i$, vary between 0 and 200 mm [30, 34, 35].

2.12.2 Superposition

The energy deposited in a point p, in a horizontal plane p_z, by a single beamlet β in a homogeneous water-equivalent phantom is given by

$$E_\beta(p) = I_\beta(p_z) \cdot k_\beta(\theta, \lambda, p_z) \ \left[\frac{\mathrm{J}}{\mathrm{m}^3}\right]. \tag{14}$$

However, as patients are obviously heterogeneous, each spatial dimension is scaled by multiplying with $\frac{\rho_{\text{water}}}{\rho(p)}$, where ρ is the local electron density and ρ_{water} is the electron density of water. These electron densities of the patient tissues are retrieved from the CT images taken before treatment planning.

Taking into account that scattered particles follow different paths through the medium, all the possible paths are combined into fewer collapsed paths and it is assumed that the heterogeneity effects can be corrected for along these paths. This is done by scaling I_β and all the origin-centered rays of the k_β functions, independently.

Scaling I_β, the effective/radiological distance between the entry point of the pencil beam and the calculation plane is calculated by

$$d_{\text{eff}}(X) = \int_X \frac{\rho(p)}{\rho_{\text{water}}} \mathrm{d}p \tag{15}$$

for an arbitrary curve X. The heterogeneity-corrected I'_β is therefore given as

$$I'_\beta(p_z) = I_\beta(p'_z) \cdot \frac{\rho(p_\beta)}{\rho_{\text{water}}}, \tag{16}$$

where, p_β is the point on the beam central axis at a depth p_z. Further, p'_z is the effective depth given by equation (15) where the path was taken from the entry point to p_β.

The lateral scatter kernel is scaled similarly, by calculating the radiological path length radially from the center of the pencil beam. Then the heterogeneity-corrected lateral kernel is given as,

$$k'_\beta(\theta, \lambda, p_z) = k_\beta\left(\theta, \frac{p'_z}{p_z}\lambda', p'_z\right) \cdot \frac{\rho(p)}{\rho_{\text{water}}}, \tag{17}$$

where λ' is the effective radius. The lateral scatter kernel at the effective depth p'_z is used, therefore the effective radius λ' is scaled by the p'_z/p_z which corrects for the diverging coor-

dinate system. Finally, the heterogeneity-corrected energy distribution for a single beamlet β is given by

$$E_\beta(p) = I'_\beta(p_z) \cdot k'_\beta(\theta, \lambda, p_z). \tag{18}$$

The superposition is performed over 16 discrete directions which corresponds to a discrete number of angular sectors. The total energy deposited in a point p is then a integral over the contributions of the individual beamlets over the full beam [30, 34, 35].

2.12.3 Build-up and Build-down Corrections

Separating the heterogeneity correction into two directions, the lateral and the depth-dependent, is definitely an approximation. However, an advantage is that the pencil-beam kernel is scaled in all dimensions by $\frac{\rho_{\text{water}}}{\rho(p)}$ when dose is calculated in a uniform phantom with an electron density which is not water-equivalent. An adequate distance from the material interface of so-called slab-like phantoms, the results are comparable to Monte Carlo simulations. Close to interface, however, the gradual build-up and build-down effects are not reproduced as scattered particles which originate before the interface are not correctly accounted for. The extension of the build-up region is determined by the mean range of the scattered particles. As the dominating scatter component is forward directed, a forward build-up convolution kernel is applied to the energy deposition. The build-up kernel k_{b} is given as

$$k_{\text{b}} = \sum_{i=1}^{2} g_i \frac{1}{\nu_i} e^{-\nu_i d}, \tag{19}$$

for $d \geq 0$, otherwise, it is zero. Here, the g_i and ν_i decide the shape of the kernel and are determined via optimization methods. Energy is preserved as $\sum g_i = 1$. Convolution with the energy density distribution is performed in terms of the effective distance as follows:

$$E_{\text{b}}(p) = \int_{t=0}^{p_z} E_{\text{total}}(p_x, p_y, t) \cdot k_{\text{b}}(d_{\text{eff}}) \cdot \frac{\rho_{\text{water}}}{\rho(p_x, p_y, t)} dt. \tag{20}$$

Here, d_{eff} is the effective distance from (p_x, p_y, p_z) to (p_x, p_y, t). Multiplication with $\frac{\rho_{\text{water}}}{\rho(p_x, p_y, t)}$ is done to change variables from effective depth to true depth. The original build-up at the surface is stretched as the energy is moved deeper. This is pre-compensated for in I_β, in equation (11), by inversely convoluting I_β with the kernel k_{b}. The scatter calculation is executed as before, except I_β is replaced by I_{pre}. When k_{b} is applied to the energy distribution, the initial build-up and any following build-up or build-down effects at heterogeneity interfaces will be reproduced similarly [34].

2.12.4 Electron Contamination Contribution

For electron contamination, the lateral scatter is not taken into account. The energy contribution is given by

$$E_{\beta,\mathrm{ec}} = \psi_{\beta,\mathrm{ec}} \cdot c_{\mathrm{ec}}(p_z) \left[\frac{\mathrm{J}}{\mathrm{m}^3}\right], \tag{21}$$

where $\psi_{\beta,\mathrm{ec}}$ is the electron contamination energy fluence, and $c_{\mathrm{ec}}(p_z)$ is an empirical curve. This curve was determined from the difference between measured and calculated depth-dose curves, and it defines the total energy deposited at a plane p_z.

2.12.5 Total Energy and Conversion to Dose

Finally, the total energy density E_{total}, which is a sum of the primary photon, extra-focal photon and electron contamination, is converted to dose,

$$D(r) = \frac{E_{\mathrm{total}}\,\rho_{\mathrm{water}}}{\rho(r)} \cdot c. \tag{22}$$

Here, c is a calibration factor which takes into account the unit conversion from $\mathrm{J/m^3}$ to Gy. [30, 34, 35].

2.13 The γ Method

The γ index was introduced in 1998, by Low *et al*. [41]. This index is used for comparing dose distributions calculated by a TPS to dose distributions measured by a phantom, as a part of patient specific quality assurance (QA). Note that the three-dimensional representation is used clinically, but the two-dimensional representation is presented here for simplicity. This method uses the distance to agreement (DTA) distribution and the percentage dose difference (DD) to determine whether a dose calculation is acceptable. In a calculated dose distribution, the DTA is the distance between a given measured point and the nearest point of the same dose. The percentage DD is simply the difference in dose between the calculated and measured dose for a given point [41, 42]. For the global γ index, the DD is normalized to the maximum dose measured and for the local γ index, the DD is normalized to the dose at each given point [43, 44].

In the two-dimensional representation, the DTA and DD are united in the form that in a three-dimensional space consisting of dose in one direction and physical distance in two directions, the acceptance criteria form an ellipsoid surface[9]. In such an ellipsoid, the γ index is the minimal radial distance between the measured and calculated points. This distance

[9] In the three-dimensional case, distance is given in three directions and dose in a forth.

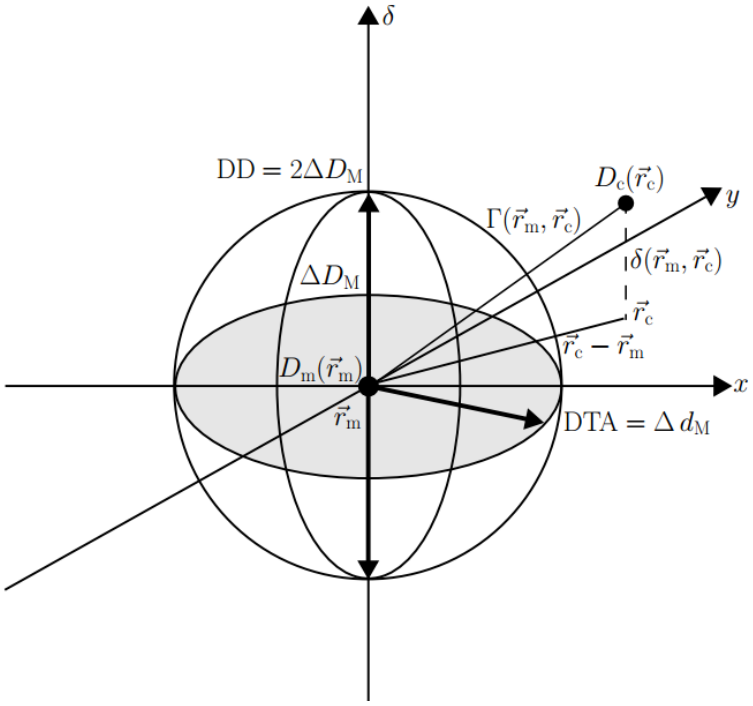

Figure 12: Two-dimensional representation of the ellipsoid surface representing the acceptance criteria. The figure is inspired by a figure in [41].

is scaled as a fraction of the acceptance criteria. The acceptance criteria are not met in the regions where $\gamma > 1$. Acceptance criteria of 3% DD and 3 mm DTA or 2% DD and 2 mm DTA are commonly used. A measurement point $\vec{r}_{\mathrm{m}}$ is situated at the center of the ellipsoid, as seen in figure 12. The x- and y-axis represent the plane in which the calculated point $\vec{r}_{\mathrm{c}}$ is located. The $\delta-$axis represent the difference between the measured dose $D_{\mathrm{m}}(\vec{r}_{\mathrm{m}})$ and the calculated dose $D_{\mathrm{c}}(\vec{r}_{\mathrm{c}})$. The DTA criterion is represented by a disk in the $\vec{r}_{\mathrm{c}} - \vec{r}_{\mathrm{m}}$ plane with a radius DTA $= \Delta d_{\mathrm{M}}$. If $D_{\mathrm{c}}(\vec{r}_{\mathrm{c}})$ lies within or intersects the disk, the DTA is inside the acceptance criterion. The DD test is represented by the two vertical arrows making up the diameter of the ellipsoid in the figure, the length of DD is $2\Delta D_{\mathrm{M}}$. A calculation point passes the DD test if $|D_{\mathrm{c}}(\vec{r}_{\mathrm{m}}) - D_{\mathrm{m}}(\vec{r}_{\mathrm{m}})| \leq \Delta D_{\mathrm{M}}$. The equation representing the normalized ellipsoid surface is given by

$$1 = \sqrt{\frac{r^2(\vec{r}_{\mathrm{m}}, \vec{r})}{\Delta d_{\mathrm{M}}^2} + \frac{\delta^2(\vec{r}_{\mathrm{m}}, \vec{r})}{\Delta D_{\mathrm{M}}^2}}, \tag{23}$$

where $r(\vec{r}_{\mathrm{m}}, \vec{r}) = |\vec{r} - \vec{r}_{\mathrm{m}}|$, and $\delta(\vec{r}_{\mathrm{m}}, \vec{r}) = D(\vec{r}) - D_{\mathrm{m}}(\vec{r}_{\mathrm{m}})$ is the DD at the position $\vec{r}_{\mathrm{m}}$. A quality index γ is given by

$$\gamma(\vec{r}_{\mathrm{m}}) = \min\{\Gamma(\vec{r}_{\mathrm{m}}, \vec{r}_{\mathrm{c}})\}, \tag{24}$$

for all $\vec{r}_{\rm c}$. Here

$$\Gamma(\vec{r}_{\rm m},\vec{r}_{\rm c}) = \sqrt{\frac{r^2(\vec{r}_{\rm m},\vec{r}_{\rm c})}{\Delta d_{\rm M}^2} + \frac{\delta^2(\vec{r}_{\rm m},\vec{r}_{\rm c})}{\Delta D_{\rm M}^2}}, \tag{25}$$

where $r(\vec{r}_{\rm m},\vec{r}_{\rm c})$=$|\vec{r}_{\rm c}-\vec{r}_{\rm m}|$, and $\delta(\vec{r}_{\rm m},\vec{r}_{\rm c}) = D_{\rm c}(\vec{r}_{\rm c}) - D_{\rm m}(\vec{r}_{\rm m})$ is the DD at the position $\vec{r}_{\rm m}$. The pass-fail criteria is therefore: $\gamma(\vec{r}_{\rm m}) \leq 1$, calculation passes, and $\gamma(\vec{r}_{\rm m}) > 1$, calculation fails [41, 42].

3 Methods and Materials

3.1 Equipment

All the patients in this study have been treated with a Varian TrueBeam™ linac, and the verification of the treatment plans has been performed with this linear accelerator. The type of MLC used was a Varian Millenium 120 MLC.

Figure 13: Varian TrueBeam™ linear accelerator

The Delta^4 phantom (ScandiDos, Uppsala, Sweden), seen in figure 14 (a), is routinely used for verification of VMAT plans at UNN. This phantom consist of 1069 p-type Silicon diode detectors making up a crossed array inside a cylinder of polymethylmethacrylate (PMMA) phantom. There is a computer software, Scandidos Delta^4, associated with the phantom in which the measured dose distribution is compared with the dose distribution calculated by the TPS. In the $6 \cdot 6$ cm central area of the phantom, the diode detectors are placed with 5 mm spacing. In the rest of the phantom, the distance between the diode detectors is 10 mm [45].

An IMRT reinforced thermoplastic Style 27 mask, Type-S™ (Civco Radiotherapy, Iowa, USA), figure 14 (b), was used to immobilize the patients during treatment. Note that this model covers both the head and the shoulders.

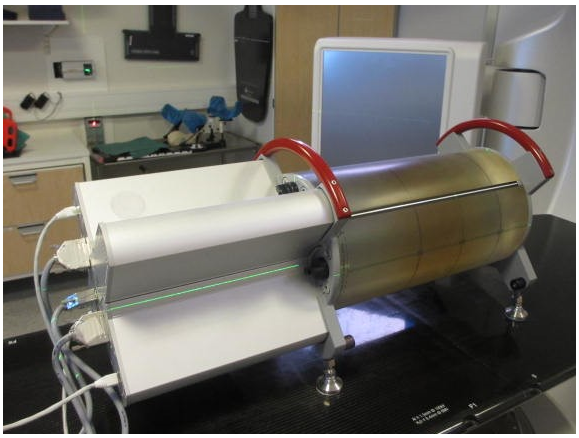

(a) The Delta^4 phantom

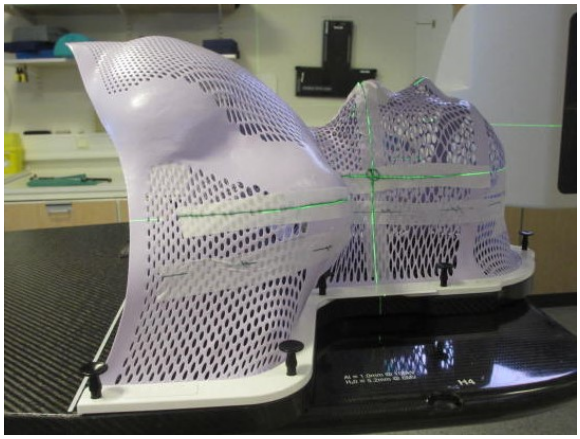

(b) Thermoplastic fixation mask

Figure 14: Equipment

3.2 H&N Radiotherapy Treatment at UNN

The guidelines at UNN for patients with curative H&N cancer undergoing radiotherapy describe that patients with macroscopic disease are prescribed 70 Gy in 35 fractions if treatment is given without chemotherapy. Alternatively can patients receive radiotherapy and chemotherapy at the same time, then 68 Gy is prescribed in 34 fractions. If the patient present with sub-clinical disease, 60 Gy is prescribed in 30 fractions [46]. In all these cases, dose is prescribed in three (or two) different dose levels, this is called the simultaneous integrated boost technique. When radiotherapy is given at the same time as chemotherapy, 68 Gy is prescribed to ITV68, which is the highest dose level. This volume consists of the primary tumor and pathological lymph nodes, GTV-T + GTV-N, see figure 15 and 16 (a)-(f). To the ITV64 intermediate dose level, 64 Gy is prescribed, shown in figure 16 (g), (h) and (i). This volume is made up of CTV64-T and CTV64-N, shown in figure 15 and 16 (a), (b) and (c), which are GTV-T + 10 mm margin and GTV-N + 5 mm margin, respectively. In the lowest dose level which receive 52 Gy, ITV52 is made up of CTV64 + elective lymph node regions, depending on the type of tumor and extent of lymph node metastases, this is shown in figure 15 and 16 (a)-(c) and (j)-(l). Note that all these volumes are modified in the presence of bone, skin and air. Further, PTV52, PTV64 and PTV68/70 are made up of ITV52, ITV64 and ITV68/70 + 5 mm margin, respectively. ITV is cropped to 1-3 mm under the skin, and PTV is cropped to 1 mm under the skin, this is due to the phenomena described in section 2.5.4. For serial OAR, a planning organ at risk volume (PRV) is also generated, this is done by expanding the OAR with 3 mm in all directions, similar to the PTV expansion from ITV [17, 46].

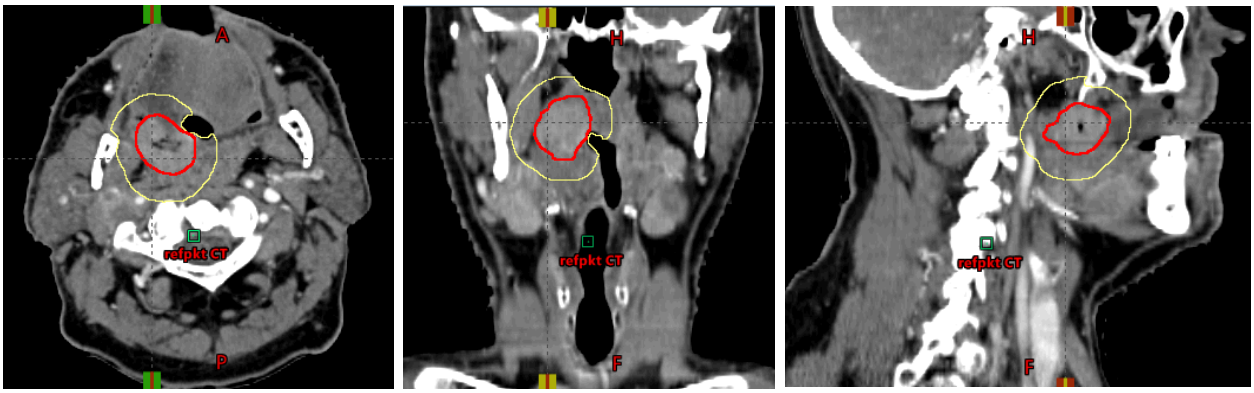

(a) (b) (c)

Figure 15: GTV-T is shown in red and CTV-T is shown in yellow, displayed in three directions.

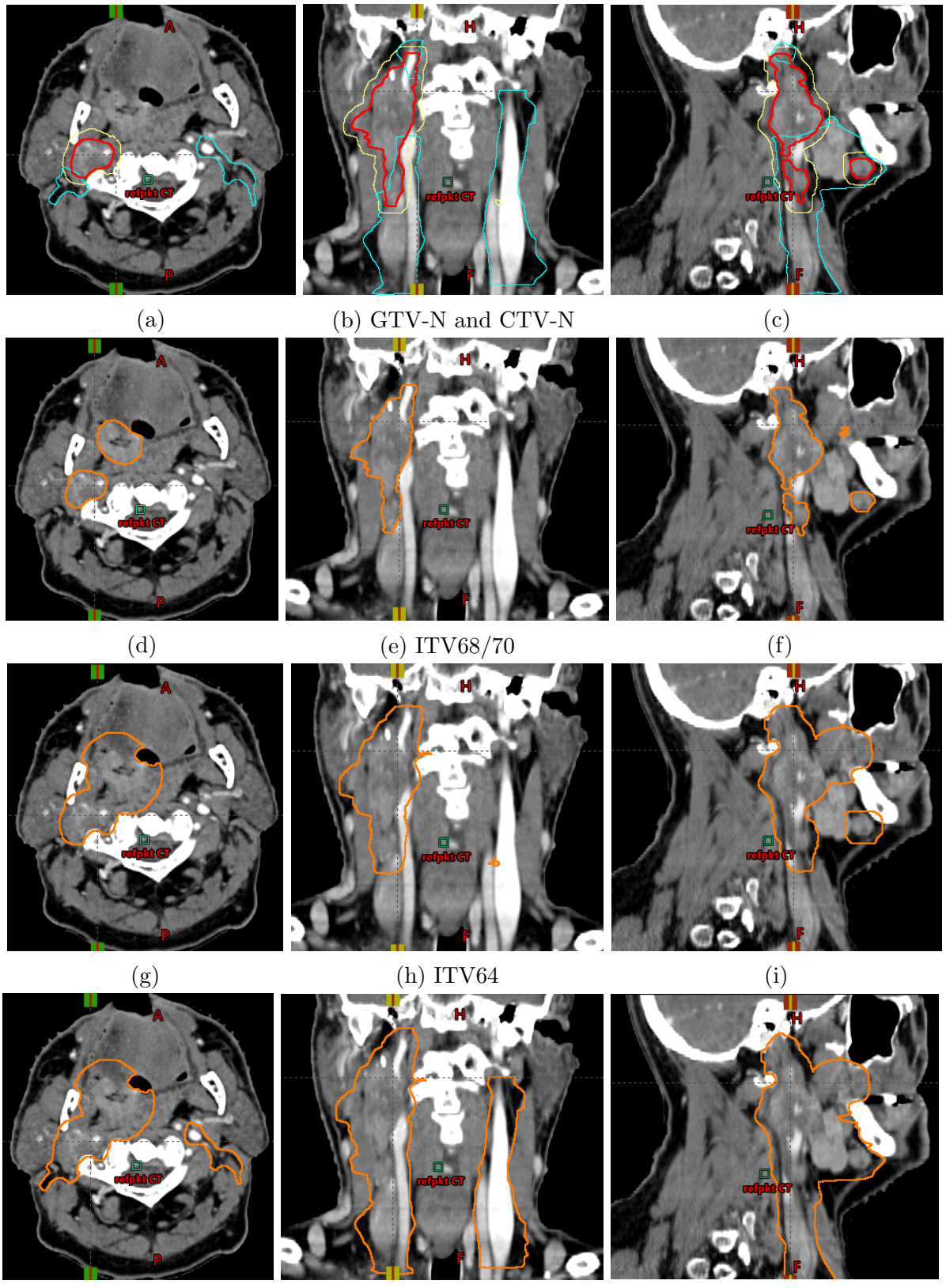

(a) (b) GTV-N and CTV-N (c)

(d) (e) ITV68/70 (f)

(g) (h) ITV64 (i)

(j) (k) ITV52 (l)

Figure 16: GTV-N is shown in red, CTV-N is shown in yellow and CTV with elective lymph nodes are shown in blue in (a), (b) and (c). ITV68 is snown in (d), (e) and (f), further ITV64 is shown in (g), (h) and (i) and ITV52 is shown in (j), (k) and (l), displayed in three directions.

3.2.1 Tolerance Constraints

The tolerance constraints of the OAR and dose requirements for target volumes are presented in table 1.

Table 1: Tolerance constraints for OAR and dose requirements for target volumes.

Priority	Organ/Structure	Constraints	References
2	PTV	$D_{98} \geq 90\%, \geq 95\%$	[28]
2	ITV	$D_{98} \geq 95\%$	[28]
1	Spinal cord	$D_{\max} \leq 50$ Gy	[28]
3	Spinal cord PRV	$D_{\max} \leq 52$ Gy	[28]
4	Parotid gland	$D_{\text{mean}} \leq 26$ Gy	[17],[28],[47]
5	Submandibular gland	$D_{\text{mean}} \leq 39$ Gy	[28]

The only absolute OAR requirement is the maximum dose to spinal cord. This means that achieving this tolerance constraint is more important than getting better dose coverage to the target volume. Note that if the volume of the spinal cord PRV where the dose exceeds 52 Gy is smaller than 0.027 cm^3, the plan is still accepted [17, 28]. For the other OAR, the dose coverage of the target volume is generally more important than meeting the respective OAR tolerance limits.

3.3 Patient Population

The patient population was chosen based on the following criteria: 2 Gy in 34 or 35 fractions, curative intent and bilateral tumor in the neck area. Patients with massive lymph node involvement were excluded. Radiotherapy treatment was prescribed in three dose levels according to the simultaneous integrated boost technique, namely ITV52, ITV64 and ITV68/ITV70. To ITV52, the dose per fraction were 1.53 Gy, to ITV64, the dose per fraction were 1.88 Gy and lastly to ITV68 and ITV70, the dose per fraction were 2 Gy. All the patients except one received chemotherapy and all patients received radiotherapy 6 days a week. The patients were immobilized using an thermoplastic fixation mask covering the head and shoulders, as shown in figure 14 (b). The diagnosis and stage of all the patients are given in table 2, none of the patients had any metastases, therefore they were all considered M0.

Table 2: Patient Characteristics

Patient	Tumor site	Stage
1	Supraglottis	T2N0
2	Tonsile	T2N0
3	Tonsile	T3N2
4	Tonsile	T2N2
5	Tonsile	T2N2
6	Hypopharynx	T4aN1
7	Tonsile	T4N2
8	Tonsile	T2N0
9	Tonsile	T3N1
10	Base of tongue	T1N1
11	Oropharynx	T2N2a
12	Base of tongue	T3N0
13	Tonsile	T4aN0
14	Base of tongue	T3N2
15	Oropharynx	T4N2

3.4 Optimization

3.4.1 Progressive Resolution Optimizer Algorithm

The progressive resolution optimizer (PRO) is the algorithm used in the optimization process, and not for the final dose calculation. The PRO algorithm generates VMAT plans based on dose-volume objectives, and where dynamic MLC, variable dose rate and variable gantry speed is applied. In the PRO algorithm, dose is calculated using a fast so-called dose multi-resolution dose calculation (MRDC), for each segment. This is a pencil beam algorithm and is not as accurate as the final dose calculation algorithm, for example AAA [30, 48].

An objective function is used to optimize the plan and evaluate its quality. This objective function is a sum of the dose-volume and other used-defined objectives. A 178 CPs, defining MLC leaf positions and MU per degree as a function of gantry angle, is optimized in all four optimizing phases. The dose calculation is progressive and performed in coarse sectors of about 18° in the first phase, up to about 2° much finer resolution in the forth phase. A trial fluence is created within a sector, optimized using all the present CPs. In each iteration, customarily about eight sectors are randomly chosen and optimized in parallel. An optimal fluence is calculated for each sector, from the fluence of the leaf sequences retrieved from the previous iteration. Several temporary leaf sequences are generated from these optimal fluences, and the combination that produces the best the objective function is applied for the next iteration [48].

Modeling leaf motion is done by interpolating leaf positions between the CPs. Further, the leaf tongues are modeled by modifying the MLC aperture as described in section 2.9, to take the tongue-and-groove effect into account.

Information is transferred to the linear accelerator and the machine control system establishes the modulation of the dose rate and gantry speed for the delivery of the plan. In the TPS, when the dose is calculated, an estimate of the dose rate and gantry speed is displayed. Note that this information is not sent to the treatment machine [30].

3.4.2 Intermediate Dose

In Eclipse^{TM}, when continuing an optimization, the dose which have already been calculated, can be used as an intermediate dose. This can be done either by selecting the "Use the current plan dose as an intermediate dose for optimization" or by selecting the "Automatic intermediate dose" when optimizing the first time. The optimization algorithm can amongst others adjust the leaf sequences for VMAT fields based on this intermediate dose. When the first round of optimization has ended, the error between the result and the dose calculation is calculated. Further, during the second round of optimization, when the optimization is finished, the differences are compensated for, trying to get better agreement [30].

3.5 Plan Uncertainty and the Width of Uncertainty Plots

A new function has been implemented in Eclipse^{TM} version 13, in which isocenter shifts can be simulated. The plan uncertainty function has been used by Stroom *et al.* [49] to evaluate uncertainties in positioning. Here, isocenter shifts of ± 0.5, ± 1, ± 1.5, ± 2 and ± 3 mm were applied along the ML-, CC- and AP-direction.

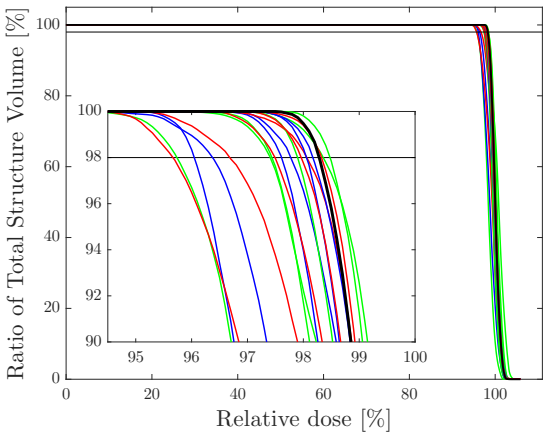

Figure 17: DVH describing the dose coverage of patient 1 in the original plan. The unperturbed plan is shown in black and the uncertainty plans in the ML-direction is shown in red, CC-direction in blue and AP-direction in green.

In several articles by Liu *et al.* [50, 51, 52, 53], three methods for quantification of robustness has been described. One of these involved finding the width of a so-called dose-volume histogram band (DVHB), which can be explained as the envelope of DVH uncertainty dose distributions. Further, the second method is the worst case analysis, in which the highest and lowest dose values in each voxel from unperturbed and perturbed dose distributions formed a similar DVH band. Also in this method the width of the DVH band was found.

Inspired by these two methods for quantifying robustness, a similar method was used in

this thesis. The width at D_{98}, meaning the difference between the furthest right plan and the furthest left plan at D_{98} was calculated. There will always be uncertainties in radiotherapy, e.g. in patient positioning, in the treatment beam and in the contouring of the target volumes and OAR. A robust plan is a plan in which the patient receives a equally good plan even in the presence of a few mm shift. A narrow width suggest a more robust plan and a broad width suggest a less robust plan. A DVH of patient 1 with all the uncertainty plans is shown in figure 17 to illustrate the concept.

3.6 Optimization Methods

As a preparation for all the analyses which was performed, all the patients were exported from the Eclipse™ TPS version 10, anonymized and imported into a test box, with the Eclipse™ version 13 installed. The dose plans were recalculated with this new version. The DVHs of the original plan and the modified plans, which are described in sections 3.6.1 and 3.6.2, were all exported as text files. Further, MATLAB® (Version 2016a, The MathWorks®, Inc., Natick, Massachusetts, USA) was used to plot graphs and calculate p-values using Wilcoxon signed rank test described in section 3.7.2, in addition medians, ranges and the conformity and homogeneity indices described in section 3.7.3 were calculated. Lastly, verification plans were made for the original and the modified plans and tested using the Delta^4 phantom.

3.6.1 Optimizing With/Without Bolus

The current practice at UNN is that during treatment planning, if the CTV is situated so close to the skin that a part of the PTV extend into air, the PTV is cropped to 1 mm inside the body structure, see section 3.2. An alternative to this procedure is to add a virtual bolus of 5 mm on the skin surface and use a PTV52/PTV64 which is not cropped to the body structure, i.e. ITV52/64 + 5 mm. Using such a virtual bolus is done to overcome the problem described in section 2.5.4. The generation of a bolus is shown in figure 18, as well as an example of the difference between a PTV which is not cropped and a PTV which is cropped to the body structure[10]. The original plans were copied for all the patients, and this alternative procedure was applied. That is, new PTVs were made and boluses were added for optimization and then removed before the final dose calculation.

[10]Two different patients are shown, one in (a) and (b), and a different in (c).

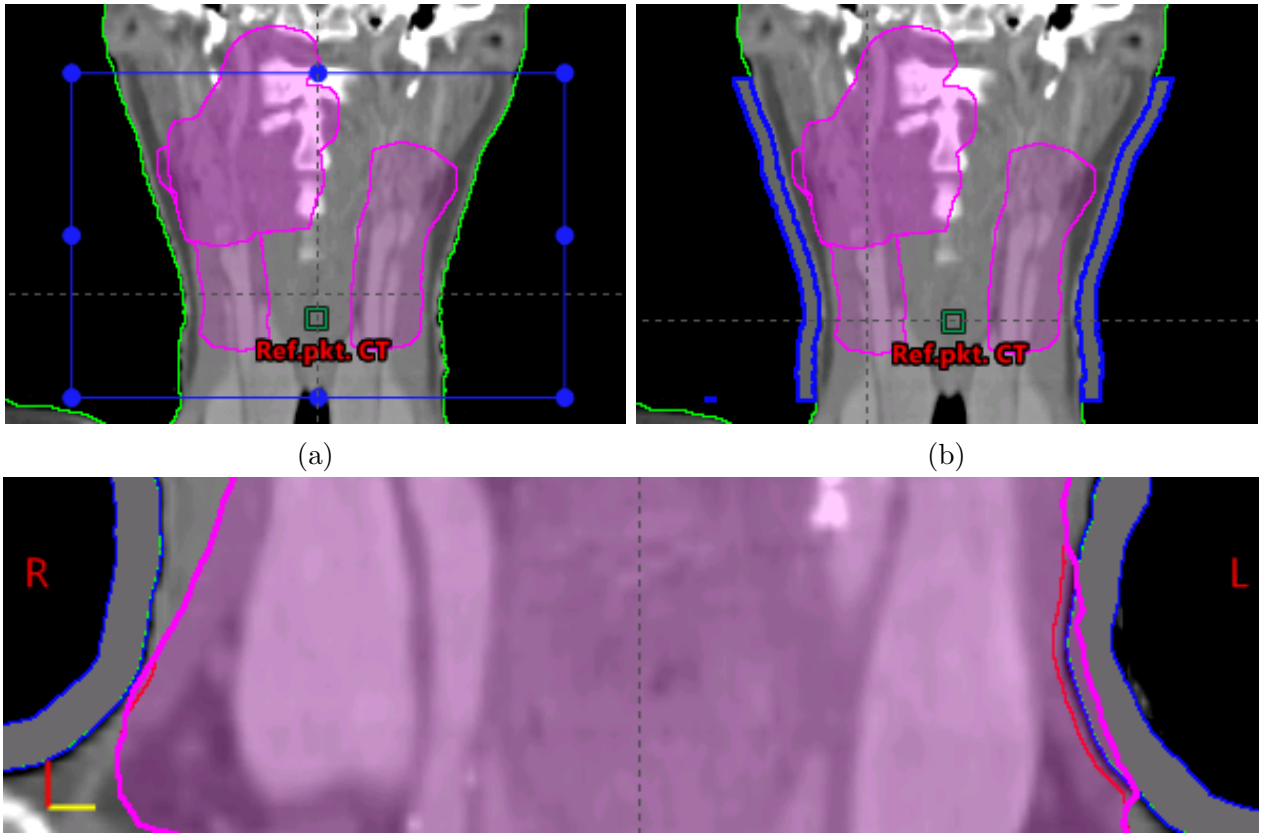

(a) (b)

(c)

Figure 18: Before bolus is generated in (a) and after in (b). PTV which is cropped to 1 mm inside the body structure in red and the new PTV which is not cropped to the body structure shown in pink, in (c).

Using the plan uncertainty tool, quite small isocenter shifts of ±1 mm and ±2 mm and larger isocenter shifts equal to the ITV to PTV margin, ±5 mm were applied to one direction at the time, in the ML-, CC- and the AP-direction. In total, 18 new plans were calculated for the original plan and for the plan which was optimized with bolus, for all the 15 patients. The width at D_{98} for ITV52, ITV64 and ITV68 was calculated for the original plan and the plan which was optimized with bolus. Further, for the OAR, the width at D_{max} of spinal cord and spinal cord PRV, and the width at D_{mean} of the right and left parotid gland and right and left submandibular gland have been found in the same way.

3.6.2 Simultaneous, Sequential and Intermediate Optimization Strategies

The original plan which had been delivered to the patient, was recalculated in the Eclipse™ TPS, version 13, and was used as a base for three different optimization strategies. In this original plan, the radiation therapists performing the planning have changed the objectives and optimized several times trying to get the best dose coverage for the target volumes at the same time as trying to minimize the dose to the OAR. It should be noted that all

radiation therapists have their own strategy when it comes to optimization, and reaching the constraints that are set. Different radiation therapists have been performing the dose planning for the patients in this study, therefore, the way the optimization is done varies between the patients. The optimization objectives that were used, are listed in appendix A.5. The simultaneous and sequential methods were used in the master thesis by Hægeland [8].

In the simultaneous optimization method, the original plan with the same objectives as was originally used, was optimized and dose was calculated three times.

For the sequential optimization strategy, first only the objectives for the target volumes, i.e. ITV and PTV, was used for optimization and dose calculation. Further, the second and third time the optimization and dose calculation was performed, all the original objectives was used, i.e. the objectives for OAR and helping structures was also included.

Lastly, for the intermediate calculation method, almost in the same way as for the sequential calculation method, in the first round of optimization, only the objectives for the target volumes, was used. In addition, the "intermediate calculation" function was used, in which an intermediate calculation started during the optimization, i.e. no "normal" dose calculation was performed before the second optimization. For the second optimization, the rest of the objectives from the original plan was also used, which was objectives for OAR and helping structures. After the second optimization, first an intermediate dose calculation and then a final dose calculation was performed.

3.6.3 With/Without Fixation Mask

Patients with H&N cancer are immobilized with a fixation mask during the CT scans and treatment delivery and this mask appears at the CT images used for treatment planning. The recalculated dose plans were copied with fixed MU and the body structure was modified to include the mask in one copy and to not include the mask in the other copy, shown in figure 19. Currently in the clinic, this mask is sometimes included in the body contour and sometimes not, depending on the person performing the planning. An investigation was done to find the dosimetric difference between including the fixation mask in the body contour, or not.

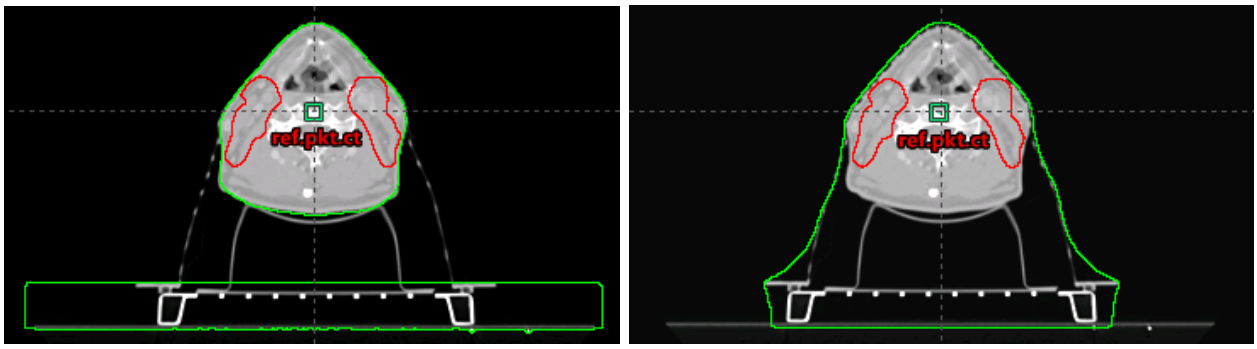

(a) Without fixation mask (b) With fixation mask

Figure 19

3.7 Statistics

3.7.1 Box plots

The red line inside the box represent the median of the sample and if the median is not located at the center of the box, this shows skewness of the sample. The top of the box is the 75th percentile and the bottom of the box represent the 25th percentile, of the sample. The length of the box is called the interquartile range, and represent the middle 50% of the observations. The whiskers are shown as black dashed lines and they are drawn from the interquartile range box and they reach all the values outside this range up to where values are considered as outliers. Outliers are observations more than 1.5 times the interquartile range, and are displayed with a red plus sign [54].

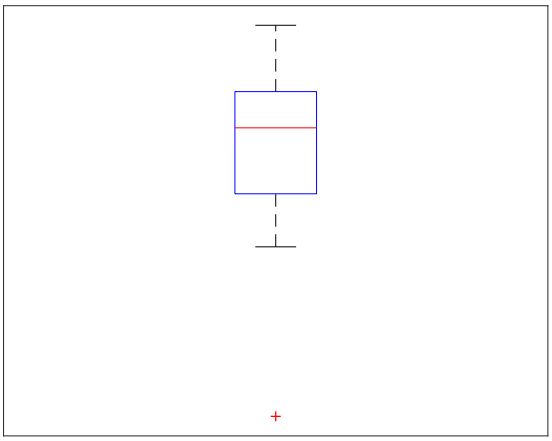

Figure 20: General box plot

3.7.2 Wilcoxon Signed Rank Test

The Wilcoxon signed rank test was applied to test whether there was a statistically significant difference between relevant parameters in the original plan and the other plans. The Wilcoxon signed rank test is a so-called nonparametric rank test, which do not require a specific distribution, e.g. a normal distribution of the data, to calculate a p-value. This is one of the reasons why it was chosen, since normally distributed data could not be assumed

with only 15 patients. Further, the samples are assumed to be dependent observations and independently drawn and finally that it is possible to compare the two values of a pair. The null hypothesis H_0 is that $\theta = 0$, meaning that there is no statistical difference in the median, θ, of the two samples. The alternative hypothesis H_A, is $\theta > 0$, meaning that there is a statistical difference in the median of the two samples, at a chosen significance level of 5%. The test is performed by subtracting one of the samples from the other, then assigning a rank to the absolute value of these values obtained. This is done by starting with the pair with the smallest difference, and then assigning ranks to the rest of the pairs in ascending order. Further, the negative differences are given a negative sign, and the positive and negative ranks are summed individually. The null hypothesis is rejected if the smallest value of these two, W_{observed} is less than or equal to a tabulated critical value W_{critical}. The p-value is defined as the probability that $W_{\text{critical}} > W_{\text{observed}}$, given that the null hypothesis is true, and it is a number between 0 and 1. Therefore, if the p-value is small, it is an indication that the null hypothesis is unlikely to be true [55, 56, 57, 58, 59].

3.7.3 Conformity and Homogeneity Indices

The conformity index (CI) describes how well the dose distribution is conformed to the size and shape of the target. It is given by,

$$CI = \frac{TV_{95\%}^2}{TV \cdot V_{95\%}}. \tag{26}$$

Here, $TV_{95\%}$ is the volume of the target covered by the 95% isodose, TV is the target volume and $V_{95\%}$ is the total volume covered by the 95% isodose. A value of 1 corresponds to a perfectly conformal plan. Several versions of the conformity index is used in the literature, but this CI includes both a over treatment ratio, $\frac{TV_{95\%}}{V_{95\%}}$, and a under treatment ratio, $\frac{TV_{95\%}}{TV}$ [60, 61].

The homogeneity index (HI) describes dose homogeneity of the target and is given by,

$$HI = \frac{D_2 - D_{98}}{D_{\text{median}}}, \tag{27}$$

where a value of 0 would mean perfect homogeneity inside the target volume [60].

3.7.4 Robustness Index

The robustness index (RI) was proposed in the master's thesis, "Optimization and verification of dosimetric robustness of VMAT dose-plans", by Hægeland [8]. It describes the

complexity of VMAT treatment plans; fewer MUs, fewer flanks, fewer islands, slow speed, smaller field size and larger opening are indicators of a simpler and more robust plan, i.e. a low RI suggest a more robust plan against external influences, and a high RI suggest a less robust plan. The robustness index is given by

$$RI = \frac{\text{Flank} \cdot \text{Speed} \cdot \text{Island} \cdot \text{Field size} \cdot \text{MU}}{\text{Opening}^2 \cdot 10^6}, \tag{28}$$

note that it has been slightly modified since the master's thesis was written, in cooperation with the author. The scripts calculating the terms of this index is given in the appendix A.7, and has been rewritten and adapted for the Eclipse$^{\text{TM}}$ TPS by Hægeland. A flank is when the long-side of a MLC leaf is exposed to an open field, see the horizontal red lines in figure 21. The tongue-and-groove effect makes a contribution to the total dose, especially in the presence of such flanks, which are often present when there are many islands in a plan. The speed is defined as the distance a MLC leaf, marked in dark grey, travels between two segments/control points, the first segment is seen in figure 21 (a) and the second segment is seen in (b). A high speed is unwanted, as this might affect the accuracy of MLC motion. The speed is seen is relation to the opening as a high speed might lead to a delay in the rearmost leaf bank, which would lead to a larger opening. Further, an island is a MLC opening surrounded by MLC leaves. Note that one pair of leaves has to be closed to make two islands, it can be seen that figures 21 (a) and (b) contain 3 islands each. The field size is simply the size of the total field limited by the X and Y-jaws, without the MLC leaves and MU is the total number of MUs in a plan. Finally, the MLC opening is the distance between two opposite leaves. The MLC flank has to be seen in relation to the opening, as the flank will have a relative bigger influence on the dose for a small opening [8].

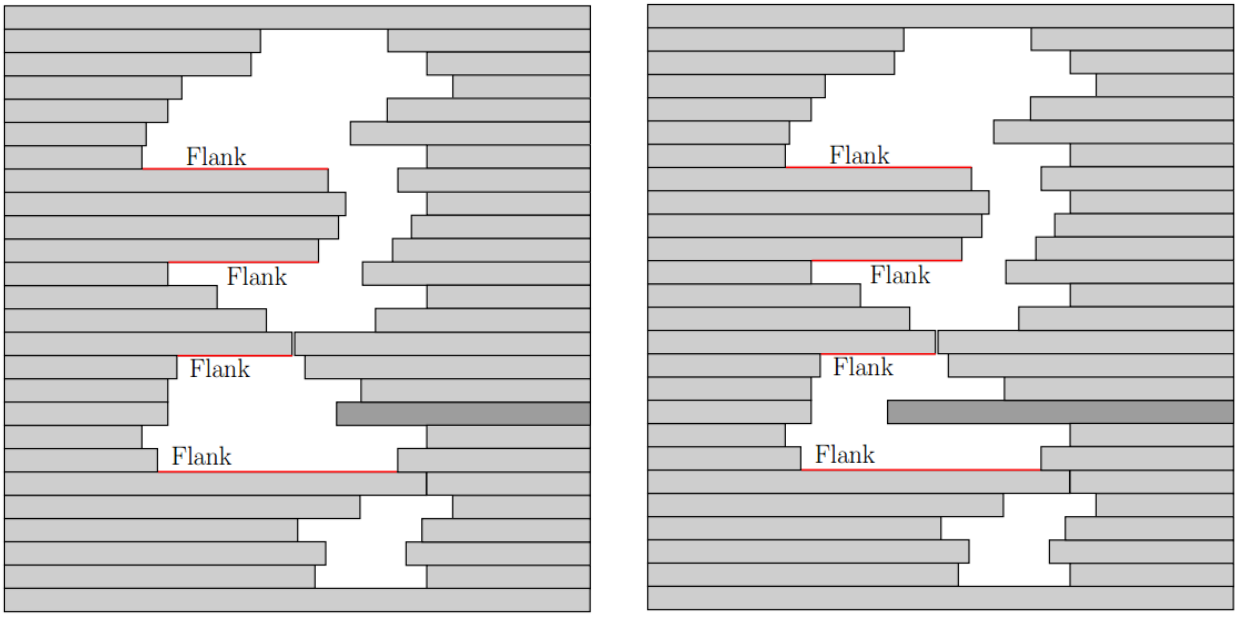

(a) (b)

Figure 21: Field opening of the MLC leaves. Some of the MLC flanks are marked as horizontal red lines, the speed is defined as the distance a MLC leaf moves between two subsequent segments, shown in dark grey, and there are three islands present in both (a) and (b).

4 Results

4.1 Optimizing With/Without Bolus

Original VMAT plans from 15 patients were compared to alternative plans optimized with a virtual bolus. These two plans were compared in terms of dose coverage, D_{98}, of the ITV52, ITV64, ITV68/70, PTV52, PTV64 and PTV68/70 volumes. In addition, $D_{\max}$ of spinal cord and spinal cord PRV and finally D_{mean} of the parotid glands and the submandibular glands, were compared. The CI and HI of PTV52, PTV64 and PTV68/70 were calculated, and the RI and γ index was plotted, for the two plans. Furthermore, uncertainty plans of ± 1 mm, ± 2 mm and ± 5 mm isocenter shifts, in the ML-,CC- and AP-directions were plotted, along with the unperturbed plans, i.e. the original plan and the plan which was optimized with bolus. The widths of these uncertainty plans were plotted and the medians and ranges were calculated. Note that the PTVs were not included in this comparison as the PTV according to definition, in section 2.2, is present to account for set up uncertainties, and it was exactly the set up uncertainties that was the subject here.

4.1.1 Dose-Volume Parameters

The D_{98} of ITV52, ITV64 and ITV68/70 in the original plan and the plan which was optimized with bolus was compared in figure 22 (a). For ITV52, the median dose was slightly larger, and the range of values was wider in the original plan than in the plan which was optimized with bolus. In the same figure, D_{98} of the ITV64 was generally higher for the plan which was optimized with bolus, but the median was still about the same as in the original plan. For this volume, all values were above the 95% limit for both plans. Further, the median of D_{98} in the ITV68/70 was higher in the plan which was optimized with bolus, in addition to the range of values being smaller.

For PTV52 in figure 22 (b), the median was above the 95% constraint in the original plan. In the plan which was optimized with bolus, the range of values was very large, however, the median was close to the 95% limit. Oppositely, for PTV64, the values of D_{98} were generally higher in the plan which was optimized with bolus, and the range of values was narrower. Lastly, for PTV68/70, the median was slightly higher for the plan which was optimized with bolus and the range of values of the two plans were almost the same.

Maximum dose of the spinal cord is displayed in figure 22 (c). The maximum dose of both the original plan and the plan which was optimized with bolus was below the absolute tolerance limit of 50 Gy. The median was lower in the plan which was optimized with bolus, but the range of values was larger than in the original plan. For the spinal cord PRV, some

values were above the constraint of 52 Gy for both plans. Also here, the median was lower in the plan which was optimized with bolus.

Mean doses of the right and left parotid gland was similarly compared in 22 (d). Clearly, the mean dose was lower in the original plan, and the range of values was much narrower. The dose was generally lower in the left parotid gland compared to the right.

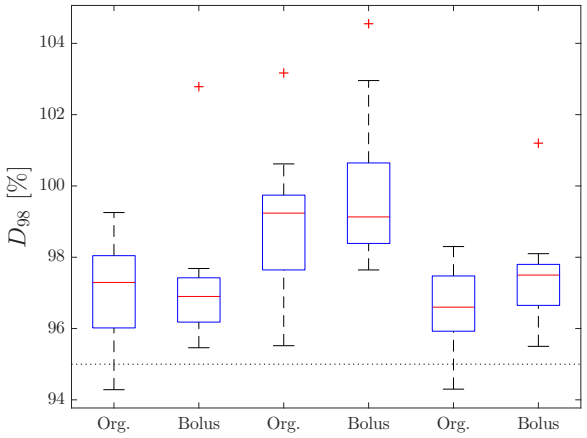

(a) ITV52 (1,2), ITV64 (3,4) and ITV68/70 (5,6)

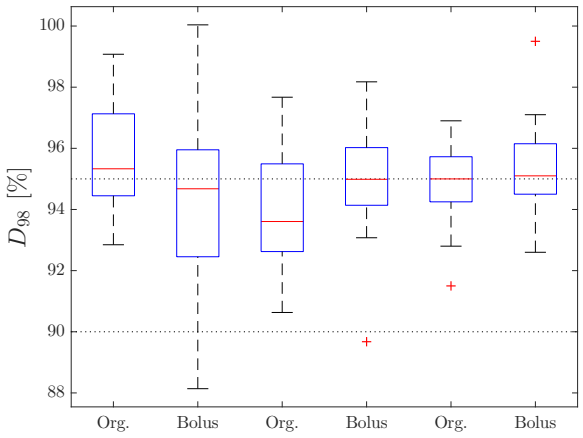

(b) PTV52 (1,2), PTV64(3,4), PTV68/70(5,6)

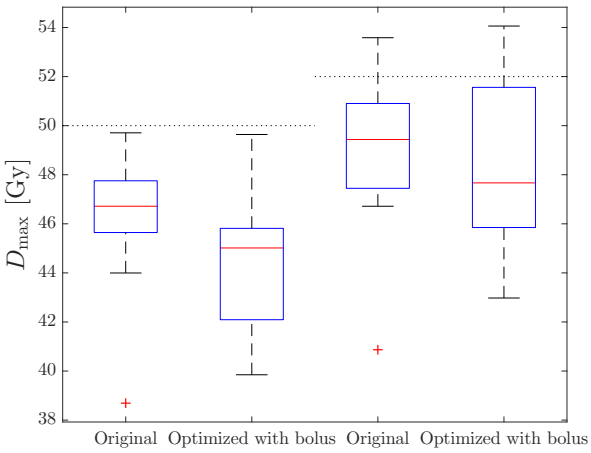

(c) Spinal cord (1,2) and spinal cord PRV (3,4)

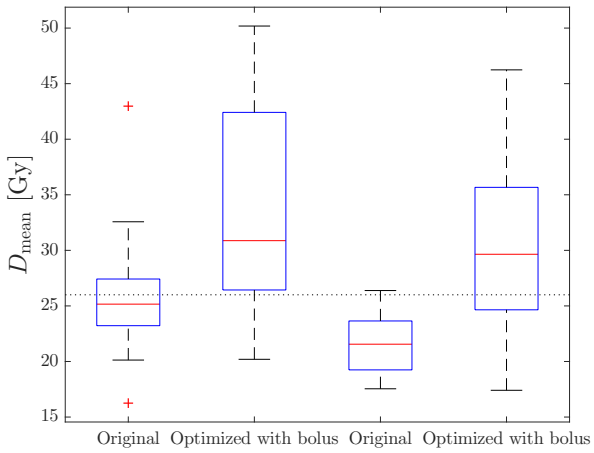

(d) Right (1,2) and left (3,4) parotid gland

Figure 22: D_{98} of ITV52, ITV64, ITV68/70, PTV52, PTV64 and PTV68/70, $D_{\max}$ of spinal cord and spinal cord PRV and D_{mean} of right and left parotid gland. The black dotted lines represent the respective tolerance constraints.

A comparison of the mean dose of the right and left submandibular gland is displayed in figure 23 (a). For the right submandibular gland, the median was about the same in the original plan and the plan which was optimized with bolus. The median dose was lower for the left submandibular gland than for the right, for both plans. Further, more patients have

lower mean doses in the original plan, as the 25th percentile was lower, this was the case for both glands.

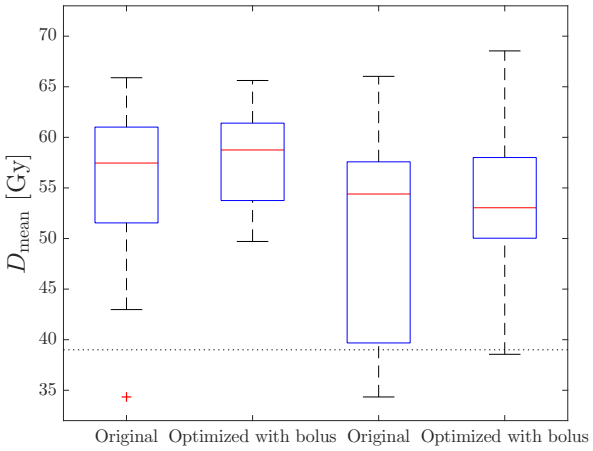

Right (1,2) and left (3,4) submand. gland.

Figure 23: D_{mean} of left and right submandibular gland. The black dotted line represent the tolerance constraint.

The p-values for all important parameters are listed in table 3, values below 0.05 means that the corresponding parameter was significantly different in the two plans. It can be seen that D_{98} of PTV52 and PTV64, D_{max} of the spinal cord and D_{mean} of the parotid and submandibular glands all have p-values below 0.05.

Table 3: p-values found using Wilcoxon signed rank test, comparing the original plan and the plan which was optimized with bolus.

	p-value
D_{98} of ITV52 [%]	0.628
D_{98} of ITV64 [%]	0.184
D_{98} of ITV68/70 [%]	0.056
D_{98} of PTV52 [%]	0.028
D_{98} of PTV64 [%]	0.032
D_{98} of PTV68/70 [%]	0.316
D_{max} of spinal cord [Gy]	0.016
D_{max} of spinal cord PRV [Gy]	0.229
D_{mean} of right parotid gland [Gy]	0.005
D_{mean} of left parotid gland [Gy]	0.002
D_{mean} of right submandibular gland [Gy]	0.040
D_{mean} of left submandibular gland [Gy]	0.011

4.1.2 Conformity and Homogeneity Indices

The CI and HI was computed for PTV52, PTV64 and PTV68/70 in the original plan and plan which was optimized with bolus. These structures were evaluated because it was the

conformity and homogeneity of the PTV that was of interest, clinically. These values, in addition to the p-values of the CI and HI for each of the PTVs is given in table 4. Recall that CI of 1 and HI of 0 mean perfect conformity and homogeneity, respectively. Note that there was only a statistically significant difference for HI of PTV52 and PTV64.

Table 4: Median conformity index CI and median homogeneity index HI with ranges, as well as p-values found using Wilcoxon signed rank text, for PTV52, PTV64 and PTV68/70 in the original plan and the plan which was optimized with bolus.

	Original		Optimized with bolus		
	Median	Range	Median	Range	p-value
PTV52					
CI	0.61	0.55 - 0.76	0.63	0.51 - 0.74	0.890
HI	0.45	0.35 - 0.51	0.48	0.31 - 0.63	0.004
PTV64					
CI	0.82	0.74 - 0.94	0.84	0.74 - 0.94	0.252
HI	0.16	0.12 - 0.19	0.14	0.11 - 0.20	0.008
PTV68/70					
CI	0.57	0.27 - 0.70	0.59	0.27 - 0.74	0.421
HI	0.08	0.05 - 0.12	0.07	0.05 - 0.10	0.121

4.1.3 Robustness Index

The RI is plotted in figure 24. Remember that a low index suggest a more robust plan. The p-value was determined to be 0.015, meaning the two plans has a significantly different RI.

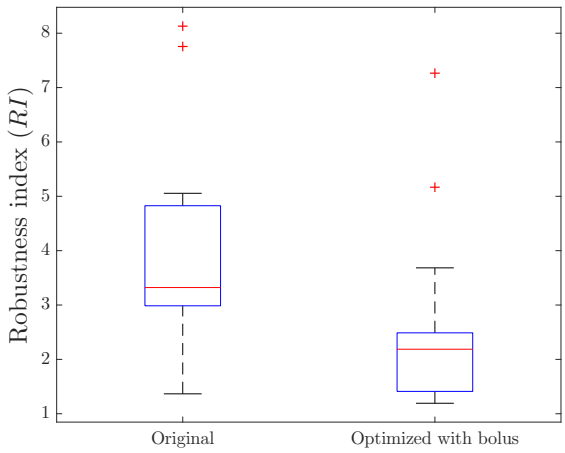

Figure 24: The robustness index is plotted for the original plan and the plan which was optimized with bolus.

4.1.4 γ Index

The global γ index is plotted for the original plan and the plan which was optimized with bolus, in figure 25. The pass-fail criteria was set to DTA = 2 mm and DD = 2%, and 95%

of the measurement points had to pass this criteria. The plan which was optimized with bolus has a higher median γ index and a narrower range of values. However, the p-value was calculated to be 0.318, and thereby, the two plans were not significantly different.

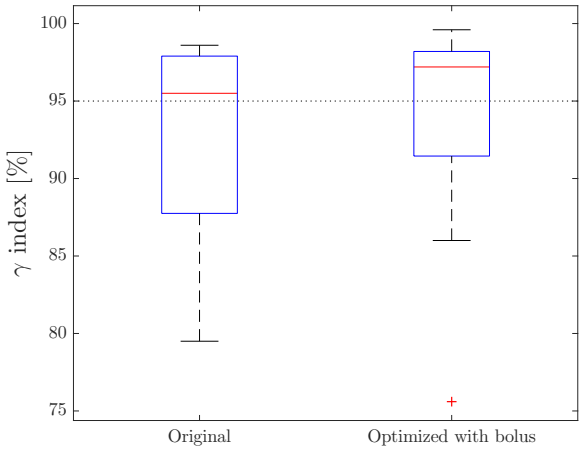

Figure 25: The pass-fail criteria is distance to agreement, DTA = 2 mm and dose difference, DD = 2%. The black dotted line represent the constraint that 95% of the measurement points need to pass the pass-fail criteria for the plan to be approved for treatment delivery.

4.1.5 Plan Uncertainty

Uncertainty plans of ±1 mm, ±2 mm and ±5 mm isocenter shift, in the ML-,CC- and AP-directions are plotted in the following along with the unperturbed plan. The plan uncertainty of D_{98} of ITV52 is plotted in figure 26, for the original plan in (a) and the plan which was optimized with bolus in (b). For patient 2 the value of D_{98} is notably higher in the plan which was optimized with bolus. This is also the case for patient 4, where the values for all the uncertainty plans and the unperturbed plan was above the tolerance constraint of 95%, contrary to in the original plan. On the other side, the values for patient 6, 10, 14 and 15 were slightly higher in the original plan.

For D_{98} of ITV64 in figure 26 (c) and (d), there was a larger spread in the uncertainty plans for ITV64 than there was for ITV52, especially for patient 6, 12 and 14. The same tendencies as for ITV52 was seen for ITV64, that some values were higher and some values were lower in the original plan compared to the plan which was optimized with bolus. In figure 26 (f) for ITV68/70, it can be seen that only patient 3 and 9 has some uncertainty plans with D_{98} under the constraint of 95%, and it was only for isocenter shifts of 5 mm. Contrary, in (e) patients 2, 4, 5, 6, 7, 9, 10 and 15 has some or all of uncertainty plans under the constraint of 95%.

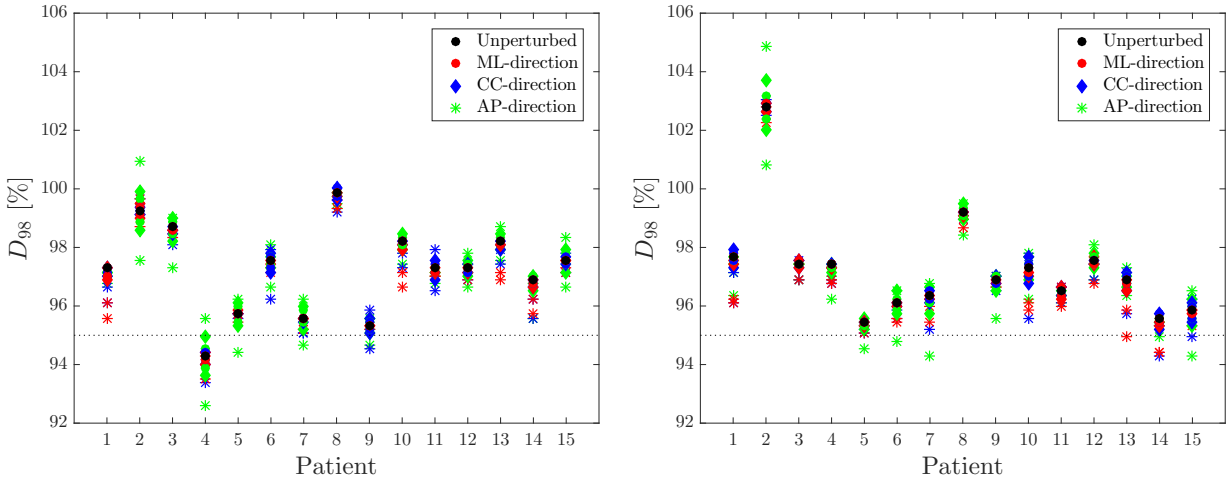

(a) ITV52, Original

(b) ITV52, Optimized with bolus

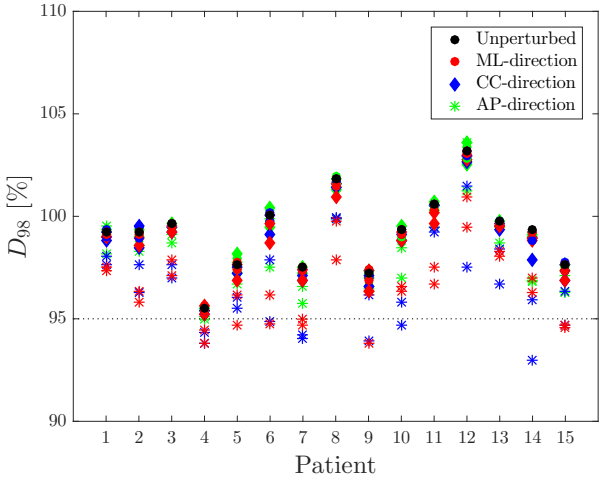

(c) ITV64, Original

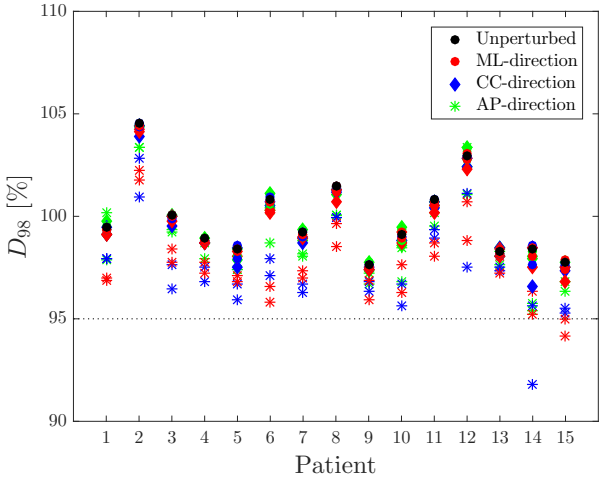

(d) ITV64, Optimized with bolus

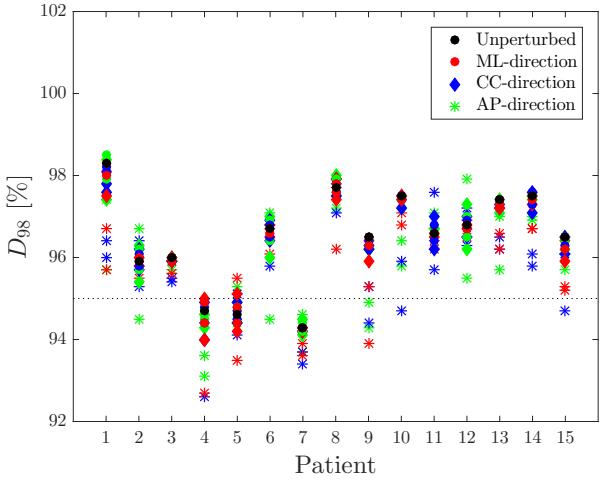

(e) ITV68/70, Original

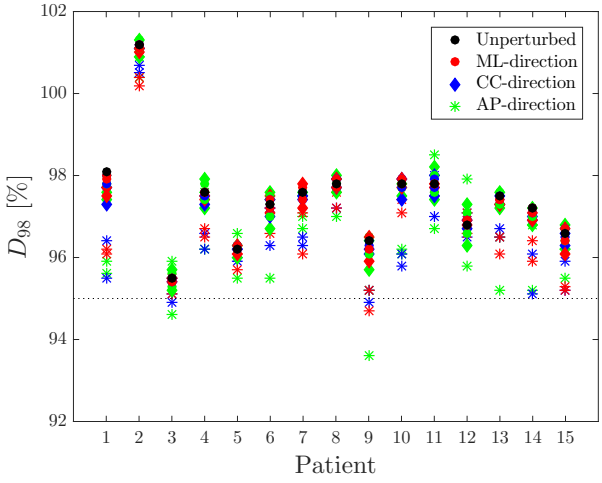

(f) ITV68/70, Optimized with bolus

Figure 26: D_{98} of ITV52, ITV64 and ITV68/70 in the original plan and the plan which was optimized with bolus. The values from the unperturbed plan are displayed as black circles. Further, isocenter shifts of ±1 mm (circles), ±2 mm (diamonds) and ±5 mm (stars), in the ML-direction (red), CC-direction (blue) and AP-direction (green), are plotted. The black dotted lines represent the tolerance constraints.

$D_{\max}$ of spinal cord is plotted in figure 27. It can be seen that all dose maximums in the unperturbed plan was below the absolute constraint of 50 Gy. However for several of the uncertainty plans, especially for 5 mm in the CC-direction (blue stars), the $D_{\max}$ was above this constraint. There was also a difference between the patients in how large the spread of the plans were, e.g. patients 5, 6 and 12 have a small spread, and patients 11, 13 and 15 have a quite large spread. The same tendencies can also be seen for spinal cord PRV, in the same figure. The width was notably larger in the plan which was optimized with bolus compared to the original plan, especially for patient 2, 9, 12 and 13.

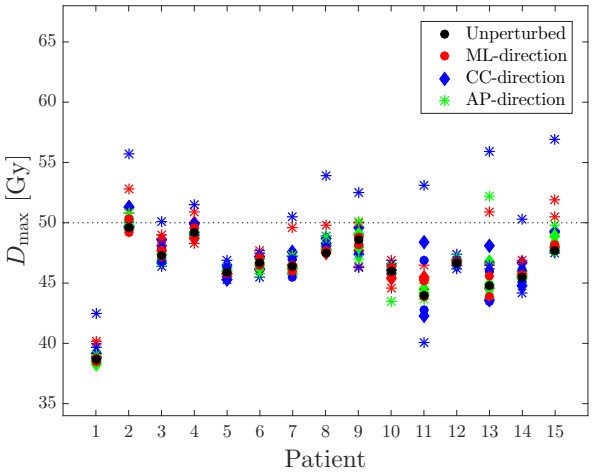

(a) Spinal cord, Original

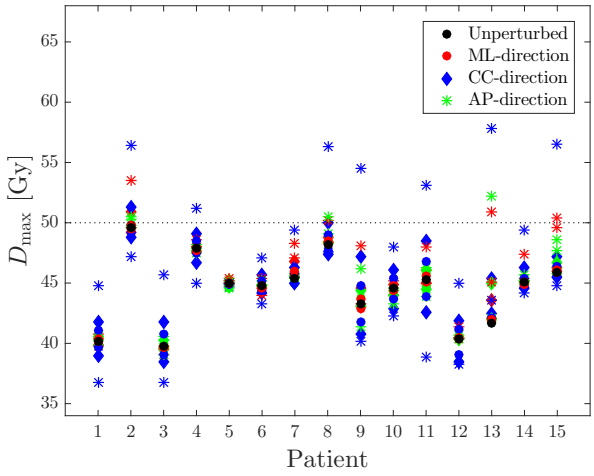

(b) Spinal cord, Optimized with bolus

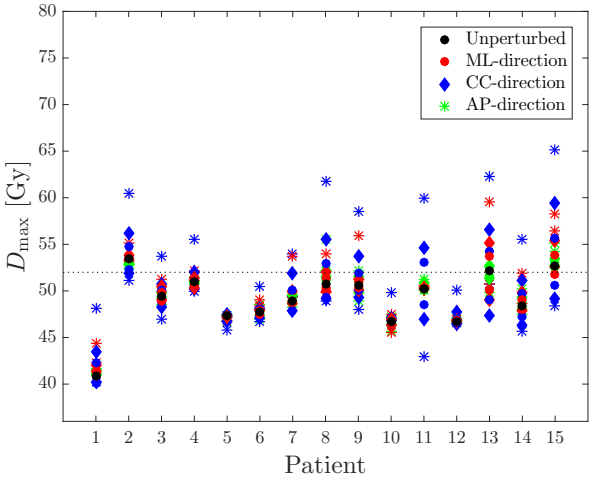

(c) Spinal cord PRV, Original

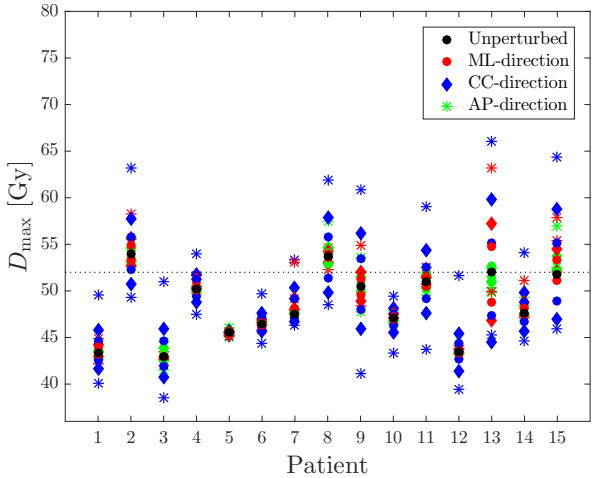

(d) Spinal cord PRV, Optimized with bolus

Figure 27: $D_{\max}$ of the spinal cord and the spinal cord PRV for the original plan and for the plan which was optimized with bolus. The values from the unperturbed plan are displayed as black circles. Further, isocenter shifts of ±1 mm (circles), ±2 mm (diamonds) and ±5 mm (stars), in the ML-direction (red), CC-direction (blue) and AP-direction (green), are plotted. The black dotted lines represent the respective tolerance constraints.

Furthermore, in figure 28, uncertainty plans of the right and left parotid gland are plotted. Clearly, the values in the plan which was optimized with bolus were for most of the patients higher than in the original plan, for both parotid glands. On the other hand, the spread of the plans is larger in the original plan.

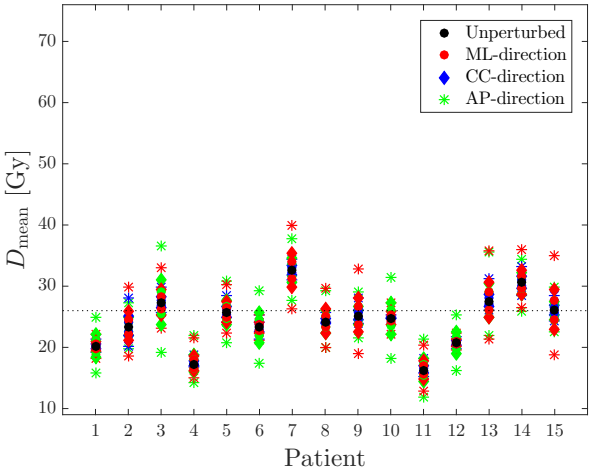

(a) Right parotid gland, Original

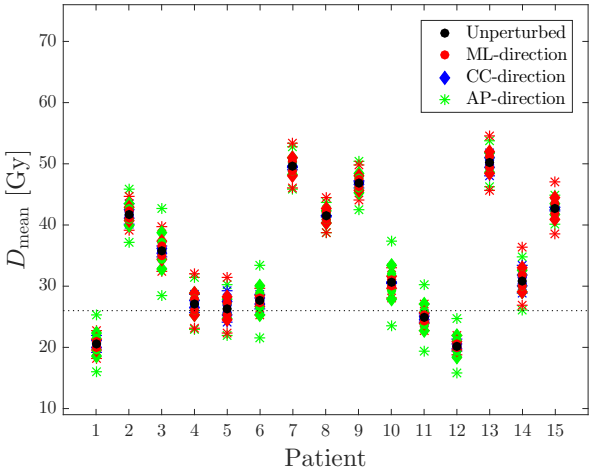

(b) Right parotid gland, Optimized with bolus

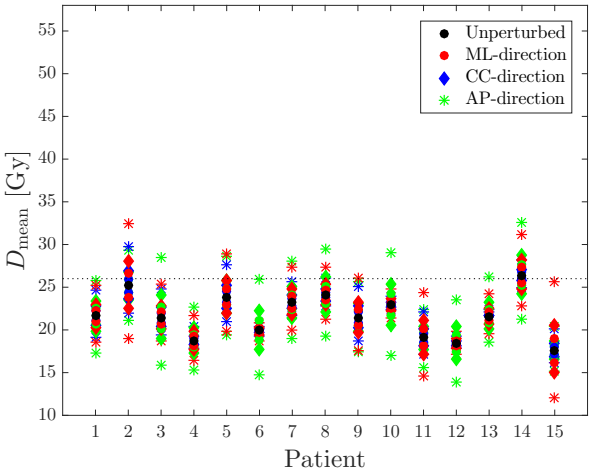

(c) Left parotid gland, Original

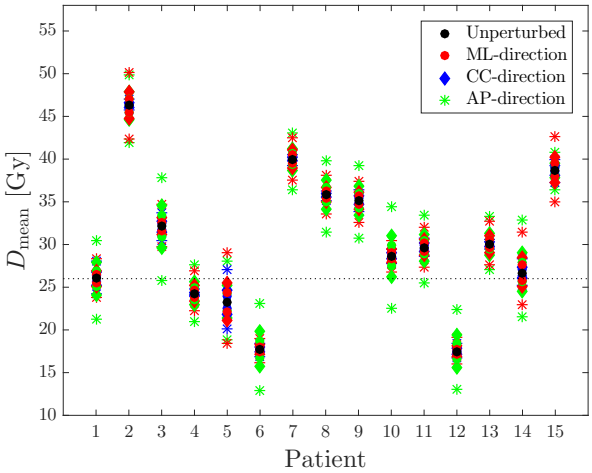

(d) Left parotid gland, Optimized with bolus

Figure 28: D_{mean} of the right and left parotid gland for the original plan and for the plan which was optimized with bolus. The values from the unperturbed plan are displayed as black circles. Further, isocenter shifts of ± 1 mm (circles), ± 2 mm (diamonds) and ± 5 mm (stars), in the ML-direction (red), CC-direction (blue) and AP-direction (green), are plotted. The black dotted lines represent the respective tolerance constraints.

The same tendencies were seen for the submandibular glands in figure 29, more patients have lower doses to these OAR in the original plan compared to the plan which was optimized with bolus.

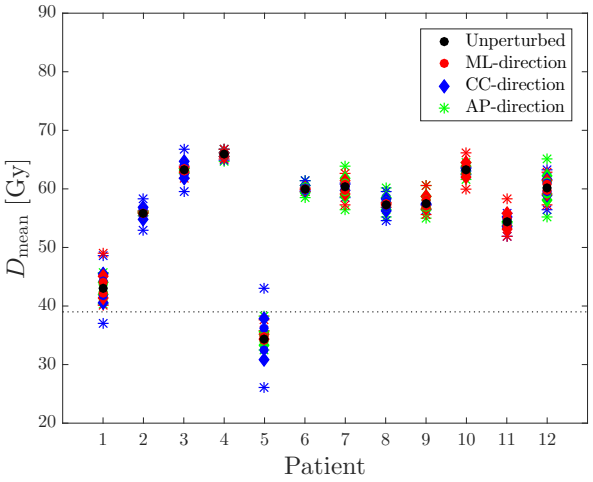

(a) Right submand. gland, Original

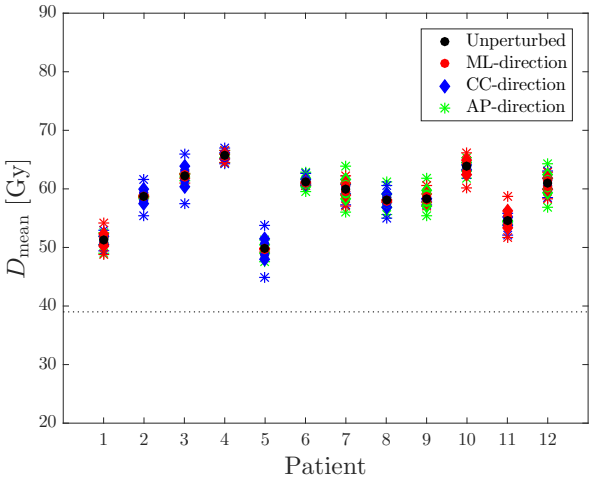

(b) Right submand. gland, Optimized with bolus

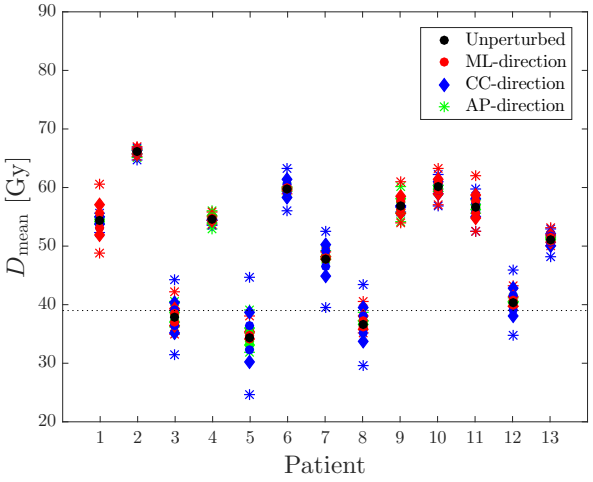

(c) Left submandibular gland, Original

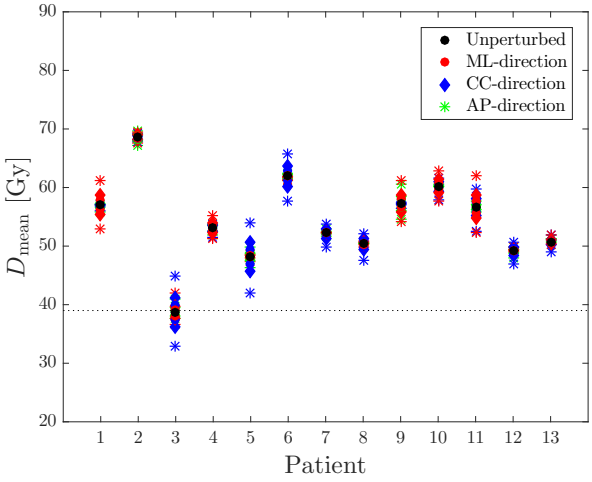

(d) Left submand. gland, Optimized with bolus

Figure 29: D_{mean} of the right and left submandibular gland for the original plan and for the plan which was optimized with bolus. The values from the unperturbed plan are displayed as black circles. Further, isocenter shifts of ±1 mm (circles), ±2 mm (diamonds) and ±5 mm (stars), in the ML-direction (red), CC-direction (blue) and AP-direction (green), are plotted. The black dotted lines represent the tolerance constraints.

In figure 30, the width at D_{98} of ITV52, ITV64 and ITV68/70 was compared for the original plan and plan which was optimized with bolus. Further, the width of D_{max} of spinal cord and spinal cord PRV and D_{mean} of the right and left parotid gland and right and left submandibular gland is plotted in figure 31. Note that this width is visualized in figure 17, in section 3.5, and also as the spread of uncertainty plans described earlier in figures 26 - 29. The median for all the patients in the original plan and plan which was optimized with bolus

Table 5: Median width and ranges of the uncertainty plots of relevant parameters. p-values were calculated using Wilcoxon signed rank test, comparing the widths of the original plan and plan which was optimized with bolus.

	Original		Optimized with bolus		
	Median width	Range	Median width	Range	p-value
D_{98} of ITV52 [%]	1.70	0.81 - 3.40	1.44	0.65 - 4.05	0.938
D_{98} of ITV64 [%]	3.61	1.81 - 6.38	3.29	1.28 - 6.80	0.169
D_{98} of ITV68/70 [%]	2.00	0.60 - 2.80	1.80	1.00 - 2.90	0.284
$D_{\max}$ of spinal cord [Gy]	5.03	1.22 - 13.06	8.02	0.82 - 16.12	< 0.001
$D_{\max}$ of spinal cord PRV [Gy]	7.96	1.63 - 16.93	12.17	0.95 - 21.49	0.004
D_{mean} of right parotid gland [Gy]	11.34	7.64 - 17.37	9.20	5.74 - 14.35	0.041
D_{mean} of left parotid gland [Gy]	9.72	7.45 - 13.66	8.48	6.20 - 12.10	0.007
D_{mean} of right submandibular gland [Gy]	6.27	1.93 - 16.98	6.43	2.71 - 8.83	0.733
D_{mean} of left submandibular gland [Gy]	9.52	2.26 - 20.15	5.24	2.62 - 12.05	0.048

is given in table 5, together with the p-values calculated. The width of $D_{\max}$ of the spinal cord and spinal cord PRV was significantly larger in the plan which was optimized with bolus. The width of D_{mean} of the right parotid gland, left parotid gland and left submandibular gland was significantly larger in the original plan.

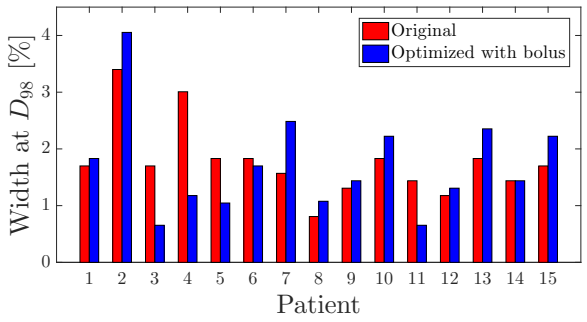

(a) ITV52

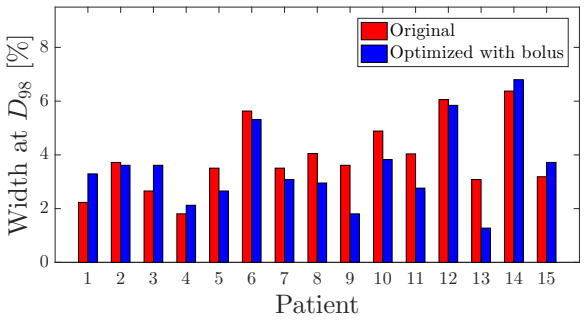

(b) ITV64

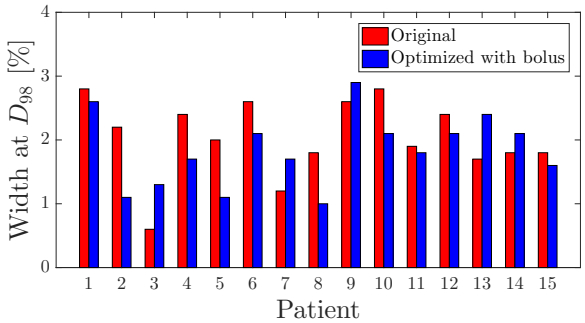

(c) ITV68/70

Figure 30: Width of the uncertainty plots for D_{98} of ITV52, ITV64 and ITV68.

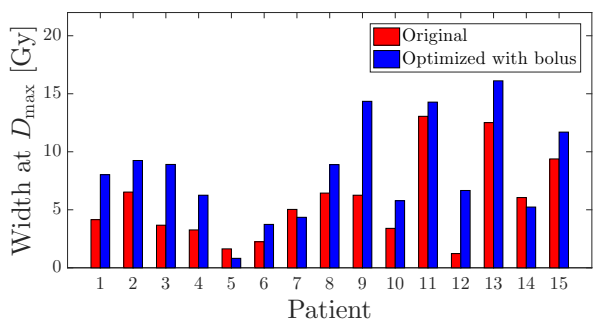

(a) Spinal cord

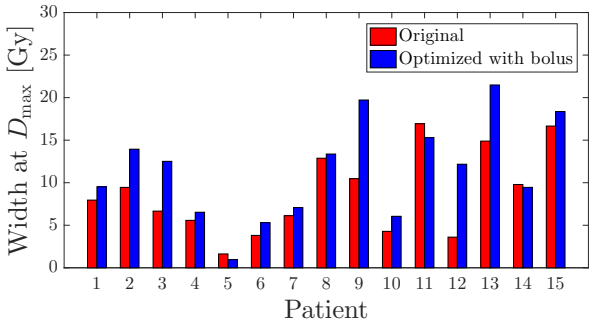

(b) Spinal cord PRV

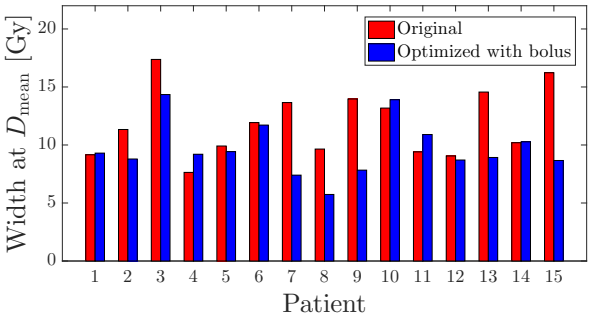

(c) Right parotid gland

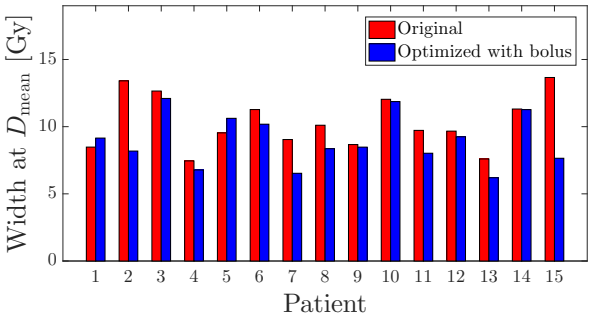

(d) Left parotid gland

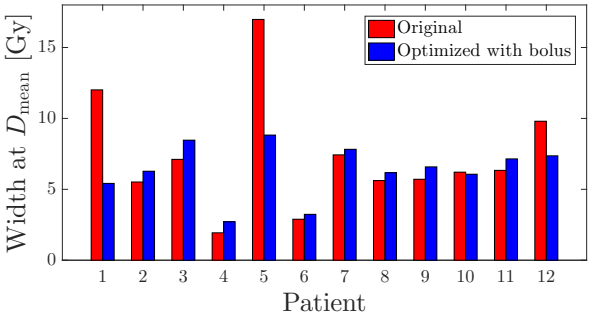

(e) Right submandibular gland

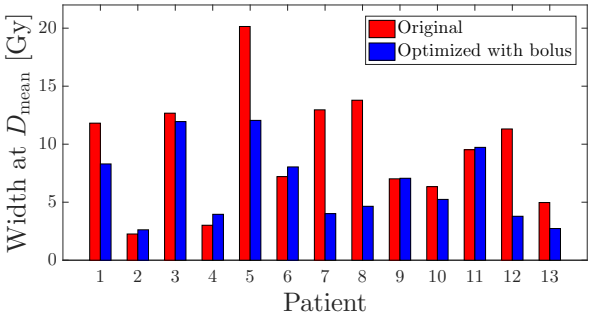

(f) Left submandibular gland

Figure 31: Width of uncertainty plots for $D_{\max}$ of spinal cord and spinal cord PRV and D_{mean} of the right and left parotid gland and the right and left submandibular gland.

4.2 Simultaneous, Sequential and Intermediate Optimization Strategies

VMAT plans with three different optimization strategies; simultaneous, sequential and intermediate, described in section 3.6.2 were compared to the original plan, for all 15 patients. This was done as before, in terms of D_{98} to ITV52, ITV64, ITV68/70, PTV52, PTV64 and PTV68/70, $D_{\max}$ to spinal cord and spinal cord PRV and D_{mean} of both the parotid glands and both the submandibular glands. Further, testing for statistical significance, each of the

three plans were compared to the original plan. CI and HI for PTV52, PTV64 and PTV68 were calculated, the RI and γ index was plotted and the indices were tested for statistical significance.

4.2.1 Dose-Volume Parameters

For D_{98} of ITV52 in figure 32 (a), it can be seen that the simultaneous, sequential and intermediate calculations were all slightly better than the original and above the limit of 95%. The median dose was the highest for the simultaneous optimization method. Further, the median of D_{98} for ITV64 was about the same for all the optimization methods. However, the 25th percentile was at the highest dose in the simultaneous method, suggesting that more patients receive a higher dose to the ITV64 in this plan.

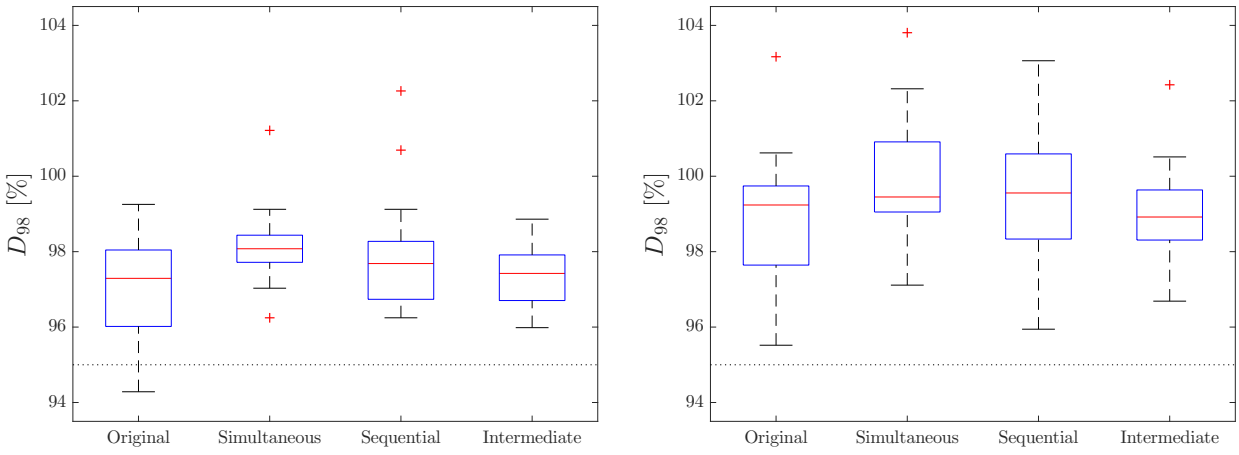

(a) ITV52 (b) ITV64

Figure 32: D_{98} of ITV52 and ITV64. The black dotted lines represent the tolerance constraints.

For D_{98} of the ITV68/70 in 33 (a), the median was lower in the original plan compared to all the other plans. In addition, not all patients have D_{98} above the constraint of 95% in the original plan, there was also an outlier below the constraint in the sequential plan.

D_{98} of PTV52 in the simultaneous plan was for almost the whole population over 95%, and the blue box was the smallest. In the same plot it can also be seen that there was a larger spread in the intermediate and sequential plans, and the dose was not over 95% in all cases. Further, for PTV64 in (c), the median dose was also in this case higher in the simultaneous method. All values were above the 90% limit. In the plot displaying D_{98} of PTV68/70, the 95% limit was on the median in the original plan, and the medians of the other methods were above this limit.

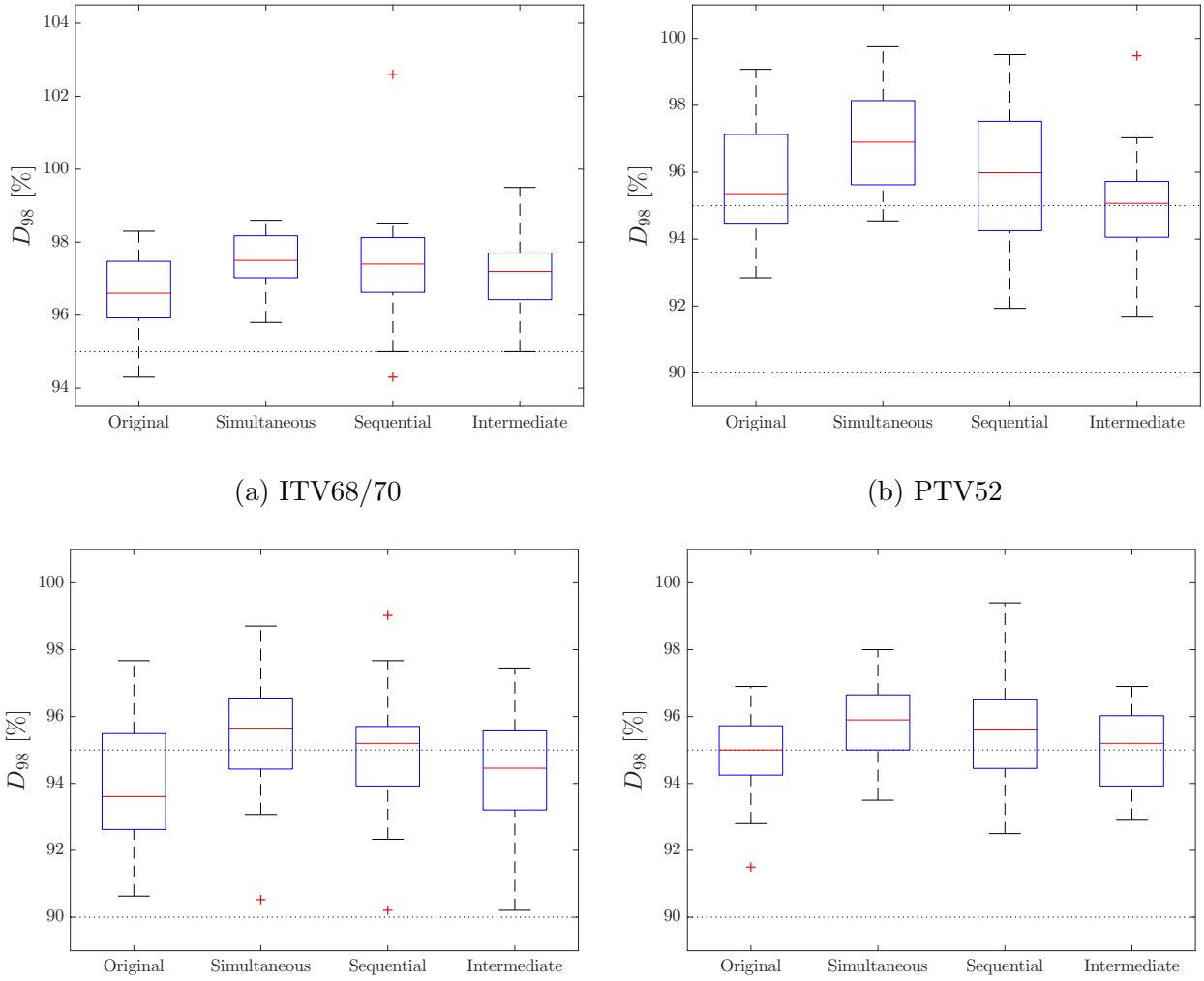

(a) ITV68/70

(b) PTV52

(c) PTV64

(d) PTV68/70

Figure 33: D_{98} of ITV68/70, PTV52, PTV64 and PTV68/70. The black dotted lines represent the respective tolerance constraints.

In figure 34 (a) it can be seen that the absolute limit of the $D_{\max}$ to the spinal cord is only held in the original plan, followed by the simultaneous plan in which one value was above the 50 Gy limit. In the same figure, for spinal cord PRV, none of the methods have all values below the 52 Gy limit, but the simultaneous method was the closest. For the D_{mean} of the right and left parotid gland in figure 34 (b), it was evident that the original plan in both cases generally has the lowest dose, and that the three other methods were quite similar. The mean dose of the right and left submandibular gland in figure 34 (c) was for all the methods, over the limit of 39 Gy, there were only a few of the patients that have doses below this limit in the original plan.

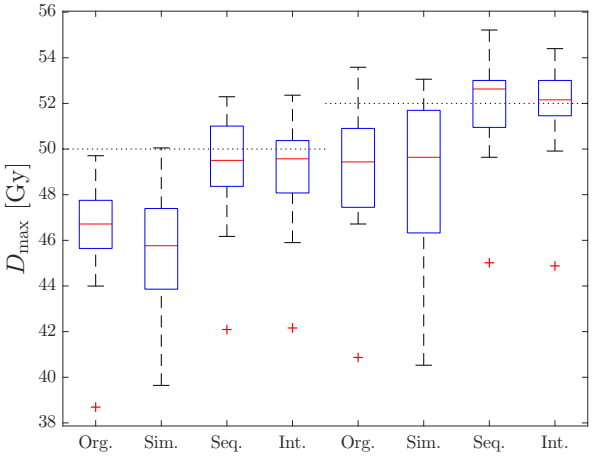

(a) Spinal cord (1-4) and spinal cord PRV (5-8).

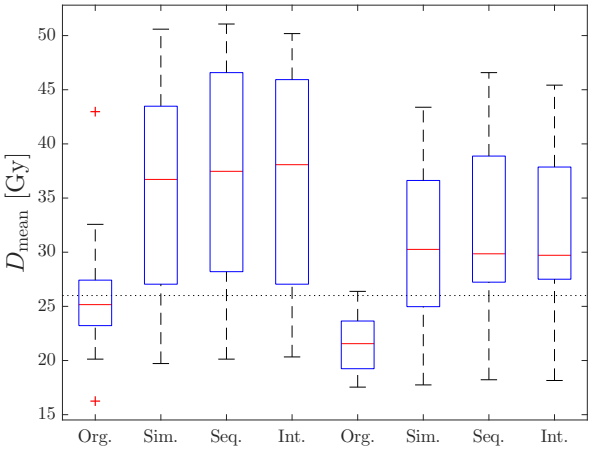

(b) Right (1-4) and left (5-8) parotid gland.

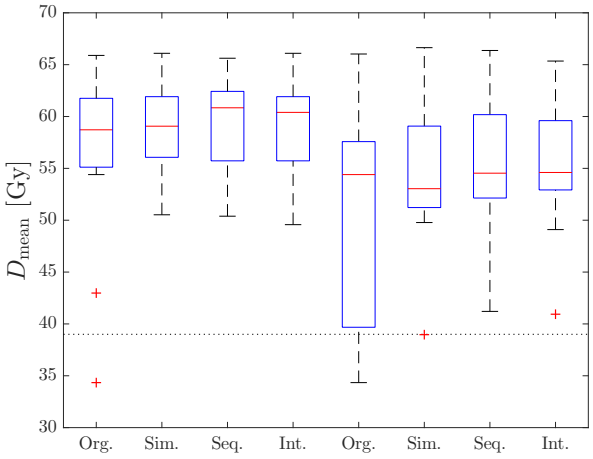

(c) Right (1-4) and left (5-8) submandibular gland.

Figure 34: Max of spinal cord and spinal cord PRV in (a), mean of left parotid gland and right parotid gland in (b), mean of right and left submandibular gland in (c). The black dotted lines represent the respective tolerance constraints.

To be able to determine whether the three different optimization strategies were different from the original one, they were tested for significance. The resulting p-values are given in table 6. It can be seen that the p-values for D_{98} of ITV52, ITV64, ITV68/70, PTV52, PTV64 and PTV68/70 in the simultaneous plan, all were under the limit of 0.05 and was therefore significantly different from the original plan. This was also the case for D_{98} of ITV68/70 in the sequential plan. $D_{\max}$ of the spinal cord and spinal cord PRV was significantly different in the intermediate and sequential plan, and D_{mean} of both parotid glands and both submandibular glands were below the limit of 0.05 for all three plans.

Table 6: p-values found using the Wilcoxon signed rank test, comparing the original plan to the plans with the simultaneous, sequential and intermediate optimization strategies.

	Original vs. Simultaneous p-value	Original vs. Sequential p-value	Original vs. Intermediate p-value
D_{98} of ITV52 [%]	0.004	0.083	0.455
D_{98} of ITV64 [%]	0.008	0.419	0.658
D_{98} of ITV68/70 [%]	0.003	0.040	0.168
D_{98} of PTV52 [%]	< 0.001	0.638	0.258
D_{98} of PTV64 [%]	< 0.001	0.140	0.727
D_{98} of PTV68/70 [%]	0.004	0.091	0.836
$D_{\max}$ of spinal cord [Gy]	0.480	< 0.001	0.003
$D_{\max}$ of spinal cord PRV [Gy]	0.323	< 0.001	< 0.001
D_{mean} of right parotid gland [Gy]	0.002	< 0.001	< 0.001
D_{mean} of left parotid gland [Gy]	0.002	< 0.001	< 0.001
D_{mean} of right submandibular gland [Gy]	0.021	0.018	0.020
D_{mean} of left submandibular gland [Gy]	0.011	0.003	0.002

4.2.2 Conformity and Homogeneity Indices

The CI and HI was computed for PTV52, PTV64 and PTV68/70 in the original, simultaneous, sequential and intermediate plan. These values, in addition to the corresponding p-values, are given in table 7, recall that CI of 1 and HI of 0 mean perfect conformity and homogeneity, respectively. It can be seen that for HI, the simultaneous optimization strategy was significantly better than the original plan for all three PTVs. For PTV52, the intermediate and sequential method has a significantly lower CI than the original plan.

Table 7: Conformity index CI and homogeneity index HI for the original, simultaneous, sequential and intermediate optimization strategies. In addition, p-values are found using Wilcoxon signed rank test, comparing the original plan to each of the other plans, individually.

	Original		Simultaneous			Sequential			Intermediate		
	Median	Range	Median	Range	p-value	Median	Range	p-value	Median	Range	p-value
PTV52											
CI	0.61	0.55 - 0.76	0.62	0.53 - 0.75	0.389	0.54	0.43 - 0.70	< 0.001	0.55	0.48 - 0.71	< 0.001
HI	0.45	0.35 - 0.51	0.43	0.34 - 0.48	0.003	0.45	0.35 - 0.50	0.890	0.45	0.35 - 0.50	0.359
PTV64											
CI	0.82	0.74 - 0.94	0.83	0.74 - 0.95	0.454	0.82	0.53 - 0.93	0.277	0.83	0.69 - 0.92	0.762
HI	0.16	0.12 - 0.19	0.13	0.11 - 0.18	< 0.001	0.14	0.11 - 0.18	0.083	0.15	0.11 - 0.18	0.330
PTV68/70											
CI	0.57	0.27 - 0.70	0.57	0.23 - 0.73	0.804	0.58	0.27 - 0.77	0.489	0.560	0.26 - 0.75	0.421
HI	0.08	0.05 - 0.12	0.07	0.05 - 0.09	< 0.001	0.08	0.05 - 0.11	0.252	0.07	0.05 - 0.10	0.303

4.2.3 Robustness Index

The RI is plotted in figure 35 for the original, simultaneous, sequential and intermediate plans. Remember that a low index suggest a more robust plan. Statistical comparisons of the plans are presented in table 8.

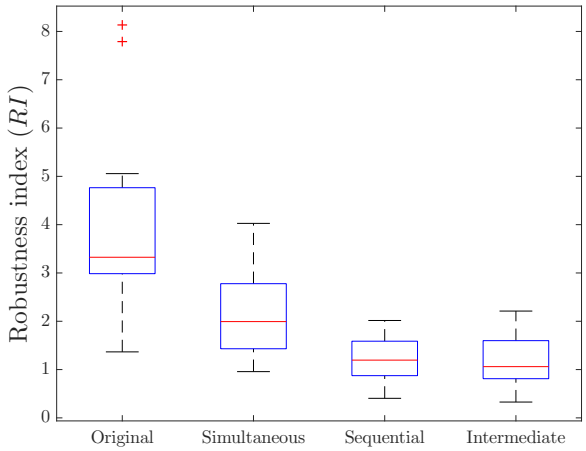

Figure 35: The robustness index is plotted for the original, simultaneous, sequential and intermediate plans.

Table 8: p-values found using Wilcoxon signed rank test comparing the RI for the original plan to the plans with the simultaneous, sequential and intermediate optimization strategies.

	Original vs. Simultaneous p-value	Original vs. Sequential p-value	Original vs Intermediate p-value
RI	0.001	< 0.001	< 0.001

4.2.4 γ Index

The global γ index is plotted in figure 36 and tested for statistical significance in table 9, for the original plan compared to the plans with the simultaneous, sequential and intermediate optimization strategies. The pass-fail criteria was set to DTA = 2 mm and DD = 2%, and 95% of the measurement points had to pass this criteria. The γ index was significantly different for the intermediate and sequential plans. These two plans does also have the highest median.

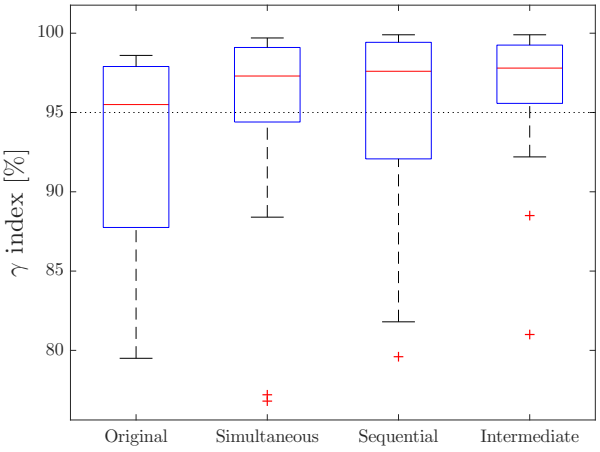

Figure 36: The γ index is plotted for the original, simultaneous, sequential and intermediate plans. The pass-fail criteria was distance to agreement, DTA = 2 mm and dose difference, DD = 2%. The black dotted line represent the constraint that 95% of the measurement points need to pass the pass-fail criteria for the plan to be approved for treatment delivery.

Table 9: p-values found using Wilcoxon signed rank test comparing the γ index for the original plan to the plans with the simultaneous, sequential and intermediate optimization strategies.

	Original vs. Simultaneous	Original vs. Sequential	Original vs Intermediate
	p-value	p-value	p-value
γ index	0.095	0.025	0.005

4.3 With/Without Fixation Mask

To identify the difference between including or not including the fixation mask in the dose calculation process, described in section 3.6.3, the maximum difference and medians with ranges for clinically relevant structures were calculated. The results are displayed in table 10. It can be seen that the differences in gray are quite small and that D_{98} of ITV52, ITV64, ITV68/70, PTV64, PTV68/70, D_{max} of spinal cord and spinal cord PRV and D_{mean} of the right parotid gland, all were significantly different. In spite of the small differences, the dose in plan without mask is consistently larger.

Table 10: The maximum dose difference and medians with ranges, seen among all the patients, between including the fixation mask or not.

	Maximum	With Mask		Without Mask		
	difference	Median	Range	Median	Range	p-value
D_{98} of ITV52 [Gy]	0.27	50.52	48.69 - 51.61	50.59	48.89 - 51.75	< 0.001
D_{98} of ITV64 [Gy]	0.27	63.51	60.79 - 65.82	63.65	61.00 - 65.89	< 0.001
D_{98} of ITV68/70 [Gy]	0.34	65.62	64.06 - 66.84	65.69	64.26 - 66.98	< 0.001
D_{98} of PTV52 [Gy]	0.14	49.44	48.01 - 51.14	49.57	48.14 - 51.14	0.935
D_{98} of PTV64 [Gy]	0.20	59.84	58.00 - 61.81	59.98	58.14 - 61.88	< 0.001
D_{98} of PTV68/70 [Gy]	0.20	64.60	61.95 - 65.76	64.74	62.08 - 65.82	< 0.001
$D_{\max}$ of spinal cord [Gy]	0.20	46.44	38.69 - 49.71	46.58	38.76 - 49.78	< 0.001
$D_{\max}$ of spinal cord PRV [Gy]	0.20	49.84	40.87 - 53.58	49.91	40.94 - 53.65	< 0.001
D_{mean} of right parotid gland [Gy]	0.07	24.68	16.25 - 33.05	24.75	16.32 - 33.12	0.016
D_{mean} of left parotid gland [Gy]	0.07	21.62	17.54 - 26.38	21.56	17.54 - 26.38	0.500

5 Discussion

This section begins with a discussion of results and then follows a more general discussion where references to literature is included.

5.1 Optimizing With/Without Bolus

5.1.1 Dose-Volume Parameters

The D_{98} of PTV52 was determined to be significantly higher in the original plan than in the plan which was optimized with bolus, see table 3. However, D_{98} of PTV64 was significantly higher in the plan which was optimized with bolus. Further, the median was higher in ITV52 and lower in ITV68/70 for the original plan compared with the plan which was optimized with bolus. This might be because in the original plan the TPS increases the fluence in the area close to the skin to compensate for low electronic build-up, which would mean increased dose. This increased fluence is unwanted and could lead to hot spots if there are even small set-up errors [62]. In the original plans, the PTVs are cropped to 1 mm under the surface, as this is the clinical practice at UNN today. In the plan which was optimized with bolus, PTV52 and PTV64 were not cropped to the skin surface during optimization and dose calculation. However, to achieve the best possible comparison and most clinically relevant values, the PTVs that were cropped to 1 mm under the skin surface were used for evaluation in this thesis. A markedly lower dose to PTV52 was seen in the plan which was optimized with bolus, for the patients in which the volume extended into air, explaining the large range of values for PTV52, in figure 22 (b). As PTV52 is a larger volume than PTV64, extending farthest out, the effect was mostly seen for this volume, and there was one patient with D_{98} below the absolute constraint of 90%, and additional two at exactly 90%. Clearly, optimizing with bolus, and then removing the bolus before the final dose calculation has lead to a lower dose in the PTV52. Note that the dose to PTV64 and PTV68/70 was still higher in the plan which was optimized with bolus, which is wanted. However, the actual clinical effect, i.e. the dose coverage of CTV52, and the amount of set-up errors present can be evaluated with cone beam (CB) CTs taken at the treatment sessions. These CBCTs should then be compared to the original planning CT.

Regarding the OAR, D_{max} of spinal cord, D_{mean} of both parotid glands and both submandibular glands were significantly different in the two plans, see table 3.

The only absolute requirement for the OAR is the maximum dose to spinal cord. This was reflected in the results as the other OAR were receiving doses that were higher than the constraints, for many of the patients. It can be seen that the median of the D_{max} to the spinal

cord was lower in the plan which was optimized with bolus and in addition, more patients were getting a lower maximum dose. In a clinical situation, if the volume of the spinal cord PRV where the dose exceeded 52 Gy was smaller than 0.027 cm^3, the plan was still accepted, see section 3.2.1. This explained why the $D_{\max}$ for some of the patients in the original plan was higher than the tolerance limit of 52 Gy. Interpreting the box plot in figure 22, most of the patients got less dose to the spinal cord PRV in the plan where the optimization was done with bolus, but a few patients got more.

Further, the D_{mean} of both the right and left parotid gland was, also in the original plan, for many of the patients higher than the tolerance limit of 26 Gy. The mean dose of the parotid glands in the plan which was optimized with bolus was significantly higher than in the original plan, and there was a much wider range of values. For several of the patients, the primary tumor is located on the right side, and therefore will the left parotid gland be spared more. If a patient has one functioning parotid gland, that is much better for quality of life than having none. Therefore, when performing the dose planning, the radiation therapist attempts to spare at least one of the parotid glands as much as possible.

There was not much difference in the mean dose to the submandibular glands in the original plan and the plan which was optimized with bolus. However, a larger part of patients get less dose in the original plan, as the 25th percentile was at a lower dose.

5.1.2 Conformity, Homogeneity, Robustness and γ Indices

Concerning the CI and HI calculated for PTV52, PTV64 and PTV68/70 in table 4, PTV64 has the highest median CI and PTV68/70 has the lowest and therefore the best HI for both the original plan and the plan which was optimized with bolus. Further, the homogeneity was second best for PTV64 and the worst for PTV52. This is expected, as good homogeneity is easier to achieve in a small volume, in addition, the PTV68/70 is also typically situated deeper into the body, and it has a less complex shape than the other two. As the p-value suggests, the HI of PTV52 was significantly better in the original plan, and the HI of PTV64 was significantly better in the plan which was optimized with bolus.

The plan which was optimized with bolus was determined to have a RI that was significantly better than the one in the original plan. This suggests that the plan which was optimized with bolus might be less complex.

The γ index describes how similar the calculated and measured dose distributions are, or to what degree the linac was able to deliver the planned dose distribution. It was evident that the plan which was optimized with bolus was the better of the two, as the median γ index was higher. However, the difference between the two plans was not statistically significant, as the p-value was above 0.05. This suggests that there were only small differences in the

two plans and that the values in one of the plans were not consistently higher. It should be noted that in the plan which was optimized with bolus, there was one outlier at about 75%. There were no outliers in the original plan, but the range of values was much wider.

5.1.3 Plan Uncertainty

For D_{98} of ITV64 and ITV68/70 it can be seen in figure 26 that only a few of the uncertainty plans, for the plan which was optimized with bolus, were below the constraint of 95%. In the original plan, on the other hand, several more uncertainty plans and even unperturbed plans were under the constraint.

For the spinal cord PRV, it can be seen that for some of the patients which have $D_{\max}$ very close to or slightly over the constraint of 52 Gy, even small isocenter shifts of 1 mm yield a $D_{\max}$ above the constraint. This was seen for example in patients 2, 8, 13 and 15, in both plans. This might be an important feature to remember, that if a value is very close to the constraint, with the uncertainties that exist in radiation therapy, the probability is high for the patient to receive a dose over the constraint.

The median widths of all three ITV uncertainty plots were wider, but not significantly wider, in the original plan compared with the plan which was optimized with bolus, see figure 30 and table 5. The width is a measure of robustness in the plan, and a narrow width means a good and robust plan.

Regarding the OAR, the widths were significantly narrower in the original plan for the spinal cord the and spinal cord PRV. However, the $D_{\max}$, seen in figure 22, were generally higher for the spinal cord PRV and significantly higher for spinal cord in the original plan. Furthermore, the widths were wider in the original plan for the left parotid gland and the submandibular glands. However, the D_{mean} were significantly higher in the plan which was optimized with bolus. It should be emphasized that in a clinical setting, where the optimization would have been done in many rounds until the desired plan was obtained, the outcome of the plan which was optimized with bolus would most likely have been much better.

Notice that only $D_{\max}$ to spinal cord/spinal cord PRV out of the OAR was generally lower in the plan which was optimized with bolus. Therefore, it is interesting that the only OAR which was given objectives for the optimization for all the patients was the spinal cord/spinal cord PRV, see appendix A.5. The left and right parotid glands were given objectives for 4 of the 15 patients and for the submandibular glands, no objectives were given for any of the patients. The four patients which had objectives for the parotids glands during optimization were patients 4, 5, 12 and 14. It can be seen for the plan which was optimized with bolus, in figure 28, that none of these patients have very high doses for the unperturbed plan. The fact that optimization objectives were not set for the submandibular glands and only

set for some of the patients for the parotid glands might be one of the reasons why the plan which was optimized with bolus yield overall higher mean doses to the parotid and submandibular glands. However, it is not necessarily bad to not set objectives for OAR that are not prioritized highly, as the optimizer then focuses more on the important target volumes.

5.2 Simultaneous, Sequential and Intermediate Optimization Strategies

5.2.1 Dose-Volume Parameters

Comparing the original with the simultaneous, sequential and intermediate optimization strategies, it was found that the original plan was significantly different from the plan with the simultaneous optimization strategy for D_{98} of ITV52, ITV64, ITV68/70, PTV52, PTV64 and PTV68/70, see table 6. In addition, the sequential plan for D_{98} of ITV68/70 was also significantly different from the original plan. Figures 32 and 33 show that the simultaneous plan was better than the original, as a higher target volume coverage was achieved. This was also the case for the sequential plan in ITV68/70. For D_{98} of ITV52 in figure 32, only in the original plan does some of the patients have D_{98} below the limit of 95%. For ITV64, all the patients have D_{98} above the 95% limit and for ITV68/70, a few of the patients have D_{98} below the 95% constraint in the original plan, and there was one patient under the constraint in the sequential plan.

For all of the patients, the D_{98} of the PTVs were above the absolute requirement of 90%, but not all were above the limit of 95%. The simultaneous optimization method have the highest median in all the PTVs and stands out as being the best method at achieving higher dose to the target volumes. Remembering that the simultaneous method was just optimizing and recalculating the original dose plan three times, suggest that it is worth the while to take the time to do this.

Regarding the OAR, D_{max} of the spinal cord and spinal cord PRV was significantly different from the original plan for the intermediate and sequential plan, but not in the simultaneous plan. D_{mean} of both the parotid glands and both submandibular glands was significantly different from the original plan for all the three other plans, as seen in table 6.

Only in the original plan was the median of the D_{mean} of the parotid glands lower than the tolerance limits. A reason for this might be that in the original plan, the radiation therapists performing the planning have changed the objectives and optimized several times trying to get the best dose coverage for the target volumes at the same time as trying to minimize the dose to the OAR. In the intermediate, simultaneous and sequential plan, the

same objectives have been used as in the original plan, but the same objectives were used in every optimization.

Only the maximum dose in the simultaneous plan is, in addition to the original plan, below the 50 Gy absolute tolerance constraint to spinal cord. A reason for this might be that in the sequential and intermediate method, the objective for the spinal cord were only used in the second and third round of optimization. This means that less time was spent optimizing for this objective than in the simultaneous plan. It should be noted that no plan would be delivered to a patient with maximum dose to spinal cord above 50 Gy, the treatment plan would have to be changed to get this dose below 50 Gy. The submandibular glands were not prioritized when it comes to getting the mean dose below 39 Gy, which was clearly seen in 34 (c). The problem in this case was most likely that these glands were very close to or in the target volume, as was seen for one patient in appendix A.1. Reducing the dose would mean reducing the dose to the target volume, which is not something you would do as it is much more important to get the prescribed dose to the target volume.

5.2.2 Conformity, Homogeneity, Robustness and γ Indices

The homogeneity index, given in table 7, was in the simultaneous plan significantly better than in the original plan for PTV52, PTV64 and PTV68/70. Although, note that the differences in median values were quite small.

Comparing the original plan to each of the simultaneous, sequential and intermediate plans, the robustness index was found to be significantly different for all three cases. Notably, the sequential and intermediate plans were the most similar amongst the four plans and have the lowest indices.

The intermediate and sequential plans have significantly higher γ index than the original plan, see figure 36. It should be noted that the patient population was limited, as there were only 15 patients. Counting how many patients that have γ index under 90%; the original plan has four, the intermediate plan has two, the simultaneous plan has three and the sequential plan has three. The values under 90% in the sequential plan were higher than the values under 90% in the simultaneous plan, which was why the range of values was larger in the sequential plan. This explains why the simultaneous plan might seem better than the sequential plan in the figure.

The intermediate and sequential plans were quite similar, especially in the OAR plots and the RI and γ indices. This is expected, as the optimization strategies were similar: first the plans were optimized and dose was calculated with just objectives for the target volumes, and the next time, the OAR objectives were added. There were tendencies towards the OAR getting more dose with these strategies, without improving the dose coverage for the target

volumes. However, these two methods performed the best in the verification process, as their γ indices were higher. In addition, their robustness index was lower, suggesting more robust plans. This suggests that the planned treatment was slightly more likely to be given accurately than for the simultaneous and original plan.

5.3 With/Without Fixation Mask

Several parameters were compared in two plans, with and without fixation mask included in the body structure, see table 10. Note that for seven of the parameters, the p-value was <0.001, this was because all, or almost all, of the 15 patients had a higher dose in the plan without mask compared to the plan with mask. The difference in gray between including or not including the fixation mask in the dose calculation was quite small. However, it seems that the dose values were systematically higher in the plan without the fixation mask. This is expected, as the attenuation of the photon beam will start a few millimeters earlier with the mask.

5.4 Discussion of General Considerations

5.4.1 Optimizing With/Without Bolus

In the literature, several methods have been proposed to avoid the overdosage problem in the build-up region, described in section 2.5.4, in the case that the PTV extend to or outside the skin surface. One method which has been described is to crop the PTV to about 3 mm under the skin surface, this was reported by Merlotti *et al.* [25] and Shiau *et al.* [26]. Shiau *et al.* investigated 5 mm and 3 mm shrinkage of the PTV, and concluded with 3 mm being the best solution. Court and Tishler [63] have investigated cropping 0, 3 and 5 mm under the surface. They have stated that the decision of which of these that should be chosen should be based on the amount of set-up uncertainties present. Further, they found that the PTV which was cropped 3 mm was more robust against set-up uncertainties of more than 2 mm, compared to the PTV which was cropped with 5 mm. Johnston *et al.* [3] and Dunlop *et al.* [60] have reported to crop the PTV with 5 mm under the skin surface. Lastly, it was described in the Danish head and neck cancer group (DAHANCA) protocol that the PTV was commonly reduced a few millimeters under the skin surface. It has been remarked that this should be done with care, as the PTV is present to account for uncertainties.

Another method was to apply a virtual bolus for the optimization and then remove it before dose calculation. Thilmann *et al.* [64] was the first to propose using a virtual bolus for treatment of breast cancer, where a bolus of 10 mm was applied when the PTV extended into air. It was concluded that the bolus had to be removed before final dose calculation, as the

dose distribution otherwise would be shifted. In addition to breast cancer, virtual bolus has also been used for total body irradiation before a stem cell transplant and for H&N cancer. Several researchers have reported the feasibility of using a virtual bolus for patients with H&N cancer [24, 25, 26, 60, 63]. Firstly, Merlotti *et al.* have stated that using a virtual bolus is advised for the cases where the CTV extend into the skin. Further, Dunlop *et al.* have used a virtual bolus of 10 mm such that the PTV always was 10 mm from the body contour or the virtual body surface. Note that the PTV was cropped to 5 mm under the skin surface. Thomas and Hoole [24] have reported that good coverage of the PTV was obtained when a virtual bolus was applied for dose calculation. Lastly, Shiau *et al.* [26] have advised of using a virtual bolus of 3.5 mm thickness when the CTV included the skin. It should be noted that IMRT had been used in all these articles and that the situation might be somewhat different with VMAT, as the treatment is given from more angles. Summing up, there seem to be a consensus in the literature that cropping the PTV to 3 mm under the skin would be a good solution to the overdosage problem in the build-up region. This will most likely improve the conformity of the PTVs, spare the skin and the optimization system will not work as hard to try to deposit dose to this region. Cropping more than 3 mm is not advised here as reducing the PTV too much could mean compromising the target coverage. Testing the approach of cropping 3 mm remains for future work.

In this thesis, ambiguous results were found but both approaches are acceptable. Neither the original plan nor the plan which was optimized with bolus showed significantly superior results for all the structures and parameters evaluated. The plan optimized with bolus performed slightly better in the ITVs for D_{98} of the uncertainty plans, for the PTVs in terms of conformity and homogeneity indices, in the γ index and for the maximum dose to spinal cord. However, it performed much worse for PTV52 and the other OAR. For the OAR, this is most likely due to the optimization objectives that had been set. On the other side, it might be the same optimization objectives that made the plan which was optimized with bolus slightly better for the ITVs.

5.4.2 Conformity and Homogeneity Indices

In the literature, different conformity and homogeneity indices are used. Therefore, only the CI and HI which had been defined in the same way as in this thesis and only the volume with the highest dose, i.e. PTV68, in the original plan was considered for comparison reasons.

First, Dunlop *et al.* [60] have reported mean CI of 0.77 and HI of 0.12 for 8 patients with nasopharygeal cancer. In that article, SmartArc VMAT plans were generated using the Philips Pinnacle version 9 TPS and 65 Gy was prescribed to the primary target and 54 Gy

to the elective target. Further, Jacob *et al.* [65] have reported HI[11] of 0.11, for nine patients with H&N cancer treated with RapidArc. Here, 50 Gy was prescribed to PTV. Van Gestel *et al.* [66] have reported a HI of 0.10 for the volume called PTV69, for five patients with oropharyngeal cancer. This value was obtained with RapidArc treatments using a Varian CLINAC 2100. Lastly, Lee *et al.* [67] have found a CI[12]for the PTV70 volume, of 0.82, for 20 patients with nasopharyngeal cancer. The values given here were obtained with the Pinnacle SmartArc system, dual arc Elekta VMAT.

Comparing to CI of 0.57 and HI of 0.08 which was calculated for the original plan in this thesis, table 4, the homogeneity is slightly better than the values in the literature, but the conformity was poorer compared to the values in the literature.

5.4.3 Robustness Index

There are many different indices or scores presented in the literature which attempts to quantify the complexity, or robustness of IMRT or VMAT plans, e.g. the modulation index proposed by Webb *et al.* [68]. Further, Mohan *et al.* [69] have found that as complexity increases, so does the fraction of radiation transmission through and scattered from the leaves, to the total delivered dose. It was also stated in the same article that to make a complex intensity pattern, more MU was required, compared to in a simpler plan. Both these effects were taken account for in the robustness index in section 3.7.4, by particularly the Flank term and the MU term, respectively. Further, H&N patients are known for needing especially complex plans. This is because of the concave shape of the target volumes, placement of OAR and prescription of high doses to the target volumes. McGarry *et al.* [70] have determined that when the minimum field size was reduced from 1 cm to 4 cm, and in addition, when the total numbers of segments was reduced, a reduction in complexity was found. Moreover, one of the features Crowe *et al.* [71] took into account in their index was the difference in area between the field apertures defined by the jaws and the smaller aperture defined by the MLCs. The same feature is similarly taken account for in the RI used in this thesis, by the Opening and Field size terms. Craft *et al.* [72], has described a situation where reducing the amount of MUs given in a plan could be done without degrading the quality of the plan, and that there will always be a trade off between complexity and treatment quality. It was pointed out by McNiven *et al.* [73] that a larger number of MUs, a larger number of segments, small segment size and complex shape were all factors associated with a high degree of complexity in a plan. But also that these were dependent on the treatment site,

[11] HI was defined as $\frac{D_2 - D_{98}}{D_{\text{prescribed}}}$, remember that the index was divided by D_{median} in this thesis. However, in practice, these values will be very similar.

[12] Compared to the CI defined in this thesis, the reciprocal was reported. The inverse value is stated here, for better comparison to the values in this thesis.

and that different sites require different degree of plan complexity [72, 73], e.g. a H&N case often require a much more complex plan than a breast case to make an acceptable treatment plan. This makes it difficult to compare different sites. In addition, there will be a trade off between complexity and the dosimetric accuracy of the plan. McNiven *et al.* presented the modulation complexity score which was defined on a fixed scale from 0 to 1 and therefore allows for better comparison between different treatment sites. This is a feature that the RI in this thesis does not contain, and which could be a considered for continued work.

The robustness index seem to be a good index describing the same tendencies as for the γ index, and it has many of the same features as other indices in the literature. It should be further developed and tested on more treatment sites, in a larger scale.

5.4.4 γ Index

For verification of VMAT plans with a Delta^4 phantom, a pass-fail criteria of DD = 3% and DTA = 3 mm is widely used in the literature [60, 67, 74, 75]. This have been debated, and some authors have stated that this criteria was not strict enough and that 2%/2 mm should be used instead [76]. This supports the decision of choosing a criteria of 2%/2 mm. In addition, the global γ index was chosen instead of the local, because of clinical relevance.

Note that for this thesis, all the plans were made in version 13 of Eclipse$^{\text{TM}}$ on a test box, manually transferred to the linac and run in service mode. Overall, the original plans had better γ values when they originally were verified before treatment. This suggests that there might be a systematic difference between the test system and the clinical version of Eclipse$^{\text{TM}}$. Therefore, all the plans would most likely get higher γ indices in a clinical situation where Eclipse$^{\text{TM}}$ version 13 would be installed.

5.4.5 Plan Uncertainty

The new plan uncertainty tool in version 13 of Eclipse$^{\text{TM}}$ has only been described by a few authors to this date. Stroom *et al.* [49] have used the plan uncertainty tool and concluded that isocenter shifts of as much as 3 mm have a modest impact on the VMAT plan quality for a single fraction of stereotactic ablative radiation therapy (SABR). They came to this conclusion by evaluated various DVH parameters, as was also done in this thesis. Further, in a article published in march of 2017, Liu *et al.* [77] studied the association of VMAT plan robustness with local failure (LF) in H&N cancer. Using plan robustness analysis, in which in addition to the nominal/unperturbed dose distribution, six perturbed plans were created by translating the CT isocenter in three directions by the 3 mm PTV margin. They concluded that possible target underdosage due to patient set-up uncertainties appeared to be

a more relevant factor associated with LF in VMAT for H&N cancer than compromized PTV coverage, at least for the patients included in that study. This suggests that it is important to investigate the subject of robustness in plans further, and that the plan uncertainty tool can be used for this purpose. Lastly, it should be noted that producing as many uncertainty plans as was done is this thesis using a test box was quite time consuming. Most likely, dose calculation would take much less time with an ordinary clinical Eclipse^{TM} licence.

5.4.6 Simultaneous, Sequential and Intermediate Optimization Strategies

How the optimization system works is not fully known, so as a way of testing this system, different optimization strategies were tried to see whether better plans could be made without much additional work. The optimization strategies of the sequential and intermediate plans were similar, first the plans were optimized with just the target volumes, i.e. ITVs and PTVs, and then secondly, the rest of the original objectives were applied too. Further, these two plans had better γ and robustness indices, than the simultaneous and original plan, seen in figures 35 and 36. This could suggest that using this order of optimization was favorable for producing less modulated and more robust plans. As briefly described in section 2.10, the optimization algorithm chooses a direction and then searches along this direction. It can be hypothesized that in the sequential method, as only the target volume objectives were used in the first optimization, a kind of direction was chosen that was beneficial for making a less complex plan. However, the dose-volume parameters were not better than in the original and simultaneous plan. Still, it is obviously better to use a plan which have a higher probability of being delivered as it was planned, than a plan that might seem better in the planning process, but have a lower probability of being delivered as planned because of technical limitations and uncertainties. Hægeland [8] also found that the sequential optimization method produced lower and therefore better RI compared to the simultaneous and original plan. It is worth noticing that Oliver *et al*. have found that increasing the optimization time and increasing the number of segments by adding an arc correlated with improvements in the DVH. Their results complies with the experiences in this thesis, where the simultaneous plan was better compared to the original plan. Remember that the simultaneous plan was just the original plan being optimized and calculated three times. During the process of optimization, more activity was seen in the optimizing window in the two first rounds of optimization than in the third. Therefore, it can be proposed that optimizing two, instead of three, additional rounds might also improve the plan quality.

5.4.7 With/Without Fixation Mask

Various researchers have stated that wearing a fixation mask during IMRT increases the skin dose [63, 78, 79]. In the article by Court and Tishler [63] it was expressed that the common practice was to include the fixation mask in the body contour. Therefore, to make the planning situation as similar as possible to the real clinical situation, it is advisable to always include the fixation mask in the body structure for the dose calculation process. It should be noted that the radiotherapy department at UNN has not experienced any difference in skin reactions before and after they started with IMRT/VMAT treatment instead of conventional radiotherapy.

5.5 Future Work

Summing up, more investigations should be done to determine whether the approach of cropping the PTV with 3 mm would be a good solution to the problem in the build-up region. Testing the robustness of this approach could be done by calculating uncertainty plans with median widths, γ indices and RI. In addition, it would be very relevant to investigate the actual set-up uncertainties present in the clinic, this could be done as mentioned before using CBCT images. To make this study as similar as possible to the clinical situation, the original optimization objectives for all the patients were used. However, for future work, it could be considered to use the same objectives for all the patients, which would allow for better comparison between the patients and between the original plan and the plan optimized with bolus. Further, uncertainty plans could be generated for the simultaneous, sequential and intermediate optimization strategies as well, to see whether the sequential and intermediate plans are more robust than the original and simultaneous also in this method of analysis. Furthermore, a possibility for future clinical work could be to only create uncertainty plans with 3 mm isocenter shifts, in stead of quite small isocenter shifts of 1 mm and quite large isocenter shifts of 5 mm, which would reduce the time. The intermediate dose function has shown to be useful, and should be further tested for more cases and treatment sites. The RI should be further developed and tested in a larger scale on more treatment sites.

6 Conclusion

By comparing original VMAT plans with plans optimized using a virtual bolus, both approaches were found to be acceptable. However, none of them were proven to be superior to the other. The plan which was optimized with bolus showed significantly better dose coverage to PTV64, lower D_{max} to the spinal cord as well as superior γ and robustness indices. The original plan showed significantly better dose coverage to PTV52 and significantly lower D_{mean} of both parotid glands and both submandibular glands. In the literature, it has been suggested to crop the PTV with 3 mm under the skin instead of 1 mm which had been done in the original plan. This should be investigated further.

The intermediate plan followed by the sequential plan had the best γ and robustness indices, suggesting they were more robust plans. Hence, the intermediate dose function should be further investigated as a method to improve practice. The simultaneous plan had the best dose coverage to target volumes, slightly better γ indices and significantly better robustness indices compared to the original plan. This implies that taking the time to optimize and calculate dose after a plan has met the tolerance criteria, is worth the while.

To make the planning situation as similar as possible to the real situation, it was concluded that the fixation mask should always be included in the body contour for dose calculation, as there was a significant difference between including and not including the mask.

References

[1] "NCCN Guidelines for treatment of cancer by site: Head and Neck Cancers," 2012. [Online]. Available: https://www.nccn.org/professionals/physician_gls/f_guidelines.asp#head-and-neck

[2] Cancer Registry of Norway, "Cancer in Norway 2015 - Cancer incidence, mortality, survival and prevalence in Norway," 2016.

[3] M. Johnston, S. Clifford, R. Bromley, M. Back, L. Oliver, and T. Eade, "Volumetric-modulated arc therapy in head and neck radiotherapy: a planning comparison using simultaneous integrated boost for nasopharynx and oropharynx carcinoma," *Clinical Oncology*, vol. 23, no. 8, pp. 503–511, 2011.

[4] J. L. Bedford, "Treatment planning for volumetric modulated arc therapy," *Medical physics*, vol. 36, no. 11, pp. 5128–5138, 2009.

[5] C. M. Nutting, J. P. Morden, K. J. Harrington, T. G. Urbano, S. A. Bhide, C. Clark, E. A. Miles, A. B. Miah, K. Newbold, M. Tanay *et al.*, "Parotid-sparing intensity modulated versus conventional radiotherapy in head and neck cancer (PARSPORT): a phase 3 multicentre randomised controlled trial," *The lancet oncology*, vol. 12, no. 2, pp. 127–136, 2011.

[6] W. F. Verbakel, J. P. Cuijpers, D. Hoffmans, M. Bieker, B. J. Slotman, and S. Senan, "Volumetric intensity-modulated arc therapy vs. conventional IMRT in head-and-neck cancer: a comparative planning and dosimetric study," *International Journal of Radiation Oncology • Biology • Physics*, vol. 74, no. 1, pp. 252–259, 2009.

[7] A. Holt, D. Van Gestel, M. Arends, E. Korevaar, D. Schuring, M. Kunze-Busch, R. Louwe, and C. van Vliet-Vroegindeweij, "Multi-institutional comparison of VMAT vs IMRT for head-and-neck cancer: A planning study," *Radiat. Oncol*, vol. 8, p. 26, 2013.

[8] C. Hægeland, "Optimization and verification of dosimetric robustness of VMAT dose-plans," Master's thesis, NTNU, 2016.

[9] P. Mayles, A. Nahum, and J.-C. Rosenwald, *Handbook of radiotherapy physics: theory and practice*. CRC Press, 2007.

[10] E. Podgorsak *et al.*, "Radiation oncology physics," *a handbook for teachers and students/EB Podgorsak.–Vienna: International Atomic Energy Agency*, vol. 657, 2005.

[11] F. H. Attix, *Introduction to radiological physics and radiation dosimetry.* John Wiley & Sons, 2008.

[12] M. J. Gazda and L. R. Coia, "Principles of radiation therapy," *Cancer Management: A Multidisciplinary Approach: Medical, surgical and radiation oncology. Melville: PRR, Inc*, pp. 9–19, 2001.

[13] P. Allisy-Roberts and J. R. Williams, *Farr's physics for medical imaging.* Elsevier Health Sciences, 2007.

[14] KVIST -gruppen, "Faglige anbefalinger for strålebehandling ved ikke-småcellet lungekreft," pp. 6–8, 12–19, 21–27, 2015.

[15] International Commission on Radiation Units, *Prescribing, recording, and reporting electron beam therapy.* Oxford University Press, 2004, no. 71.

[16] Statens strålevern, "Volum og doser i ekstern stråleterapi," *Strålevernrapport*, no. 9, pp. 22–25, 2012.

[17] "Retningslinjer for strålebehandling i DAHANCA," 2013, retrieved January 30 2017. [Online]. Available: https://www.dahanca.oncology.dk/Brows_Web_Guidelines

[18] Genetics Home Reference, "head and neck squamous cell carcinoma," 2017, retrieved March 26 2017. [Online]. Available: https://ghr.nlm.nih.gov/condition/head-and-neck-squamous-cell-carcinoma

[19] National Cancer Institute, "Head and Neck Cancers," 2017, retrieved March 26 2017. [Online]. Available: https://www.cancer.gov/types/head-and-neck/head-neck-fact-sheet

[20] "Kreft i svelg," retrieved March 28 2017. [Online]. Available: http://oncolex.no/Hodehals/Diagnoser/Svelg

[21] "Kreft i strupehode," retrieved March 14 2017. [Online]. Available: http://oncolex.no/Home/Hodehals/Diagnoser/Strupe.aspx

[22] K. Edmunds and J. Bedford, "Assessment of the robustness of volumetric-modulated arc therapy for lung radiotherapy," *The British journal of radiology*, vol. 86, no. 1023, p. 20120498, 2013.

[23] T. Nguyen, A. Hoole, N. Burnet, and S. Thomas, "The optimization of intensity modulated radiotherapy in cases where the planning target volume extends into the build-up region," *Physics in medicine and biology*, vol. 54, no. 8, p. 2511, 2009.

[24] S. J. Thomas and A. C. Hoole, "The effect of optimization on surface dose in intensity modulated radiotherapy (IMRT)," *Physics in medicine and biology*, vol. 49, no. 21, p. 4919, 2004.

[25] A. Merlotti, D. Alterio, R. Vigna-Taglianti, A. Muraglia, L. Lastrucci, R. Manzo, G. Gambaro, O. Caspiani, F. Miccichè, F. Deodato *et al.*, "Technical guidelines for head and neck cancer IMRT on behalf of the Italian association of radiation oncology-head and neck working group," *Radiation Oncology*, vol. 9, no. 1, p. 264, 2014.

[26] A.-C. Shiau, P.-L. Lai, J.-A. Liang, P.-W. Shueng, W.-L. Chen, and W.-P. Kuan, "Dosimetric verification of surface and superficial doses for head and neck IMRT with different PTV shrinkage margins," *Medical physics*, vol. 38, no. 3, pp. 1435–1443, 2011.

[27] L. Djupvik, "Kurativ strålebehandling av ØNH," 2017, unpublished.

[28] K. Marienhagen, "ØNH-cancer: Risikoorganer og toleransegrenser," 2017, attached in Appendix A.8.

[29] "Inside a Varian linear accelerator, Dose shaping," 2017, retrieved May 23 2017. [Online]. Available: http://newsroom.varian.com/imagegallery?cat=2471

[30] *Eclipse Photon and Electron Algorithms 13.6 Reference Guide*, P1008611-003-C ed., Varian Medical Systems, Inc, 3100 Hansen Way, Palo Alto, CA 94304-1030,USA, 2015.

[31] Intensity Modulated Radiation Therapy Collaborative Working Group and others, "Intensity-modulated radiotherapy: current status and issues of interest," *International Journal of Radiation Oncology • Biology • Physics*, vol. 51, no. 4, pp. 880–914, 2001.

[32] A. Ahnesjö, B. Hårdemark, U. Isacsson, and A. Montelius, "The IMRT information process—mastering the degrees of freedom in external beam therapy," *Physics in Medicine and Biology*, vol. 51, no. 13, p. R381, 2006.

[33] K. Otto, "Volumetric modulated arc therapy: IMRT in a single gantry arc," *Medical physics*, vol. 35, no. 1, pp. 310–317, 2008.

[34] L. Tillikainen, H. Helminen, T. Torsti, S. Siljamäki, J. Alakuijala, J. Pyyry, and W. Ulmer, "A 3D pencil-beam-based superposition algorithm for photon dose calculation in heterogeneous media," *Physics in medicine and biology*, vol. 53, no. 14, p. 3821, 2008.

[35] L. Tillikainen, S. Siljamäki, H. Helminen, J. Alakuijala, and J. Pyyry, "Determination of parameters for a multiple-source model of megavoltage photon beams using optimization methods," *Physics in medicine and biology*, vol. 52, no. 5, p. 1441, 2007.

[36] F. E. Boas and D. Fleischmann, "Ct artifacts: causes and reduction techniques," *Imaging in Medicine*, vol. 4, no. 2, pp. 229–240, 2012.

[37] J. H. Hubbell and S. M. Seltzer, "Tables of x-ray mass attenuation coefficients and mass energy-absorption coefficients 1 keV to 20 MeV for elements Z= 1 to 92 and 48 additional substances of dosimetric interest," National Inst. of Standards and Technology-PL, Gaithersburg, MD (United States). Ionizing Radiation Div., Tech. Rep., 1995.

[38] W. Ulmer, J. Pyyry, and W. Kaissl, "A 3D photon superposition/convolution algorithm and its foundation on results of Monte Carlo calculations," *Physics in medicine and biology*, vol. 50, no. 8, p. 1767, 2005.

[39] W. Ulmer and D. Harder, "Applications of a triple Gaussian pencil beam model for photon beam treatment planning," *Zeitschrift für Medizinische Physik*, vol. 6, no. 2, pp. 68–74, 1996.

[40] W. Ulmer and D. v. Harder, "A triple Gaussian pencil beam model for photon beam treatment planning," *Zeitschrift für medizinische Physik*, vol. 5, no. 1, pp. 25–30, 1995.

[41] D. A. Low, W. B. Harms, S. Mutic, and J. A. Purdy, "A technique for the quantitative evaluation of dose distributions," *Medical physics*, vol. 25, no. 5, pp. 656–661, 1998.

[42] D. A. Low and J. F. Dempsey, "Evaluation of the gamma dose distribution comparison method," *Medical physics*, vol. 30, no. 9, pp. 2455–2464, 2003.

[43] L. Vieillevigne, J. Molinier, T. Brun, and R. Ferrand, "Gamma index comparison of three VMAT QA systems and evaluation of their sensitivity to delivery errors," *Physica Medica*, vol. 31, no. 7, pp. 720–725, 2015.

[44] L. Masi, F. Casamassima, R. Doro, and P. Francescon, "Quality assurance of volumetric modulated arc therapy: Evaluation and comparison of different dosimetric systems," *Medical physics*, vol. 38, no. 2, pp. 612–621, 2011.

[45] J. L. Bedford, Y. K. Lee, P. Wai, C. P. South, and A. P. Warrington, "Evaluation of the Delta4 phantom for IMRT and VMAT verification," *Physics in medicine and biology*, vol. 54, no. 9, p. N167, 2009.

[46] K. Marienhagen, "Retningslinjer ØNH, legedel," 2016, attached in Appendix A.9.

[47] J. O. Deasy, V. Moiseenko, L. Marks, K. C. Chao, J. Nam, and A. Eisbruch, "Radiotherapy dose–volume effects on salivary gland function," *International Journal of Radiation Oncology • Biology • Physics*, vol. 76, no. 3, pp. S58–S63, 2010.

[48] E. Vanetti, G. Nicolini, J. Nord, J. Peltola, A. Clivio, A. Fogliata, and L. Cozzi, "On the role of the optimization algorithm of rapidarc® volumetric modulated arc therapy on plan quality and efficiency," *Medical physics*, vol. 38, no. 11, pp. 5844–5856, 2011.

[49] J. Stroom, S. Vieira, D. Mateus, C. Greco, A. Fogliata, G. Nicolini, A. Clivio, E. Vanetti, and L. Cozzi, "On the robustness of VMAT-SABR treatment plans against isocentre positioning uncertainties," *Radiation Oncology*, vol. 9, no. 1, p. 196, 2014.

[50] W. Liu, S. H. Patel, J. J. Shen, Y. Hu, D. P. Harrington, X. Ding, M. Y. Halyard, S. E. Schild, W. W. Wong, G. A. Ezzell *et al.*, "Robustness quantification methods comparison in volumetric modulated arc therapy to treat head and neck cancer," *Practical radiation oncology*, vol. 6, no. 6, pp. e269–e275, 2016.

[51] W. Liu, Z. Liao, S. E. Schild, Z. Liu, H. Li, Y. Li, P. C. Park, X. Li, J. Stoker, J. Shen *et al.*, "Impact of respiratory motion on worst-case scenario optimized intensity modulated proton therapy for lung cancers," *Practical radiation oncology*, vol. 5, no. 2, pp. e77–e86, 2015.

[52] W. Liu, X. Zhang, Y. Li, and R. Mohan, "Robust optimization of intensity modulated proton therapy," *Medical physics*, vol. 39, no. 2, pp. 1079–1091, 2012.

[53] W. Liu, S. J. Frank, X. Li, Y. Li, P. C. Park, L. Dong, X. Ronald Zhu, and R. Mohan, "Effectiveness of robust optimization in intensity-modulated proton therapy planning for head and neck cancers," *Medical physics*, vol. 40, no. 5, 2013.

[54] The Mathworks, Inc., "Box plots," retrieved March 14 2017. [Online]. Available: https://se.mathworks.com/help/stats/box-plots.html

[55] J. D. Gibbons and S. Chakraborti, *Nonparametric statistical inference*. Springer, 2011.

[56] F. Wilcoxon, "Individual comparisons by ranking methods," *Biometrics bulletin*, vol. 1, no. 6, pp. 80–83, 1945.

[57] W. W. LaMorte, "Wilcoxon Signed Rank Test," 2016, retrieved February 6 2017. [Online]. Available: http://sphweb.bumc.bu.edu/otlt/MPH-Modules/BS/BS704_Nonparametric/BS704_Nonparametric6.html

[58] "Assumptions of the Wilcoxon Sign Test," retrieved February 6 2017. [Online]. Available: http://www.statisticssolutions.com/assumptions-of-the-wilcox-sign-test/

[59] NIST/SEMATECH e-Handbook of Statistical Methods, "7.1.3.1. Critical values and p values," 2013, retrieved February 6 2017. [Online]. Available: http://www.itl.nist.gov/div898/handbook/prc/section1/prc131.htm

[60] A. Dunlop, L. Welsh, D. McQuaid, J. Dean, S. Gulliford, V. Hansen, S. Bhide, C. Nutting, K. Harrington, and K. Newbold, "Brain-sparing methods for IMRT of head and neck cancer," *PloS one*, vol. 10, no. 3, p. e0120141, 2015.

[61] I. Paddick, "A simple scoring ratio to index the conformity of radiosurgical treatment plans: technical note," *Journal of neurosurgery*, vol. 93, no. Supplement 3, pp. 219–222, 2000.

[62] G. Moliner, F. Izar, R. Ferrand, M. Bardies, S. Ken, and L. Simon, "Virtual bolus for total body irradiation treated with helical tomotherapy," *Journal of Applied Clinical Medical Physics*, vol. 16, no. 6, 2015.

[63] L. E. Court and R. B. Tishler, "Experimental evaluation of the impact of different head-and-neck intensity-modulated radiation therapy planning techniques on doses to the skin and shallow targets," *International Journal of Radiation Oncology • Biology • Physics*, vol. 69, no. 2, pp. 607–613, 2007.

[64] C. Thilmann, K. H. Grosser, B. Rhein, A. Zabel, M. Wannenmacher, and J. Debus, "Virtueller Bolus zur inversen Bestrahlungsplanung bei intensitätsmodulierter Radiotherapie des Mammakarzinoms im Rahmen der adjuvanten Therapie," *Strahlentherapie und Onkologie*, vol. 178, no. 3, pp. 139–146, 2002.

[65] V. Jacob, W. Bayer, S. T. Astner, R. Busch, and P. Kneschaurek, "A planning comparison of dynamic IMRT for different collimator leaf thicknesses with helical tomotherapy and RapidArc for prostate and head and neck tumors," *Strahlentherapie und Onkologie*, vol. 186, no. 9, pp. 502–510, 2010.

[66] D. Van Gestel, C. van Vliet-Vroegindeweij, F. Van den Heuvel, W. Crijns, A. Coelmont, B. De Ost, A. Holt, E. Lamers, Y. Geussens, S. Nuyts *et al.*, "RapidArc, SmartArc and TomoHD compared with classical step and shoot and sliding window intensity modulated radiotherapy in an oropharyngeal cancer treatment plan comparison," *Radiation Oncology*, vol. 8, no. 1, p. 37, 2013.

[67] T.-F. Lee, H.-M. Ting, P.-J. Chao, and F.-M. Fang, "Dual arc volumetric-modulated arc radiotherapy (VMAT) of nasopharyngeal carcinomas: a simultaneous integrated

boost treatment plan comparison with intensity-modulated radiotherapies and single arc VMAT," *Clinical Oncology*, vol. 24, no. 3, pp. 196–207, 2012.

[68] S. Webb, "Use of a quantitative index of beam modulation to characterize dose conformality: illustration by a comparison of full beamlet IMRT, few-segment IMRT (fsIMRT) and conformal unmodulated radiotherapy," *Physics in medicine and biology*, vol. 48, no. 14, p. 2051, 2003.

[69] R. Mohan, M. Arnfield, S. Tong, Q. Wu, and J. Siebers, "The impact of fluctuations in intensity patterns on the number of monitor units and the quality and accuracy of intensity modulated radiotherapy," *Medical physics*, vol. 27, no. 6, pp. 1226–1237, 2000.

[70] C. K. McGarry, C. D. Chinneck, M. M. O'Toole, J. M. O'Sullivan, K. M. Prise, and A. R. Hounsell, "Assessing software upgrades, plan properties and patient geometry using intensity modulated radiation therapy (IMRT) complexity metrics," *Medical physics*, vol. 38, no. 4, pp. 2027–2034, 2011.

[71] S. Crowe, T. Kairn, J. Kenny, R. Knight, B. Hill, C. M. Langton, and J. Trapp, "Treatment plan complexity metrics for predicting IMRT pre-treatment quality assurance results," *Australasian physical & engineering sciences in medicine*, vol. 37, no. 3, pp. 475–482, 2014.

[72] D. Craft, P. Süss, and T. Bortfeld, "The tradeoff between treatment plan quality and required number of monitor units in intensity-modulated radiotherapy," *International Journal of Radiation Oncology • Biology • Physics*, vol. 67, no. 5, pp. 1596–1605, 2007.

[73] A. L. McNiven, M. B. Sharpe, and T. G. Purdie, "A new metric for assessing IMRT modulation complexity and plan deliverability," *Medical physics*, vol. 37, no. 2, pp. 505–515, 2010.

[74] A. Bertelsen, C. R. Hansen, J. Johansen, and C. Brink, "Single arc volumetric modulated arc therapy of head and neck cancer," *Radiotherapy and Oncology*, vol. 95, no. 2, pp. 142–148, 2010.

[75] B. Liu, J. Adamson, A. Rodrigues, F. Zhou, F.-f. Yin, and Q. Wu, "A novel technique for VMAT QA with EPID in cine mode on a Varian TrueBeam linac," *Physics in medicine and biology*, vol. 58, no. 19, p. 6683, 2013.

[76] G. Heilemann, B. Poppe, and W. Laub, "On the sensitivity of common gamma-index evaluation methods to MLC misalignments in Rapidarc quality assurance," *Medical physics*, vol. 40, no. 3, 2013.

[77] W. Liu, S. H. Patel, D. P. Harrington, Y. Hu, X. Ding, J. Shen, M. Y. Halyard, S. E. Schild, W. W. Wong, G. E. Ezzell *et al.*, "Exploratory study of the association of volumetric modulated arc therapy (VMAT) plan robustness with local failure in head and neck cancer," *Journal of Applied Clinical Medical Physics*, 2017.

[78] N. Lee, C. Chuang, J. M. Quivey, T. L. Phillips, P. Akazawa, L. J. Verhey, and P. Xia, "Skin toxicity due to intensity-modulated radiotherapy for head-and-neck carcinoma," *International Journal of Radiation Oncology • Biology • Physics*, vol. 53, no. 3, pp. 630–637, 2002.

[79] S. W. Hadley, "Effects of immobilization mask material on surface dose," *Journal of Applied Clinical Medical Physics*, vol. 6, no. 1, 2005.

[80] The Mathworks, Inc, "Reading Arbitrary Format Text Files with TEXTSCAN," 2017, retrieved May 26 2017. [Online]. Available: https://se.mathworks.com/help/matlab/examples/reading-arbitrary-format-text-files-with-textscan.html

A Appendix

A.1 Supplements to H&N Radiotherapy Treatment at UNN

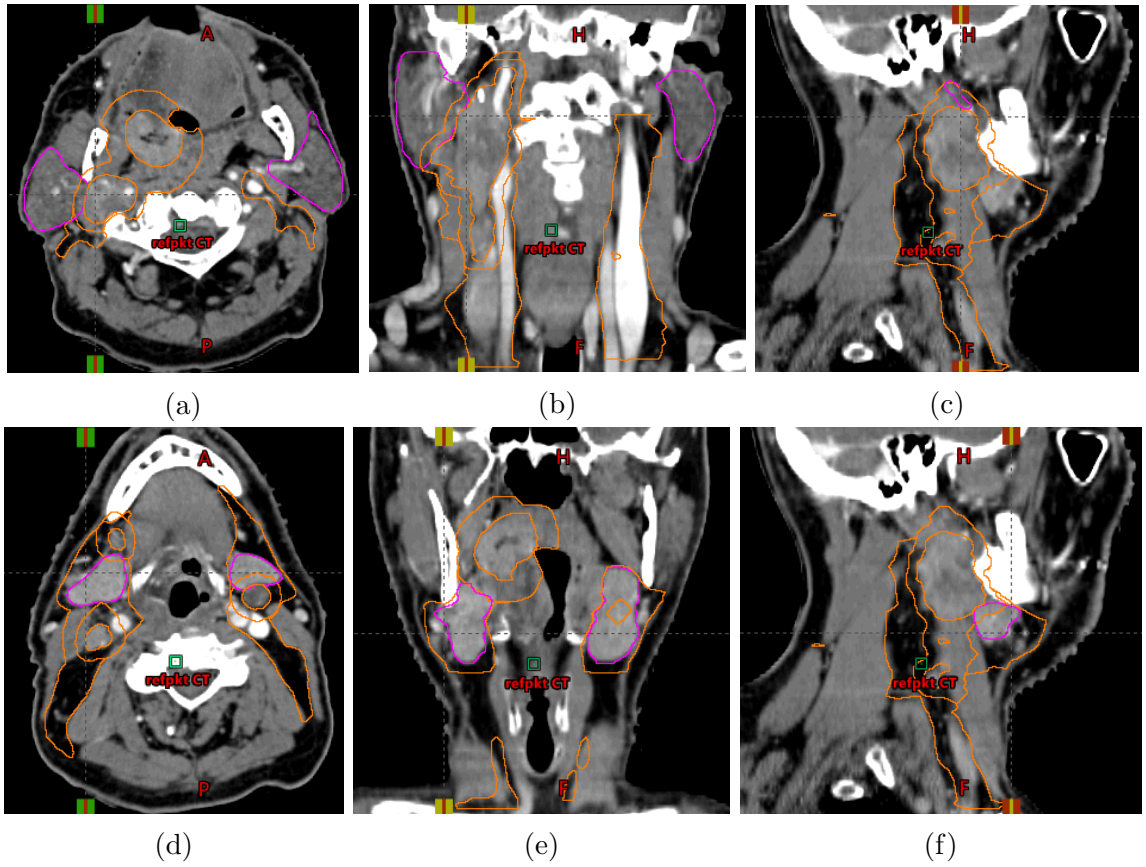

(a) (b) (c)

(d) (e) (f)

Figure 37: All three ITV's are shown in orange and in (a). (b) and (c) the parotid glands shown in pink. in (d). (e) and (f). the submandibular glands are shown in pink.

A.2 Uncertainty Plans

(a) Mean of uncertainty plans, D_{98} of ITV52.

	Original	Optimized with bolus	
	Mean	Mean	p-value
Unperturbed plan	97.27	97.27	0.628
+1 mm ML-direc.	97.23	97.27	0.669
−1 mm ML-direc.	97.26	97.25	0.609
+1 mm CC-direc.	97.19	97.27	0.689
−1 mm CC-direc.	97.31	97.27	0.552
+1 mm AP-direc.	97.37	97.30	0.551
−1 mm AP-direc.	97.16	97.19	0.609
+2 mm ML-direc.	97.18	97.18	0.569
−2 mm ML-direc.	97.23	97.18	0.515
+2 mm CC-direc.	97.12	97.22	0.702
−2 mm CC-direc.	97.31	97.23	0.497
+2 mm AP-direc.	97.42	97.32	0.462
−2 mm AP-direc.	97.04	97.10	0.570
+5 mm ML-direc.	96.67	96.60	0.552
−5 mm ML-direc.	96.83	96.65	0.453
+5 mm CC-direc.	96.71	96.87	0.773
−5 mm CC-direc.	97.11	96.84	0.351
+5 mm AP-direc.	97.45	97.21	0.296
−5 mm AP-direc.	96.51	96.52	0.497

(b) Mean of uncertainty plans, D_{98} of ITV64.

	Original	Optimized with bolus	
	Mean	Mean	p-value
Unperturbed plan	99.19	99.86	0.182
+1 mm ML-direc.	99.06	99.77	0.103
−1 mm ML-direc.	99.13	99.76	0.296
+1 mm CC-direc.	99.08	99.76	0.188
−1 mm CC-direc.	99.13	99.79	0.203
+1 mm AP-direc.	99.14	99.84	0.124
−1 mm AP-direc.	99.18	99.81	0.199
+2 mm ML-direc.	98.69	99.54	0.057
−2 mm ML-direc.	98.87	99.54	0.336
+2 mm CC-direc.	98.79	99.55	0.178
−2 mm CC-direc.	98.87	99.56	0.124
+2 mm AP-direc.	99.06	99.71	0.172
−2 mm AP-direc.	99.09	99.73	0.236
+5 mm ML-direc.	96.32	97.52	0.013
−5 mm ML-direc.	96.74	97.61	0.148
+5 mm CC-direc.	96.54	97.65	0.071
−5 mm CC-direc.	96.67	97.30	0.160
+5 mm AP-direc.	98.11	98.61	0.668
−5 mm AP-direc.	98.33	98.98	0.221

(a) Mean of uncertainty plans, D_{98} of ITV68.

	Original	Optimized with bolus	
	Mean	Mean	p-value
Unperturbed plan	96.47	97.43	0.056
+1 mm ML-direc.	96.39	97.39	0.019
−1 mm ML-direc.	96.45	97.41	0.071
+1 mm CC-direc.	96.36	97.35	0.051
−1 mm CC-direc.	96.49	97.45	0.042
+1 mm AP-direc.	96.37	97.31	0.073
−1 mm AP-direc.	96.51	97.47	0.067
+2 mm ML-direc.	96.28	97.27	0.011
−2 mm ML-direc.	96.39	97.35	0.094
+2 mm CC-direc.	96.20	97.21	0.057
−2 mm CC-direc.	96.48	97.35	0.047
+2 mm AP-direc.	96.24	97.15	0.101
−2 mm AP-direc.	96.47	97.45	0.034
+5 mm ML-direc.	95.61	96.61	0.006
−5 mm ML-direc.	95.82	96.65	0.330
+5 mm CC-direc.	95.36	96.40	0.055
−5 mm CC-direc.	95.86	96.61	0.066
+5 mm AP-direc.	95.62	96.32	0.400
−5 mm AP-direc.	96.00	96.75	0.157

(a) Mean of uncertainty plans, $D_{\max}$ of spinal cord.

	Original	Optimized with bolus	
	Mean	Mean	p-value
Unperturbed plan	46.30	44.46	0.017
+1 mm ML-direc.	46.47	44.55	0.013
−1 mm ML-direc.	46.29	44.48	0.016
+1 mm CC-direc.	46.87	45.15	0.010
−1 mm CC-direc.	45.91	43.88	0.006
+1 mm AP-direc.	46.25	44.60	0.046
−1 mm AP-direc.	46.29	44.41	0.012
+2 mm ML-direc.	46.72	44.81	0.013
−2 mm ML-direc.	46.53	44.62	0.008
+2 mm CC-direc.	47.58	46.23	0.034
−2 mm CC-direc.	45.87	43.44	0.000
+2 mm AP-direc.	46.51	44.90	0.034
−2 mm AP-direc.	46.32	44.43	0.016
+5 mm ML-direc.	47.99	46.25	0.003
−5 mm ML-direc.	47.02	45.57	0.115
+5 mm CC-direc.	50.75	50.68	0.988
−5 mm CC-direc.	45.91	42.59	0.000
+5 mm AP-direc.	46.98	45.73	0.149
−5 mm AP-direc.	46.36	44.59	0.009

(b) Mean of uncertainty plans, $D_{\max}$ of spinal cord PRV.

	Original	Optimized with bolus	
	Mean	Mean	p-value
Unperturbed plan	49.14	48.48	0.235
+1 mm ML-direc.	49.34	48.84	0.446
−1 mm ML-direc.	48.95	48.25	0.296
+1 mm CC-direc.	50.33	50.07	0.923
−1 mm CC-direc.	48.18	47.03	0.091
+1 mm AP-direc.	49.22	48.54	0.235
−1 mm AP-direc.	49.16	48.42	0.366
+2 mm ML-direc.	49.70	49.28	0.751
−2 mm ML-direc.	49.04	48.23	0.367
+2 mm CC-direc.	51.71	51.68	0.989
−2 mm CC-direc.	47.60	45.80	0.004
+2 mm AP-direc.	49.34	48.62	0.211
−2 mm AP-direc.	49.14	48.50	0.382
+5 mm ML-direc.	51.28	50.61	0.258
−5 mm ML-direc.	49.94	48.96	0.252
+5 mm CC-direc.	55.50	55.58	0.967
−5 mm CC-direc.	47.23	44.22	0.000
+5 mm AP-direc.	49.68	48.98	0.288
−5 mm AP-direc.	49.05	48.60	0.599

(a) Mean of uncertainty plans, D_{mean} of right parotid gland.

	Original	Optimized with bolus	
	Mean	Mean	p-value
Unperturbed plan	24.33	34.44	$3.052{\cdot}10^{-4}$
+1 mm ML-direc.	23.43	33.78	$4.272{\cdot}10^{-4}$
−1 mm ML-direc.	25.28	35.11	$3.052{\cdot}10^{-4}$
+1 mm CC-direc.	24.07	34.28	$4.272{\cdot}10^{-4}$
−1 mm CC-direc.	24.64	34.59	$3.052{\cdot}10^{-4}$
+1 mm AP-direc.	25.37	35.34	$4.272{\cdot}10^{-4}$
−1 mm AP-direc.	23.32	33.52	$3.052{\cdot}10^{-4}$
+2 mm ML-direc.	22.57	33.13	$4.272{\cdot}10^{-4}$
−2 mm ML-direc.	26.27	35.78	$3.052{\cdot}10^{-4}$
+2 mm CC-direc.	23.84	34.13	$4.272{\cdot}10^{-4}$
−2 mm CC-direc.	24.98	34.74	$3.052{\cdot}10^{-4}$
+2 mm AP-direc.	26.42	36.23	$4.272{\cdot}10^{-4}$
−2 mm AP-direc.	22.33	32.59	$3.052{\cdot}10^{-4}$
+5 mm ML-direc.	20.29	31.31	0.001
−5 mm ML-direc.	29.42	37.86	$1.831{\cdot}10^{-4}$
+5 mm CC-direc.	23.38	33.64	$4.272{\cdot}10^{-4}$
−5 mm CC-direc.	26.16	35.16	$1.831{\cdot}10^{-4}$
+5 mm AP-direc.	29.64	38.77	$8.545{\cdot}10^{-4}$
−5 mm AP-direc.	19.53	29.78	$3.052{\cdot}10^{-4}$

(b) Mean of uncertainty plans, D_{mean} of left parotid gland.

	Original	Optimized with bolus	
	Mean	Mean	p-value
Unperturbed plan	21.69	30.13	0.002
+1 mm ML-direc.	22.44	30.69	0.002
−1 mm ML-direc.	20.98	29.57	0.002
+1 mm CC-direc.	21.32	29.89	0.002
−1 mm CC-direc.	22.10	30.36	0.002
+1 mm AP-direc.	22.63	31.00	0.002
−1 mm AP-direc.	20.78	29.25	0.002
+2 mm ML-direc.	23.22	31.26	0.002
−2 mm ML-direc.	20.29	29.03	0.002
+2 mm CC-direc.	20.97	29.66	0.002
−2 mm CC-direc.	22.54	30.60	0.002
+2 mm AP-direc.	23.59	31.87	0.002
−2 mm AP-direc.	19.89	28.37	0.002
+5 mm ML-direc.	25.70	32.97	0.001
−5 mm ML-direc.	18.51	27.47	0.002
+5 mm CC-direc.	20.16	28.98	0.002
−5 mm CC-direc.	24.03	31.31	0.002
+5 mm AP-direc.	26.54	34.41	0.002
−5 mm AP-direc.	17.39	25.76	0.002

(a) Mean of uncertainty plans, D_{mean} of right submandibular gland.

	Original	Optimized with bolus	
	Mean	Mean	p-value
Unperturbed plan	56.29	58.72	0.042
+1 mm ML-direc.	55.93	58.40	0.034
−1 mm ML-direc.	56.69	59.02	0.027
+1 mm CC-direc.	55.73	58.26	0.064
−1 mm CC-direc.	56.85	59.15	0.027
+1 mm AP-direc.	56.08	58.45	0.042
−1 mm AP-direc.	56.51	58.97	0.027
+2 mm ML-direc.	55.59	58.07	0.034
−2 mm ML-direc.	57.10	59.32	0.027
+2 mm CC-direc.	55.15	57.79	0.092
−2 mm CC-direc.	57.37	59.55	0.016
+2 mm AP-direc.	55.88	58.17	0.042
−2 mm AP-direc.	56.73	59.20	0.034
+5 mm ML-direc.	54.79	57.05	0.064
−5 mm ML-direc.	58.45	60.13	0.110
+5 mm CC-direc.	53.36	56.22	0.176
−5 mm CC-direc.	58.82	60.61	0.021
+5 mm AP-direc.	55.29	57.27	0.092
−5 mm AP-direc.	57.37	59.80	0.052

(b) Mean of uncertainty plans, D_{mean} of left submandibular gland.

	Original	Optimized with bolus	
	Mean	Mean	p-value
Unperturbed plan	50.52	54.17	0.010
+1 mm ML-direc.	50.72	54.42	0.010
−1 mm ML-direc.	50.37	53.93	0.008
+1 mm CC-direc.	49.69	53.67	0.006
−1 mm CC-direc.	51.32	54.65	0.010
+1 mm AP-direc.	50.56	54.13	0.010
−1 mm AP-direc.	50.51	54.22	0.010
+2 mm ML-direc.	50.97	54.68	0.010
−2 mm ML-direc.	50.27	53.70	0.006
+2 mm CC-direc.	48.83	53.14	0.003
−2 mm CC-direc.	52.07	55.09	0.027
+2 mm AP-direc.	50.63	54.10	0.013
−2 mm AP-direc.	50.53	54.26	0.008
+5 mm ML-direc.	51.98	55.48	0.021
−5 mm ML-direc.	50.27	53.09	0.033
+5 mm CC-direc.	46.16	51.43	0.005
−5 mm CC-direc.	54.06	56.24	0.040
+5 mm AP-direc.	50.98	53.99	0.013
−5 mm AP-direc.	50.73	54.43	0.008

A.3 γ Index

The VMAT plans has two arcs which are called field 1 and field 2.

Table 16: Local γ index with DTA = 3 mm and DD = 3%

Patient	Original			Optimized with bolus		
number	Sum	Field 1	Field 2	Sum	Field 1	Field 2
1	91.1	94.8	95.4	95.9	95.5	97.9
2	91.3	93.7	94.4	99.3	99.4	97.8
3	87.9	96	93.7	86	90.9	94.2
4	97.2	97.6	97	97.2	98.5	98.1
5	99.9	100	100	97.2	96.2	96.2
6	95.7	97.5	97.7	97.5	98.3	96.2
7	98.6	99	97.8	99.2	98.5	98.4
8	97.4	99.2	98.4	94.8	92.1	97.6
9	91.2	96.9	93.9	92.9	97.4	96.5
10	98.9	99.6	96.7	99	99.7	99.1
11	95.7	97.5	97.9	99	98.7	97.7
12	98.7	98.4	98.7	97.5	97.6	96.7
13	99.1	98.9	99.7	98.8	99.3	98.7
14	99.6	99.3	97.4	99.6	99.5	99.5
15	98.1	97.6	99	98.6	97.9	99.1

Table 17: Local γ index with DTA = 3 mm and DD = 3%

Patient	Original			Intermediate			Simultaneous			Sequential		
number	Sum	Field 1	Field 2	Sum	Field 1	Field 2	Sum	Field 1	Field 2	Sum	Field 1	Field 2
1	91.1	94.8	95.4	95.9	97.2	95	93	95.5	95.1	90.6	94.9	92.9
2	91.3	93.7	94.4	99.1	98.2	97.9	97.6	97.1	96.4	98.1	96.5	96
3	87.9	96	93.7	90.8	89.2	95.2	86.6	89.9	94.7	89.7	88.8	95.4
4	97.2	97.6	97	93.8	96.1	96.5	98.8	99.1	97.5	95	97.3	95.7
5	99.9	100	100	97.6	98.2	97.4	98.2	98.7	97.8	99	98.4	98.3
6	95.7	97.5	97.7	98.7	99.9	98.7	99.6	99.9	99.1	97.9	98.3	97.2
7	98.6	99	97.8	99.1	99.8	99	99.5	99.1	99.4	99.5	99.5	99
8	97.4	99.2	98.4	98.7	97.6	98.6	97.4	97.8	98.3	98.8	97.5	99
9	91.2	96.9	93.9	97.2	97.7	98.8	86.9	89.7	93.8	95.3	90.3	98.3
10	98.9	99.6	96.7	99.9	99.9	100	99.7	99.9	98.8	99.7	100	99.4
11	95.7	97.5	97.9	99.9	100	100	100	100	100	96.2	96.7	98.6
12	98.7	98.4	98.7	99.7	99.8	98.7	98.7	97.9	97.4	99.8	99.4	100
13	99.1	98.9	99.7	99.4	98.9	99.2	99.3	99	99.3	99.3	99.2	99.1
14	99.6	99.3	97.4	99.1	99.1	99.1	99	99.2	99.6	99.7	99.6	99.6
15	98.1	97.6	99	99.8	99.1	99.1	99.4	99.8	99.5	100	99.4	99.1

Table 18: Global γ index with DTA = 2 mm and DD = 2%

Patient	Original			Optimized with bolus		
number	Sum	Field 1	Field 2	Sum	Field 1	Field 2
1	86.3	93.9	91.5	90.7	95.7	96.2
2	81	93.3	92.1	97.4	99.5	97.7
3	79.5	96	95.4	75.6	87.1	93.4
4	95.5	99.5	96.1	94.5	98.6	98.7
5	97.4	99.6	97.2	93.7	97	95.5
6	92.3	98.4	94.9	96.2	99.1	97.8
7	97.9	99.2	97.3	97.9	99.4	98.2
8	92.1	98.5	93.1	89.7	96	96.7
9	83.9	97.7	89.8	86	97.9	97.2
10	98.5	99.6	99.4	98.9	99.9	99.4
11	93.5	98.7	96.7	97.2	99.5	99
12	98.4	99.7	99.7	97.6	97.8	98.5
13	97.9	98.9	99.5	99.6	99.8	99
14	98.6	99.9	99.8	98.3	99.6	98.8
15	95.8	98.7	98.4	98.8	99.4	99.7

Table 19: Global γ index with DTA = 2 mm and DD = 2%

Patient	Original			Intermediate			Simultaneous			Sequential		
number	Sum	Field 1	Field 2	Sum	Field 1	Field 2	Sum	Field 1	Field 2	Sum	Field 1	Field 2
1	86.3	93.9	91.5	88.5	94	92.6	88.4	94.8	92.3	81.8	92	89.1
2	81	93.3	92.1	96.1	99.4	98.6	94.7	98.7	95.7	95.1	99	98
3	79.5	96	95.4	81	90.5	96.7	76.8	89.6	93.3	79.6	88.5	96.9
4	95.5	99.5	96.1	92.2	96	98.6	97.4	99.1	99.2	91.3	97.2	97.8
5	97.4	99.6	97.2	96.8	99.3	99	97.3	98.4	98.6	97.6	99.8	99.5
6	92.3	98.4	94.9	98.9	99.7	97.8	99.5	99.6	99.2	97.6	99.5	97.6
7	97.9	99.2	97.3	99.3	99.2	99.1	99.1	99.2	98.7	99.2	99.1	98.3
8	92.1	98.5	93.1	97	98.2	98.2	94.3	99	97.4	96.8	98.5	98.6
9	83.9	97.7	89.8	95.4	99.4	98.5	77.2	89.8	94.9	89.6	95.4	99.1
10	98.5	99.6	99.4	99.9	99.7	99.7	99.1	100	98.4	99.7	99.9	99.3
11	93.5	98.7	96.7	97.8	99.6	99.3	96.5	98.6	99.3	94.4	98.6	99.1
12	98.4	99.7	99.7	99.4	99.7	98.5	99.4	97.4	98.5	99.1	99.5	99.5
13	97.9	98.9	99.5	99.9	100	99.7	98.4	99.5	99.3	99.9	100	99.8
14	98.6	99.9	99.8	98.4	99.7	98.8	97.3	100	99	99.5	100	99.5
15	95.8	98.7	98.4	99.1	99.8	99.4	99.7	99.9	100	99.7	99.9	99.5

Table 20: Local γ index with DTA = 2 mm and DD = 2%

Patient	Original			Optimized with bolus		
number	Sum	Field 1	Field 2	Sum	Field 1	Field 2
1	67.4	80.1	79.2	74.9	83.4	84
2	65.9	79.3	75.9	89.4	91.8	90.4
3	57.7	81.1	75.2	46.9	61	66.5
4	83.1	90.1	89.9	81	88.4	89.1
5	97.4	99.6	97.2	79.4	88.2	82.4
6	78.5	86.1	85.5	82.5	90.7	82.1
7	85.4	90.6	82.7	89.7	90.9	88.1
8	85.3	91.2	89.5	73.9	75.1	83.2
9	70.6	86.4	77.8	73.1	83.7	84.2
10	90.3	95.6	83.8	92.7	95.4	92.7
11	80.6	90.8	88.8	88.4	92.4	87.6
12	89.7	89.8	92.4	80.8	86.7	85.7
13	91.3	92.8	94.2	91.2	93.9	93.4
14	95	95.2	90.4	94	92	95.4
15	83.1	89	89	90	90.5	92.9

Table 21: Local γ index with DTA = 2 mm and DD = 2%

Patient	Original			Intermediate			Simultaneous			Sequential		
number	Sum	Field 1	Field 2	Sum	Field 1	Field 2	Sum	Field 1	Field 2	Sum	Field 1	Field 2
1	67.4	80.1	79.2	77.1	84.3	81.5	72.2	82.1	80.8	63.5	77.1	74.5
2	65.9	79.3	75.9	88.9	87.2	88.2	75.9	87	83.7	84.1	83.9	84.7
3	57.7	81.1	75.2	52.5	57.7	79.1	50.4	65	70.3	59.2	60.3	82
4	83.1	90.1	89.9	73.1	79.9	84.9	90.6	94.5	91.1	73.9	84.1	83.9
5	97.4	99.6	97.2	85.9	88.4	91.9	85.9	90.3	91.4	89.7	91.4	92.9
6	78.5	86.1	85.5	91.2	95.8	86.8	93.8	94.6	93.4	82.9	90.4	83.8
7	85.4	90.6	82.7	93.4	94.2	92.1	91.7	92.3	91.2	91.5	94.2	91.9
8	85.3	91.2	89.5	87.7	85.9	94.9	85.5	84.7	89.9	86.5	84.2	90.8
9	70.6	86.4	77.8	86.8	85.7	94	86.9	89.7	93.8	95.3	90.3	98.3
10	90.3	95.6	83.8	97.3	97.1	94.9	93	97.6	91.7	98.3	98.9	95.1
11	80.6	90.8	88.8	92.9	92.2	92.4	86.4	90.2	90.1	81	84.5	88.9
12	89.7	89.8	92.4	96	97	93.6	88.4	88.7	89.3	94.2	95	94.8
13	91.3	92.8	94.2	93.7	94.5	95.7	92.1	92.6	95.4	95.6	96.9	95.9
14	95	95.2	90.4	93.2	95.7	94	90.8	93.3	94.7	95.1	96.4	96.8
15	83.1	89	89	95	95.7	93.3	95.3	93.9	95.9	96.6	96.3	94.1

Table 22: p-values found using Wilcoxon signed rank test comparing the γ index for the original plan to the plans with the simultaneous, sequential and intermediate optimization strategies.

	Original vs. Simultaneous	Original vs. Sequential	Original vs. Intermediate
Local 2/2 sum	0.083	0.064	0.040
Local 2/2 field 1	0.629	0.847	0.679
Local 2/2 field 2	0.034	0.050	0.017
Local 3/3 sum	0.210	0.032	0.027
Local 3/3 field 1	0.639	0.989	0.399
Local 3/3 field 2	0.124	0.193	0.065
Global 2/2 sum	0.095	0.025	0.005
Global 2/2 field 1	0.990	0.866	0.483
Global 2/2 field 2	0.027	0.012	0.002

A.4 Robustness Index

Table 23: The terms used in the calculation of the RI, as well as the RI, for the original plan.

				Original			
Patient Number	Flank [mm/CP]	Speed [mm/CP]	Island [1/CP]	Field size [$mm^2/10^2$]	MU [MU]	Opening [mm/CP]	RI [$mm^2 \cdot MU/CP$]
1	9.6	2.9	7.2	249	380	24.8	3.1
2	10.4	3.2	10	420	456	28	8.1
3	9.9	3.4	9.4	344	418	30	5.1
4	9.8	3.2	10.3	426	382	32.4	5.0
5	10.6	3.1	8.5	430	360	34.6	3.6
6	9.6	2.9	7.5	329	380	30.3	2.8
7	10.8	3.3	8.3	439	362	39.9	3.0
8	11	3.3	8.5	340	352	34.5	3.1
9	11.5	3.5	9.6	484	422	31.9	7.8
10	9.8	3	8.7	360	378	28.5	4.3
11	9.1	3.1	8.2	340	370	29.6	3.3
12	9.5	2.7	6.5	290	304	32.8	1.4
13	7.7	2.6	8.6	254	384	23	3.2
14	10.4	3.1	6.6	353	334	35.3	2.0
15	11.6	3.2	9.4	480	372	39.3	4.0

Table 24: The terms used in the calculation of the RI, as well as the RI, for the plan which was optimized with bolus.

				Optimized with bolus			
Patient Number	Flank [mm/CP]	Speed [mm/CP]	Island [1/CP]	Field size [$mm^2/10^2$]	MU [MU]	Opening [mm/CP]	RI [$mm^2 \cdot MU/CP$]
1	9.4	3	6.5	249	366	25.8	2.5
2	10.8	3.2	6.1	420	351	37.3	2.2
3	9.3	3.5	7.9	344	429	27.1	5.2
4	9.7	3.2	8.5	426	370	33.6	3.7
5	10.4	3.5	9.9	430	439	30.6	7.3
6	10.2	2.8	5.8	329.	308	36.6	1.3
7	11.3	3.2	5.7	439	307	47.1	1.3
8	10.2	3.1	5.8	340	313	38.8	1.3
9	11.8	3.4	6.1	484	335	40.5	2.4
10	9.5	3	6.8	360	316	34.5	1.9
11	9.4	2.9	5.8	340	475	32.7	2.4
12	9.6	2.9	7.3	290	319	30.4	2.0
13	8.7	2.8	6.8	254	346	25.8	2.2
14	10.5	3.1	6.1	353	321	35.8	1.8
15	12.5	3	6.4	480	280	52	1.2

Table 25: The terms used in the calculation of the RI, as well as the RI, for the simultaneous plan.

				Simultaneous			
Patient Number	Flank [mm/CP]	Speed [mm/CP]	Island [1/CP]	Field size [$mm^2/10^2$]	MU [MU]	Opening [mm/CP]	RI [$mm^2 \cdot MU/CP$]
1	9.3	2.9	6.6	249	381	24.7	2.8
2	10.9	3	6.1	420	347	38.2	2.0
3	9.4	3.4	7.3	344	416	28.8	4.0
4	10.6	3.2	8.7	426	351	35.5	3.5
5	11	3.2	7.9	430	381	34.3	3.9
6	9.9	2.7	5	329	330	35.9	1.1
7	12.3	3.2	5.5	439	306	49.9	1.2
8	10.9	3.1	5.9	340	320	39	1.4
9	12.3	3.4	6.6	484	345	40.8	2.8
10	10.1	3	6.1	360	304	36.1	1.6
11	9.6	3	5.5	340	340	33	1.7
12	10	2.9	6.7	290	320	30.7	1.9
13	8.7	2.8	7.2	254	363	26	2.4
14	11	3.1	6.5	353	337	35	2.2
15	12.8	2.8	6.1	480	273	54.7	1.0

Table 26: The terms used in the calculation of the robustness index RI, as well as the RI, for the sequential plan.

				Sequential			
Patient Number	Flank [mm/CP]	Speed [mm/CP]	Island [1/CP]	Field size [$mm^2/10^2$]	MU [MU]	Opening [mm/CP]	RI [$mm^2 \cdot MU/CP$]
1	10.3	2.8	4.7	249	291	33.7	0.9
2	10.9	3.1	5.4	420	355	38.4	1.8
3	10	3.2	5.5	344	347	36.2	1.6
4	10.1	3.1	6.9	426	295	43.9	1.4
5	10.3	3.3	5.5	430	309	40.2	1.5
6	9.8	2.4	3.9	329	268	44.7	0.4
7	12.1	3.2	5.1	439	292	53	0.9
8	10.2	3.1	5.1	340	304	42.7	0.9
9	12.9	3.4	5.2	484	330	42.6	2.0
10	10.9	3.2	5.8	360	321	36.4	1.8
11	10.2	3.2	5.2	340	317	36.9	1.3
12	9.2	3.1	5.4	290	283	35.9	1.0
13	9.4	2.5	4.6	254	269	35.9	0.6
14	10.5	3.2	5.2	353	304	39.6	1.2
15	11.7	3	5.2	480	259	58.5	0.7

Table 27: The terms used in the calculation of the RI, as well as the RI, for the intermediate plan.

Intermediate							
Patient Number	Flank $[\text{mm/CP}]$	Speed $[\text{mm/CP}]$	Island $[1/\text{CP}]$	Field size $[\text{mm}^2/10^2]$	MU $[\text{MU}]$	Opening $[\text{mm/CP}]$	RI $[\text{mm}^2 \cdot \text{MU/CP}]$
1	9.9	3	4.7	249	300	32.9	1.0
2	11	3.3	5.6	420	364	37.5	2.2
3	9.9	3.5	5.7	344	353	35.5	1.9
4	9.9	3.1	6.7	426	284	45	1.2
5	10.2	3.4	5.5	430	316	39.4	1.7
6	10	2.6	3.9	329	270	43	0.5
7	12	3.2	5	439	288	53.2	0.9
8	10.4	3.3	5.1	340	300	43.5	0.9
9	12.4	3.5	5.5	484	324	42.1	2.1
10	8.8	2.7	3.9	360	258	49.5	0.3
11	10.3	3.3	5.2	340	316	37.1	1.4
12	9.4	3.1	5.5	290	286	35.4	1.1
13	9.4	2.5	4.6	254	266	36.1	0.6
14	10.8	3.3	5	353	306	39	1.3
15	11.5	3.1	5.5	480	268	56.3	0.8

A.5 Optimization Objectives

Table 28: Patient 1

	Objective	Volume [%]	Dose [Gy]	Priority
Brain stem PRV	Upper	0	37	90
Spinal cord PRV	Upper	0.0	39	50
ITV52	Lower	100	52	130
ITV64	Lower	100	64	130
ITV68	Lower	100	68	130
PTV68	Upper	0.3	70	130
	Lower	100	68	130
Z-PTV52	Upper	0	54	130
	Lower	100	50	140
Z-PTV64	Upper	0	66	130
	Lower	100	62	140
Z-Ring 10	Upper	3.7	53.4	80
	Upper	15	45.9	80
	Upper	24.5	40.9	80
	Upper	38.5	33.8	80
	Upper	79.0	23.8	80
Z-zzz	Upper	0	40	90
	Upper	10.5	36.1	80
	Upper	20.6	33.0	70

Table 29: Patient 2

	Objective	Volume [%]	Dose [Gy]	Priority
Spinal cord	Upper	0	47	120
Spinal cord PRV	Upper	0	49	120
ITV68	Lower	100	67	130
Z-PTV52	Upper	0	54	120
	Lower	100	51	160
Z-PTV64	Upper	0	66	120
	Lower	100	62	140
Z-PTV68	Upper	0	70	120
	Lower	100	66	140
Dose 107%	Upper	0	67	120
Z-Body	Upper	15	15	50
	Upper	0	20	50
	Upper	20	10	50

Table 30: Patient 3

	Objective	Volume [%]	Dose [Gy]	Priority
Spinal cord	Upper	0	43	50
Spinal cord PRV	Upper	0	49	100
Z-PTV52	Upper	0	54	120
	Lower	100	51	170
Z-PTV64	Upper	0	66	120
	Lower	100	62	140
PTV68	Upper	0	70	120
	Lower	100	65	140
Z-Body	Upper	0	30	80
Z-Ring	Upper	0	45	100
	Upper	51.2	31.0	50
	Upper	27.7	40.7	90
	Upper	80.0	46.3	50

Table 31: Patient 4

	Objective	Volume [%]	Dose [Gy]	Priority
Mandible	Upper	0	65	80
Spinal cord PRV	Upper	0	49	90
Z-Parotid gland right	Upper	0	30	80
Z-Parotid gland left	Upper	0	30	80
ITV52	Lower	100	52	130
ITV64	Lower	100	64	130
ITV68	Lower	100	68	130
PTV68	Upper	0	69	125
	Lower	100	67	125
Z-PTV52 +1mm	Upper	0	53	120
	Lower	100	51	120
Z-PTV64 +1mm	Upper	0	65	125
	Lower	100	63	125
Z-Body - PTV	Upper	0	40	60
	Upper	10	25	60
	Upper	15	15	50

Table 32: Patient 5

	Objective	Volume [%]	Dose [Gy]	Priority
Spinal cord	Upper	0	46	130
Spinal cord PRV	Upper	0	48	130
Z-Parotid gland right	Upper	0	23	70
Z-Parotid gland left	Upper	0	20	90
ITV52	Lower	0	50	140
Z-PTV52 + 2 mm	Upper	0	53	100
	Lower	100	51	160
Z-PTV64 + 2 mm	Upper	0	64	110
	Lower	100	62	110
Z-PTV68	Upper	0	70	110
	Lower	100	67	100
Z-Body - PTV	Upper	0	50	90
	Upper	10	45	70
Dose 70Gy	Upper	0	70	90
Helping volume	Upper	0	45	90

Table 33: Patient 6

	Objective	Volume [%]	Dose [Gy]	Priority
Spinal cord	Upper	0	48	100
Spinal cord PRV	Upper	0	49	110
PTV68	Upper	0	68	120
	Lower	100	65	110
Z-Munnhule - PTV52	Upper	0	35	90
Z-PTV52	Upper	0	54	120
	Lower	100	50	140
Z-PTV64	Upper	0	66	120
	Lower	100	62	120
Helping contour	Upper	0	45	70

Table 34: Patient 7

	Objective	Volume [%]	Dose [Gy]	Priority
Brain stem	Upper	0	45	90
Spinal cord	Upper	0	44	90
Spinal cord PRV	Upper	0	46	90
ITV52	Upper	100	51.5	130
ITV64	Upper	100	63.5	130
ITV68	Upper	100	68.5	130
PTV68	Upper	0	69	120
	Lower	100	67	120
Z-PTV52	Upper	0	53	120
	Lower	100	51	120
Z-PTV64	Upper	0	65	120
	Lower	100	63	120
Z-Body52	Upper	10	16	100
	Upper	40	2	100
	Upper	0	42	100
	Upper	20	8	100
Z-Body64	Upper	10	43.0	100
	Upper	40	11.5	100
	Upper	0	55	100
	Upper	20	34	100
	Upper	50	5	100

Table 35: Patient 8

	Objective	Volume [%]	Dose [Gy]	Priority
Brain stem	Upper	0	50	90
Brain stem PRV	Upper	0	55	90
Spinal cord PRV	Upper	0	48	90
ITV52	Lower	100	52	130
ITV64	Lower	100	64	130
ITV68	Lower	100	68	130
Z-PTV52	Upper	0	54	120
	Lower	100	52	125
Z-PTV64	Upper	0	65	120
	Lower	100	63	120
Z-PTV68	Upper	0	70	120
	Lower	100	68	120
Z-Body	Upper	0	30	50
	Upper	10	20	50
	Upper	15	15	50

Table 36: Patient 9

	Objective	Volume [%]	Dose [Gy]	Priority
Spinal cord	Upper	0	48	80
Spinal cord PRV	Upper	0	50	100
ITV52	Lower	100	51	130
ITV68	Lower	100	67	130
Z-PTV52	Upper	0	54	120
	Lower	100	51	140
Z-PTV64	Upper	0	66	120
	Lower	100	61	130
PTV68	Upper	0	70	120
	Lower	100	64	130
Z-bakspar	Upper	0	40	90
Z-Body-PTV	Upper	10	25	80
	Upper	20	10	50
	Upper	15	15	50

Table 37: Patient 10

	Objective	Volume [%]	Dose [Gy]	Priority
Mandible	Upper	0	68	70
Spinal cord PRV	Upper	0	48	90
ITV52	Lower	100	52	130
ITV64	Lower	100	64	130
ITV68	Lower	100	68	130
Z-PTV52 + 1 mm	Upper	0	56	120
	Lower	100	51	125
Z-PTV64 + 1 mm	Upper	0	65	120
	Lower	100	63	120
Z-PTV68 + 1 mm	Upper	0	69	120
	Lower	100	67	120
Z-Body-PTV	Upper	15	18	50
	Upper	10	28	50
	Upper	0	40	60

Table 38: Patient 11

	Objective	Volume [%]	Dose [Gy]	Priority
Spinal cord PRV	Upper	0	50	80
Z-PTV52	Upper	0	54	120
	Lower	100	50	150
Z-PTV64	Upper	0	66	120
	Lower	100	62	130
Z-PTV68	Upper	0	70	120
	Lower	100	65	130
Z-Body	Upper	15	15	50
	Upper	0	20	50
	Upper	20	10	50

Table 39: Patient 12

	Objective	Volume [%]	Dose [Gy]	Priority
Spinal cord	Upper	0	48	100
Spinal cord PRV	Upper	0	50	100
Z-Parotid gland right	Upper	0	28	90
Z-Parotis gland left	Upper	0	26	90
Z-PTV52 + 2 mm	Upper	0	54	150
	Lower	100	52	250
Z-PTV64 + 2 mm	Upper	0	65	200
	Lower	100	63	160
Z-PTV68 + 2 mm	Upper	0	69	200
	Lower	100	68	200
Body	Upper	10	30	80
Dose 69	Upper	0	69	160
Dose 70	Upper	0	70	140
Helping contour2	Upper	0	25	120
Helping contour	Upper	0	35	100

Table 40: Patient 13

	Objective	Volume [%]	Dose [Gy]	Priority
Brain stem PRV	Upper	10	45	90
Spinal cord PRV	Upper	0	42	90
Temporal lapp	Upper	0	25	85
Z Larynx	Upper	0	30	90
ITV52	Lower	100	51.5	130
ITV64	Lower	100	63.5	130
ITV68	Lower	100	67.5	130
Z-PTV52	Upper	0	53	120
	Lower	100	51	120
Z-PTV64	Upper	0	65	120
	Lower	100	63	120
PTV68	Upper	0	69	120
	Lower	100	67	120
Z-Body	Upper	0	48	70
	Upper	10	25	70
	Upper	15	18	70
Z-Body52	Upper	0	38	70
	Upper	10	15.4	70
	Upper	15	7.5	70

Table 41: Patient 14

	Objective	Volume [%]	Dose [Gy]	Priority
Spinal cord PRV	Upper	0	45	80
Z Parotid gland right	Upper	0	20	45
Z Parotid gland left	Upper	0	25	60
ITV52	Lower	0	52	145
ITV64	Lower	0	64	140
ITV68	Lower	0	68	140
Z-PTV52	Upper	0	54	140
	Lower	100	50	140
Z-PTV64	Upper	0	66	130
	Lower	100	62	140
PTV68	Upper	0	70	130
	Lower	100	67	140
Z-Body	Upper	0	30	50

Table 42: Patient 15

	Objective	Volume [%]	Dose [Gy]	Priority
Brain stem	Upper	0	50	80
Spinal cord	Upper	0	47	100
Spinal cord PRV	Upper	0	48	200
Z-PTV52	Upper	0	54	120
	Lower	100	50	150
Z-PTV64	Upper	0	66	120
	Lower	100	61	130
PTV68	Upper	0	70	120
	Lower	100	65	130
Z-Back help	Upper	0	47	200
Z-Body	Upper	10	25	50
	Upper	15	20	50
	Upper	25	10	50

A.6 Matlab Functions and Scripts

A.6.1 Extract Data

```
% This function is used in all the other scripts.
% It extracts data from .txt files and separates all the structures into blocks.
function [Data, Structure, HeaderLines, NumRows, NumCols, NumBlocks]=ExtractData(s)

fileID = fopen(s,'r');
Intro = textscan(fileID,'%s',15,'Delimiter','\n');
Block = 1;
Structure = textscan(fileID,'%s',18,'Delimiter','\n');
NumCols = 3;
while (~feof(fileID))
   InputText = textscan(fileID,'%s',1,'delimiter','\n');
   HeaderLines{Block,1} = InputText{1};
   FormatString = '%f%f%f';
   InputText = textscan(fileID,FormatString,'delimiter',',');
   Data{Block,1} = cell2mat(InputText);
   [NumRows,NumCols] = size(Data{Block});
   Block = Block+1;
end
Data=Data(~cellfun('isempty',Data));
fclose(fileID);
NumBlocks = Block-1;

end
```

This script is based on the script in [80].

A.6.2 Fix Header

```
% This function, or variants of this function is used in all the other scripts.
% It removes all the headerlines from the .txt file, except the names of the structures.
function Temp = FixHeader(Structure, HeaderLines, NumBlocks)
Temp=HeaderLines;
for i = 1:NumBlocks
    if ismember('Relative dose [%]       Dose [Gy] Ratio of Total Structure Volume [%]',Temp{i});
        Temp{i} = [];
    elseif ismember('Dose [Gy]   Relative dose [%] Ratio of Total Structure Volume [%]',Temp{i});
        Temp{i} = [];
    elseif ismember('Course:',Temp{i});
        Temp{i} = [];
    elseif ismember('Dose Cover.[%]:',Temp{i});
        Temp{i} = [];
    elseif ismember('Sampling Cover.[%]:',Temp{i});
        Temp{i} = [];
    elseif ismember('Approval Status: Approved',Temp{i});
        for i0=0:14 %i0~=3 is used for FixHeaderVolume, i0~=8 is used for FixHeaderMean
            %if i0~=10 is used for FixHeaderMedian, i0~=7 is used for FixHeaderMax
            %Temp{i+i0} = [];
            %end
        Temp{i+i0} = [];
        end
    elseif ismember('Approval Status: Unapproved',Temp{i});
        for i1=0:14 %i1~=3 is used for FixHeaderVolume, i1~=8 is used for FixHeaderMean
            %if i1~=10 is used for FixHeaderMedian, i1~=7 is used for FixHeaderMax
            %Temp{i+i1} = [];
            %end
        Temp{i+i1} = [];
        end
    else
        Temp{i}=Temp{i};
    end
end
Temp=Temp(~cellfun('isempty',Temp));
%Temp=[Structure{1,1}(6);Temp]; used for FixHeaderVolume
%Temp=[Structure{1,1}(10);Temp]; used for FixHeaderMedian, FixHeaderMean, FixHeaderMax
Temp=[Structure{1,1}(2);Temp];
% This last part is used for the uncertainty plans.
%k=1;
%n=(2*length(Data))/42;
%for m=1:n;
%    for j=k:2:(k+38)
%        Temp{j}=[Temp{j+1},Temp{j}];
%        Temp{j+1}=[];
%    end
%k=k+3+38;
%end
end
```

A.6.3 Extract and Plot D_{98} of ITV52, see figure 22

```
% This script calculates D98 of ITV52 for both the original plan and plan optimized with bolus.
% The same script is used to calculated D98 of PTV, where ITV is replaced by PTV.
% The same script is used for all the other plans, only the input file is changed.
s1='pas';
s2='_dvh_org.txt';
for n=1:15
[Data, Structure, HeaderLines, NumRows, NumCols, NumBlocks]=ExtractData(strcat(s1,num2str(n),s2));
Temp=FixHeader(Structure, HeaderLines, NumBlocks);
eval(sprintf('PatientOrg%d=[Temp Data]',n));
T=length(Temp);
    for j = 1:T
    % The volume and dose columns from the ITV structure is retrieved.
    % Multiply by 100 and divide by 52 to convert from absolute dose [Gy] to relative dose [%].
        if ismember('Structure: ITV 0-52Gy',Temp{j});
            eval(sprintf('Yo%d = PatientOrg%d{%d,2}(:,3)', n,n,j)); % Volume
            eval(sprintf('Xo%d = (100*PatientOrg%d{%d,2}(:,2))./52',n,n,j)); % Dose
        break;
        elseif ismember('Structure: ITV52Gy',Temp{j});
            eval(sprintf('Yo%d = PatientOrg%d{%d,2}(:,3)', n,n,j)); % Volume
            eval(sprintf('Xo%d = (100*PatientOrg%d{%d,2}(:,2))./52',n,n,j)); % Dose
        break;
        end
    end
end
s3='_dvh_bolus.txt';
for n = 1:15
[Data, Structure, HeaderLines, NumRows, NumCols, NumBlocks]=ExtractData(strcat(s1,num2str(n),s3));
Temp=FixHeader(Structure, HeaderLines, NumBlocks);
eval(sprintf('PatientBolus%d=[Temp Data]',n));
T=length(Temp);
    for j = 1:T
    % The volume and dose columns from the PTV structure is retrieved.
    % Multiply by 100 and divide by 52 to convert from absolute dose [Gy] to relative dose [%].
        if ismember('Structure: ITV 0-52Gy',Temp{j});
            eval(sprintf('Yb%d = PatientBolus%d{%d,2}(:,3)', n,n,j)); % Volume
            eval(sprintf('Xb%d = (100*PatientBolus%d{%d,2}(:,2))./52',n,n,j)); % Dose
            break;
        elseif ismember('Structure: ITV52Gy',Temp{j});
            eval(sprintf('Yb%d = PatientBolus%d{%d,2}(:,3)', n,n,j)); %Volume
            eval(sprintf('Xb%d = (100*PatientBolus%d{%d,2}(:,2))./52',n,n,j)); % Dose
        break;
        end
    end
end
% To make the column vectors the same length.
for u=1:15
    eval(sprintf('Yb%d=[Yb%d;zeros([1110-length(Yb%d) 1])]',u,u,u));
    eval(sprintf('Yo%d=[Yo%d;zeros([1110-length(Yo%d) 1])]',u,u,u));
    eval(sprintf('Xb%d=[Xb%d;zeros([1110-length(Xb%d) 1])]',u,u,u));
    eval(sprintf('Xo%d=[Xo%d;zeros([1110-length(Xo%d) 1])]',u,u,u));
end
```

```
Yb=[Yb1 Yb2 Yb3 Yb4 Yb5 Yb6 Yb7 Yb8 Yb9 Yb10 Yb11 Yb12 Yb13 Yb14 Yb15];
Yo=[Yo1 Yo2 Yo3 Yo4 Yo5 Yo6 Yo7 Yo8 Yo9 Yo10 Yo11 Yo12 Yo13 Yo14 Yo15];

diff1=zeros([15 1]);
index1=zeros([15 1]);
diff2=zeros([15 1]);
index2=zeros([15 1]);
for i=1:15
% Finds the index at 98% of the volume.
    [diff1(i),index1(i)] = min(abs(Yo(:,i)-98.0));
% Retrieves the dose value at the previously found index.
    eval(sprintf('D98org52(%d)=Xo%d(index1(%d))',i,i,i));
    [diff2(i),index2(i)] = min(abs(Yb(:,i)-98.0));
    eval(sprintf('D98bolus52(%d)=Xb%d(index1(%d))',i,i,i));
end

% Repeated for ITV64 and ITV68, where Xo and Xb is divided by 64 and 68 respectively.

% p-values are calculated using the built in Matlab function signrank which represent
% Wilcoxon signed rank test.
p_52=signrank(D98org52,D98bolus52);
p_64=signrank(D98org64,D98bolus64);
p_68=signrank(D98org68,D98bolus68);
% Median values are calculated using the built in Matlab function median
median_org52=median(D98org52);
median_bol52=median(D98bolus52);
median_org64=median(D98org64);
median_bol64=median(D98bolus64);
median_org68=median(D98org68);
median_bol68=median(D98bolus68);

YMatrix1=[D98org52;D98bolus52;D98org64;D98bolus64;D98org68;D98bolus68];

% The last part of the script, from here, is used to plot all the figures in this thesis,
% only the vectors in YMatrix1 and the names are changed.
set(0,'DefaultAxesFontName', 'CMU Serif')
figure1 = figure;
axes1 = axes('Parent',figure1);
hold(axes1,'on');
f=ones(18,1)*95;
ff=plot(0:0.5:8.5,f);
Y=transpose(YMatrix1);
plot1=boxplot(Y);
set(ff,'Color',[0 0 0],'LineStyle',':');
uistack(plot1(:,:), 'top')
uistack(ff,'bottom')
ax = gca;
ax.XAxis.TickLabelInterpreter = 'latex';
ax.YAxis.TickLabelInterpreter = 'latex';
set(axes1,'XTick',[1 2 3 4 5 6],'XTickLabel',...
    {'Org.','Bolus','Org.','Bolus','Org.','Bolus'},'Fontsize',11);
ylabel('${D}_{98}$ [\%]','FontSize',16,'FontName','CMU Serif','Interpreter','latex');
box(axes1,'on');
```

A.6.4 Extract $D_{\max}$ of Spinal Cord, see figure 23 (a)

```
% The maximum dose printed in the header of the .txt file is retrieved for the spinal cord
% in the original plan.
s1='pas';
s2='_dvh_org.txt';
for n=[1,2,3,4,5,6,7,9,10,11,12,13,14,15]
[Data, Structure, HeaderLines, NumRows, NumCols, NumBlocks]=ExtractData(strcat(s1,num2str(n),s2));
Temp=FixHeaderMax(Structure, HeaderLines, NumBlocks);
T=length(Temp);
% Multiply by 68 and divide by 100 to convert from relative dose [%] to absolute dose [Gy]
    for j = 1:T
        if ismember('Structure: Medulla',Temp{j});
            [Beg,Number]=strsplit(char(Temp{j+1}),': ');
            eval(sprintf('MaxOrg(%d)=(68.*str2num(Beg{2}))./100',n));
        break;
        elseif ismember('Structure: SpinalCord',Temp{j});
            [Beg,Number]=strsplit(char(Temp{j+1}),': ');
            eval(sprintf('MaxOrg(%d)=(68.*str2num(Beg{2}))./100',n));
        break;
        end
    end
end

for n=8
[Data, Structure, HeaderLines, NumRows, NumCols, NumBlocks]=ExtractData(strcat(s1,num2str(n),s2));
Temp=FixHeaderMax(Structure, HeaderLines, NumBlocks);
T=length(Temp);
% Multiply by 70 (patient 8 has a prescription of 70Gy) and divide by 100 to convert from
% relative dose [%] to absolute dose [Gy]
    for j = 1:T
        if ismember('Structure: Medulla',Temp{j});
            [Beg,Number]=strsplit(char(Temp{j+1}),': ');
            eval(sprintf('MaxOrg(%d)=(70.*str2num(Beg{2}))./100',n));
        break;
        end
    end
end
% Repeated for spinal cord PRV in the original plan.
% Further, by changing s2 to the name of the .txt file of the plan which was optimized with bolus,
% spinal cord and spinal cord PRV is retrieved.
% The same script is used for the other plans, by changing the inputfile.

% Wilcoxon signed rank test is applied.
p_spi=signrank(MaxOrg,MaxBolus);
p_prv=signrank(MaxOrgPRV,MaxBolusPRV);
```

A.6.5 Extract D_{mean} of Right Parotid Gland, see figure 23 (b)

```
% The mean value printed in the header of the .txt file is retrieved for the right
% parotid gland in the original plan.
% The exact same code is used for submandibular gland, only the names of the structures are changed.
s1='pas';
s2='_dvh_org.txt';
for  n=[1,2,3,4,5,6,7,9,10,11,12,13,14,15]
[Data, Structure, HeaderLines, NumRows, NumCols, NumBlocks]=ExtractData(strcat(s1,num2str(n),s2));
Temp=FixHeaderMean(Structure, HeaderLines, NumBlocks);
T=length(Temp);
% Multiply by 68 and divide by 100 to convert from relative dose [%] to absolute dose [Gy].
    for j = 1:T
        if ismember('Structure: Parotis ho',Temp{j});
            [Beg,Number]=strsplit(char(Temp{j+1}),': ');
            eval(sprintf('MeanOrgR(%d)=(68.*str2num(Beg{2}))./100',n));
        break;
        elseif ismember('Structure: ParotidGland_R',Temp{j});
            [Beg,Number]=strsplit(char(Temp{j+1}),': ');
            eval(sprintf('MeanOrgR(%d)=(68.*str2num(Beg{2}))./100',n));
        break;
        elseif ismember('Structure: ParotidGland_ R',Temp{j});
            [Beg,Number]=strsplit(char(Temp{j+1}),': ');
            eval(sprintf('MeanOrgR(%d)=(68.*str2num(Beg{2}))./100',n));
        break;
        end
    end
end
%Patient 8 has a prescription of 70Gy
for  n=8
[Data, Structure, HeaderLines, NumRows, NumCols, NumBlocks]=ExtractData(strcat(s1,num2str(n),s2));
Temp=FixHeaderMean(Structure, HeaderLines, NumBlocks);
T=length(Temp);
    for j = 1:T
         if ismember('Structure: Parotis ho',Temp{j});
            [Beg,Number]=strsplit(char(Temp{j+1}),': ');
            eval(sprintf('MeanOrgR(%d)=(70.*str2num(Beg{2}))./100',n));
         break;
         end
    end
end
% Repeated for left parotid gland in the original plan, and for right and left parotid
% gland in the plan optimized with bolus.
% Further, by changing the inputfile, the same script is used for all the other plans.

% Wilcoxon signed rank test is applied
p_R=signrank(MeanOrgR,MeanBolusR);
p_L=signrank(MeanOrgL,MeanBolusL);

YMatrix1=[MeanOrgR;MeanBolusR;MeanOrgL;MeanBolusL];
Y=transpose(YMatrix1);
```

A.6.6 Extract and Calculate CI and HI for PTV52, see table 4

```
% CI and HI are calculated for PTV52 in the original plan.
% Calculations are equivalent for PTV64 and PTV68, but the structure names are changed and
% Xo is divided by 64 and 68, respectively. The scripts are also equal for PTV52, PTV64 and
% PTV68 in the plan which was optimized with bolus.
s1='pas';
s2='_dvh_org.txt';
for k=1:15
[Data, Structure, HeaderLines, NumRows, NumCols, NumBlocks]=ExtractData(strcat(s1,num2str(k),s2));
Temp=FixHeader(Structure, HeaderLines, NumBlocks);
eval(sprintf('PatientOrg%d=[Temp Data]',k));
T=length(Temp);
    for j = 1:T
    % The volume and dose columns from the PTV structure is retrieved.
    % Multiply by 100 and divide by 52 to convert from absolute dose [Gy] to relative dose [%].
        if ismember('Structure: PTV 0-52Gy',Temp{j});
            eval(sprintf('Yo%d = PatientOrg%d{%d,2}(:,3)', k,k,j)); % Volume
            eval(sprintf('Xo%d = (100*PatientOrg%d{%d,2}(:,2))./52',k,k,j)); % Dose
        break;
        elseif ismember('Structure: PTV52Gy',Temp{j});
            eval(sprintf('Yo%d = PatientOrg%d{%d,2}(:,3)', k,k,j)); % Volume
            eval(sprintf('Xo%d = (100*PatientOrg%d{%d,2}(:,2))./52',k,k,j)); % Dose
        break;
        end
    end
end
% To make the column vectors the same length.
for u=1:15
    eval(sprintf('Yo%d=[Yo%d;zeros([1110-length(Yo%d) 1])]',u,u,u));
    eval(sprintf('Xo%d=[Xo%d;zeros([1110-length(Xo%d) 1])]',u,u,u));
end
Yo=[Yo1 Yo2 Yo3 Yo4 Yo5 Yo6 Yo7 Yo8 Yo9 Yo10 Yo11 Yo12 Yo13 Yo14 Yo15];
Xo=[Xo1 Xo2 Xo3 Xo4 Xo5 Xo6 Xo7 Xo8 Xo9 Xo10 Xo11 Xo12 Xo13 Xo14 Xo15];

% The median dose [%] to the PTV is retrieved
for n = 1:15
[Data, Structure, HeaderLines, NumRows, NumCols, NumBlocks]=ExtractData(strcat(s1,num2str(n),s2));
Temp=FixHeaderMedian(Structure, HeaderLines, NumBlocks);
T=length(Temp);
    for j = 1:T
        if ismember('Structure: PTV 0-52Gy',Temp{j});
            [beg,number]=strsplit(char(Temp{j+1}),': ');
            eval(sprintf('MedOrg(%d)=str2num(beg{2})',n));
        break;
        elseif ismember('Structure: PTV52Gy',Temp{j});
            [beg,number]=strsplit(char(Temp{j+1}),': ');
            eval(sprintf('MedOrg(%d)=str2num(beg{2})',n));
        break;
        end
    end
end
% The volume and dose columns from the body structure is retrieved.
```

```
for n=1:15
[Data, Structure, HeaderLines, NumRows, NumCols, NumBlocks]=ExtractData(strcat(s1,num2str(n),s2));
Temp=FixHeader(Structure, HeaderLines, NumBlocks);
T=length(Temp);
    for j = 1:T
    % Multiply by 100 and divide by 52 to convert from absolute dose [Gy] to relative dose [%].
        if ismember('Structure: BODY',Temp{j});
            eval(sprintf('YBo%d = PatientOrg%d{%d,2}(:,3)', n,n,j));  % Volume
            eval(sprintf('XBo%d = (100*PatientOrg%d{%d,2}(:,2))./52',n,n,j)); % Dose
        break;
        end
    end
end
% To make the column vectors the same length.
for u=1:15
    eval(sprintf('YBo%d=[YBo%d;zeros([1110-length(YBo%d) 1])]',u,u,u));
    eval(sprintf('XBo%d=[XBo%d;zeros([1110-length(XBo%d) 1])]',u,u,u));
end
YBo=[YBo1 YBo2 YBo3 YBo4 YBo5 YBo6 YBo7 YBo8 YBo9 YBo10 YBo11 YBo12 YBo13 YBo14 YBo15];
XBo=[XBo1 XBo2 XBo3 XBo4 XBo5 XBo6 XBo7 XBo8 XBo9 XBo10 XBo11 XBo12 XBo13 XBo14 XBo15];

% The PTV volume [cm^3] is retrieved.
for n=1:15
[Data, Structure, HeaderLines, NumRows, NumCols, NumBlocks]=ExtractData(strcat(s1,num2str(n),s2));
Temp=FixHeaderVolume(Structure, HeaderLines, NumBlocks);
T=length(Temp);
    for j = 1:T
        if ismember('Structure: PTV 0-52Gy',Temp{j});
            [beg,number]=strsplit(char(Temp{j+1}),': ');
            eval(sprintf('VolumePTV(%d)=str2num(beg{2})',n));
        break;
        elseif ismember('Structure: PTV52Gy',Temp{j});
            [beg,number]=strsplit(char(Temp{j+1}),': ');
            eval(sprintf('VolumePTV(%d)=str2num(beg{2})',n));
        break;
        end
    end
end
% Volume of the body structure [cm^3] is retrieved.
for n=1:15
[Data, Structure, HeaderLines, NumRows, NumCols, NumBlocks]=ExtractData(strcat(s1,num2str(n),s2));
Temp=FixHeaderVolume(Structure, HeaderLines, NumBlocks);
T=length(Temp);
    for j = 1:T
        if ismember('Structure: BODY',Temp{j});
            [beg,number]=strsplit(char(Temp{j+1}),': ');
            eval(sprintf('VolumeBody(%d)=str2num(beg{2})',n));
        break;
        end
    end
end

for h=1:15
    % D98 is found
    [diff1(h),index1(h)] = min(abs(Yo(:,h)-98.0));
```

```
    eval(sprintf('D98org(%d)=Xo(index1(%d),%d)',h,h,h));
    % D2 is found
    [diff2(h),index2(h)] = min(abs(Yo(:,h)-2.0));
    eval(sprintf('D2org(%d)=Xo(index2(%d),%d)',h,h,h));
    % HI is calculated
    eval(sprintf('HI(%d)=(D2org(%d)-D98org(%d))/MedOrg(%d)',h,h,h,h));
    % Volume of PTV [%] receiving 95% dose
    eval(sprintf('[diff3(%d),index3(%d)]=min(abs(Xo(:,%d)-95))',h,h,h));
    eval(sprintf('V95(%d)=Yo(index3(%d),%d)',h,h,h));
    % Volume of body [%] receiving 95% dose
    eval(sprintf('[diff4(%d),index4(%d)]=min(abs(XBo(:,%d)-95))',h,h,h));
    eval(sprintf('VB95(%d)=YBo(index4(%d),%d)',h,h,h));
end

% Median, maximum and minimum values are calculated
median_HI=median(HI);
max_HI=max(HI);
min_HI=max(HI);

for i=1:15
    % Volume of body [%] receiving 95% dose times total volume of body [cm^3]
    VBody95(i)=(VB95(i)*VolumeBody(i))/100;
    % Volume of PTV [%] receiving 95% dose times total volume of PTV [cm^3]
    VPTV95(i)=(V95(i)*VolumePTV(i))/100;
    % CI is calculated
    CI(i)=((VPTV95(i)).^2)./(VolumePTV(i).*VBody95(i));
end

% Median, maximum and minimum values are calculated
median_CI=median(CI);
max_CI=max(CI);
min_CI=min(CI);
% Wilcoxon signed rank test is applied.
p_CI=signrank(CI,CIB);
p_HI=signrank(HI,HIB);
% HIB and CIB is from the equivalent script for the plan which was optimized with bolus
```

A.6.7 Extract Uncertainty Plans for D_{98} of ITV52, see figure 26 (a)

```
% D98 is calculated for all the uncertainty plans of ITV52.
% The same script is used for ITV64, ITV68, PTV52, PTV64 and PTV68, in both the original plan
% and the plan optimized with bolus.
s1='pas';
s2='_dvh_uncert_orginalplan.txt';
Yun=zeros([1220,10*21]);
Xun=zeros([1220,10*21]);
for s = 1:15
[Data, Structure, HeaderLines, NumRows, NumCols, NumBlocks]=ExtractData(strcat(s1,num2str(s),s2));
Temp=FixHeader(Data, Structure, HeaderLines, NumBlocks);
eval(sprintf('PasientUncertOrg%d=[Temp Data]',s));
T=length(Temp);
    for q = 1:T
    % The volume and dose columns from the ITV structure is retrieved for the unperturbed plan
    % and all the uncertainty plans (here 21 in total).
    % Multiply by 100 and divide by 52 to convert from absolute dose [Gy] to relative dose [%].
        if ismember('Structure: ITV 0-52Gy',Temp{q});
            for p=0:20;
                eval(sprintf('Yun%d = PasientUncertOrg%d{%d,2}(:,3)',p,s,q+p)); % Volume
                eval(sprintf('Xun%d = (100*PasientUncertOrg%d{%d,2}(:,2))./52',p,s,q+p)); % Dose
                % To make the column vectors the same length.
                eval(sprintf('Yun%d=[Yun%d;zeros([1220-length(Yun%d) 1])]',p,p,p));
                eval(sprintf('Xun%d=[Xun%d;zeros([1220-length(Xun%d) 1])]',p,p,p));
            end
            Yun(:,((s-1)*21+1):s*21)=[Yun0,Yun1,Yun2,Yun3,Yun4,Yun5,Yun6,Yun7,Yun8,Yun9,...
            Yun10,Yun11,Yun12,Yun13,Yun14,Yun15,Yun16,Yun17,Yun18,Yun19,Yun20];
            Xun(:,((s-1)*21+1):s*21)=[Xun0,Xun1,Xun2,Xun3,Xun4,Xun5,Xun6,Xun7,Xun8,Xun9,...
            Xun10,Xun11,Xun12,Xun13,Xun14,Xun15,Xun16,Xun17,Xun18,Xun19,Xun20];
            break;
        elseif ismember('Structure: ITV52Gy',Temp{q});
            for p=0:20;
                eval(sprintf('Yun%d = PasientUncertOrg%d{%d,2}(:,3)',p,s,q+p)); % Volume
                eval(sprintf('Xun%d = (100*PasientUncertOrg%d{%d,2}(:,2))./52',p,s,q+p)); % Dose
                % To make the column vectors the same length.
                eval(sprintf('Yun%d=[Yun%d;zeros([1220-length(Yun%d) 1])]',p,p,p));
                eval(sprintf('Xun%d=[Xun%d;zeros([1220-length(Xun%d) 1])]',p,p,p));
            end
            Yun(:,((s-1)*21+1):s*21)=[Yun0,Yun1,Yun2,Yun3,Yun4,Yun5,Yun6,Yun7,Yun8,Yun9,...
            Yun10,Yun11,Yun12,Yun13,Yun14,Yun15,Yun16,Yun17,Yun18,Yun19,Yun20];
            Xun(:,((s-1)*21+1):s*21)=[Xun0,Xun1,Xun2,Xun3,Xun4,Xun5,Xun6,Xun7,Xun8,Xun9,...
            Xun10,Xun11,Xun12,Xun13,Xun14,Xun15,Xun16,Xun17,Xun18,Xun19,Xun20];
            break;
        end
    end
end

for f=1:21*15
    % Finds the index at 98% of the volume.
    eval(sprintf('[diff1(%d),index1(%d)]=min(abs(Yun(:,%d)-98))',f,f,f));
    % Retrieves the dose value at the previously found index.
    eval(sprintf('D98un(%d)=Xun(index1(%d),%d)',f,f,f));
```

```
end
for h=1:15
    eval(sprintf('D98uncer%d=D98un(((%d-1)*21+1):%d*21)',h,h,h));
end

% The order of the uncertainty plans was wrong, and is corrected here.
D98uncer4(1,22)=D98uncer4(1,14);
D98uncer4(1,23)=D98uncer4(1,15);
for a=14:19
    D98uncer4(1,a)=D98uncer4(1,a+2);
end
D98uncer4(1,20)=D98uncer4(1,22);
D98uncer4(1,21)=D98uncer4(1,23);
D98uncer4(1,23)=0;
D98uncer4(1,22)=0;
D98uncer4=D98uncer4(D98uncer4~=0);

% This vector is used further for plotting.
D98=[D98uncer1;D98uncer2;D98uncer3;D98uncer4;D98uncer5;D98uncer6;D98uncer7;D98uncer8;D98uncer9;
    D98uncer10;D98uncer11;D98uncer12;D98uncer13;D98uncer14;D98uncer15];

% The width of the uncertainty plot is calculated.
width=zeros([15,1]);
for s=1:15
    width(s)=max(D98(s,1:19))-min(D98(s,1:19));
end
```

A.6.8 Extract Uncertainty Plans for $D_{\max}$ of Spinal Cord, see figure 27

```
% Calculating Dmax of the spinal cord for all the unperturbed, and all the uncertainty plans,
% the script is equivalent for spinal cord PRV, except that the structure name is changed.
% The script is also equivalent for the plan which was optimized with bolus.
s1='pas';
s2='_dvh_uncert_orginalplan.txt';
for i = 1:15
[Data, Structure, HeaderLines, NumRows, NumCols, NumBlocks]=ExtractData(strcat(s1,num2str(i),s2));
Temp=FiksHeader2(Data, Structure, HeaderLines, NumBlocks);
eval(sprintf('PatientOrg%d=[Temp Data]',i));
T=length(Temp);
    for j = 1:T
    % The volume and dose columns from the spinal cord structure is retrieved
    % for the unperturbed plan and all the uncertainty plans (here, 21 in total).
        if ismember('Structure: SpinalCord',Temp{j});
            for p=0:20
                eval(sprintf('V=PatientOrg%d{j+p,2}(:,3)',i));  % Volume [%]
                % Only non-zero elements are used.
                V=V(V~=0);
                eval(sprintf('D=PatientOrg%d{j+p,2}(:,2)',i)); % Dose [Gy]
                % Dose elements corresponding to zero volume is set to 0.
                D(length(V)+1:length(D),1)=0;
                % Only non-zero elements are used.
                D=D(D~=0);
                % The first element was a zero.
                D=[0;D];
                % Saves the Dmax for the 21 plans, it is the dose at the smallest non-zero
                % volume element.
                eval(sprintf('MaxOrg%d=(D(length(V),1))',p));
            end
            % Collecting Dmax for all the 15 patients, Max1 is for patient 1, etc.
            eval(sprintf('Max%d=[MaxOrg0 MaxOrg1 MaxOrg2 MaxOrg3 MaxOrg4 MaxOrg5 MaxOrg6
            MaxOrg7 MaxOrg8 MaxOrg9 MaxOrg10 MaxOrg11 MaxOrg12 MaxOrg13 MaxOrg14 MaxOrg15
            MaxOrg16 MaxOrg17 MaxOrg18 MaxOrg19 MaxOrg20]',i));
        break;
        end
        if ismember('Structure: Medulla',Temp{j});
            for p=0:20
                % Volume [%]
                eval(sprintf('V=PatientOrg%d{j+p,2}(:,3)',i));
                % Only non-zero elements are used.
                V=V(V~=0);
                % Dose [Gy]
                eval(sprintf('D=PatientOrg%d{j+p,2}(:,2)',i));
                % Dose elements corresponding to zero volume is set to 0.
                D(length(V)+1:length(D),1)=0;
                % Only non-zero elements are used.
                D=D(D~=0);
                % The first element was a zero
                D=[0;D];
                 % Saves the Dmax for the 21 plans, it is the dose at the smallest non-zero
                 % volume element.
```

```
                eval(sprintf('MaxOrg%d=(D(length(V),1))',p));
            end
            % Collecting Dmax for all the 15 patients, Max1 is for patient 1, etc.
            eval(sprintf('Max%d=[MaxOrg0 MaxOrg1 MaxOrg2 MaxOrg3 MaxOrg4 MaxOrg5 MaxOrg6
            MaxOrg7 MaxOrg8 MaxOrg9 MaxOrg10 MaxOrg11 MaxOrg12 MaxOrg13 MaxOrg14 MaxOrg15
            MaxOrg16 MaxOrg17 MaxOrg18 MaxOrg19 MaxOrg20]',i));
        break;
        end
   end
end

%The order of the uncertainty plans was wrong and needed correcting for patient 4.
Max4(1,22)=Max4(1,14);
Max4(1,23)=Max4(1,15);
for a=14:19
    Max4(1,a)=Max4(1,a+2);
end
Max4(1,20)=Max4(1,22);
Max4(1,21)=Max4(1,23);
Max4(1,23)=0;
Max4(1,22)=0;
Max4=Max4(Max4~=0);
MaxUn=[Max1; Max2; Max3; Max4; Max5; Max6; Max7; Max8; Max9; Max10; Max11; Max12; Max13; Max14;
Max15];
Y=transpose(MaxUn);

% Here only the 19 first plans are used.
X1=1:15;
for a=1:19
    plot1(a)=plot(X1,MaxUn(:,a));
    hold on;
end

% The width of the uncertainty plot is calculated.
clear s;
width=zeros([15,1]);
for s=1:15
    width(s)=max(MaxUn(s,1:19))-min(MaxUn(s,1:19));
end
```

A.6.9 Extract Uncertainty Plans for D_{mean} of Right Parotid Gland, see figure 28

```
% Calculating and plotting the mean dose of the right parotid gland.
% The script is equivalent for the left parotid gland and for the left and right submandibular
% glands. The mean dose is calculated using the mean value theorem for integrals approximated
% with Riemann sums. (Elements of V = 100% are removed to obtain a function D(V))
s1='pas';
s2='_dvh_uncert_orginalplan.txt';
Yun=zeros([1220,15*21]);
Xun=zeros([1220,15*21]);
for s = 1:15
[Data, Structure, HeaderLines, NumRows, NumCols, NumBlocks]=ExtractData(strcat(s1,num2str(s),s2));
Temp=FixHeader(Data, Structure, HeaderLines, NumBlocks);
eval(sprintf('PasientUncertOrg%d=[Temp Data]',s));
T=length(Temp);
    for q = 1:T
    % The volume and dose columns from the right parotid gland structure is retrieved for
    % the unperturbed plan and all the uncertainty plans (here, 21 in total).
        if ismember('Structure: ParotidGland_R',Temp{q});
            for p=0:20;
                eval(sprintf('V=PasientUncertOrg%d{q+p,2}(:,3)',s)); % Volume [%]
                % Only non-zero elements are used.
                V=V(V~=0);
                eval(sprintf('D=PasientUncertOrg%d{q+p,2}(:,2)',s)); % Dose [Gy]
                % Dose elements corresponding to zero volume is set to 0.
                D(length(V)+1:length(D),1)=0;
                % Only non-zero elements are used.
                D=D(D~=0);
                % The first element equals zero.
                D=[0;D];
                temp=0;
                counter=0;
                    % Integral approximation.
                    for i=1:(length(V)-1);
                        % Removes all elements of 100.
                        if V(i+1)~=100
                            % Adding one term to the sum.
                            temp=temp+D(i+1)*(V(i)-V(i+1));
                        else
                        % Counting the number of 100's
                        counter=counter+1;
                        end
                    end
                % Normalizing the integral
                temp=(1/(V(counter)-V(length(V))))*temp;
                % Saves the Dmean for all the 21 plans.
                eval(sprintf('Meanorg%d=temp',p));
            end
            % Collecting Dmean for all the 15 patients. Mean1 is for patient 1, etc.
            eval(sprintf('Mean%d=[Meanorg0 Meanorg1 Meanorg2 Meanorg3 Meanorg4 Meanorg5 Meanorg6
            Meanorg7 Meanorg8 Meanorg9 Meanorg10 Meanorg11 Meanorg12 Meanorg13 Meanorg14 Meanorg15
```

```
            Meanorg16 Meanorg17 Meanorg18 Meanorg19 Meanorg20]',s));
            break;
        end
        if ismember('Structure: Parotis ho',Temp{q});
            for p=0:20;
                eval(sprintf('V=PasientUncertOrg%d{q+p,2}(:,3)',s));  % Volume [%]
                % Only non-zero elements are used.
                V=V(V~=0);
                eval(sprintf('D=PasientUncertOrg%d{q+p,2}(:,2)',s)); % Dose [Gy]
                % Dose elements corresponding to 0 volume is set to zero.
                D(length(V)+1:length(D),1)=0;
                % Only non-zero elements are used.
                D=D(D~=0);
                % The first element equals zero.
                D=[0;D];
                temp=0;
                counter=0;
                    % Integral approximation.
                    for i=1:(length(V)-1);
                        % Removes all elements of 100.
                        if V(i+1)~=100
                        % Adding one term to the sum.
                        temp=temp+D(i+1)*(V(i)-V(i+1));
                        else
                        % Counting the number of 100's.
                        counter=counter+1;
                        end
                    end
                % Normalizing the integral.
                temp=(1/(V(teller)-V(length(V))))*temp;
                % Saves the Dmean for all the 21 plans.
                eval(sprintf('Meanorg%d=temp',p));
            end
            % Collecting Dmean for all the 15 patients. Mean1 is for patient 1, etc.
            eval(sprintf('Mean%d=[Meanorg0 Meanorg1 Meanorg2 Meanorg3 Meanorg4 Meanorg5 Meanorg6
            Meanorg7 Meanorg8 Meanorg9 Meanorg10 Meanorg11 Meanorg12 Meanorg13 Meanorg14 Meanorg15
            Meanorg16 Meanorg17 Meanorg18 Meanorg19 Meanorg20]',s));
          break;
        end
    end
end
%The order of the uncertainty plans was wrong and needed correcting for patient 4.
Mean4(1,22)=Mean4(1,14);
Mean4(1,23)=Mean4(1,15);
for a=14:19
Mean4(1,a)=Mean4(1,a+2);
end
Mean4(1,20)=Mean4(1,22);
Mean4(1,21)=Mean4(1,23);
Mean4(1,23)=0;
Mean4(1,22)=0;
Mean4=Mean4(Mean4~=0);
MeanUn=[Mean1; Mean2; Mean3; Mean4; Mean5; Mean6; Mean7; Mean8; Mean9; Mean10; Mean11;
        Mean12; Mean13; Mean14; Mean15];
```

```
% Here only the 19 first plans are used.
X1=1:15;
for a=1:19
    plot1(a)=plot(X1,MeanUn(:,a));
    hold on;
end

Y=transpose(MeanUn);

% The width of the uncertainty plot is calculated.
clear s;
width=zeros([15,1]);
for s=1:15
    width(s)=max(MeanUn(s,1:19))-min(MeanUn(s,1:19));
end
```

A.7 Scripts made by Camilla Hægeland

These scripts are used to calculate the Flank, Island, Speed and Opening terms of the RI.

A.7.1 Average Flank

```
using System;
using System.Linq;
using System.Windows;
using System.Windows.Controls;
using System.Collections;
using System.Collections.Generic;
using VMS.TPS.Common.Model.Types;
using VMS.TPS.Common.Model.API;
using System.Text;

namespace VMS.TPS
{
  class Script
  {
    public Script()
    {
    }

    public void Execute(ScriptContext context /*, System.Windows.Window window*/)
    {
      if (context.Patient == null)
      {
        MessageBox.Show("Please load a patient!");
        return;
      }

      int numBeams, indeksY1, indeksY2, islands, feil; //, numControlPts, numLeaves;
      numBeams = indeksY1 = indeksY2 = feil = islands = 0; // = numControlPts = numLeaves;

      //Liste for å registrere summen av flanken for MLC blad i hendholdvis venstre og høyre MLC bank
      //Summerer over hver enkelt beam/arc
      List<float> flankeLeft = new List<float>();
      List<float> flankeRight = new List<float>();

      //Summerer over alle beams/arcs
      List<float> AllflankeLeft = new List<float>();
      List<float> AllflankeRight = new List<float>();

      //Endelig gjennomsnitt
      List<float> AllFlanke = new List<float>();

      //Liste for å registrere totalt antall øyer for hver beam/arc
      List<int> øyer = new List<int>();
      List<double> AllØyer = new List<double>();

      // Display additional information. Use the active plan if available.
      PlanSetup CurrentPlan = context.PlanSetup != null ? context.PlanSetup : context.PlansInScope.ElementAt(0);

      foreach (var beam in CurrentPlan.Beams) //itererer gjennom alle beams
      {
            islands = 0; //setter antall øyer til 0 for hver beam/arc
            numBeams++;

            for(int i=0; i<beam.ControlPoints.Count; i++) //itererer gjennom alle kontrollpunktene i beam-en
            {
                islands = 0;
                //Finner plasseringen til Y1 og Y2 som tilsvarer MLC leaf posisjonen
                indeksY1 = Convert.ToInt32(beam.ControlPoints[i].JawPositions.Y1);
                indeksY2 = Convert.ToInt32(beam.ControlPoints[i].JawPositions.Y2);

                if (indeksY1<-100 && indeksY2>100){
                    indeksY1 = (200+indeksY1)/10 + 1;
                    indeksY2 = (indeksY2-100)/10 + 50;}
```

```
else if (indeksY1>-100 && indeksY2>100){
    indeksY1 = (100 + indeksY1)/5 + 11;
    indeksY2 = (indeksY2-100)/10 + 50;
}
else if (indeksY1<-100 && indeksY2<100){
    indeksY1 = (200+indeksY1)/10 + 1;
    indeksY2 = (100 + indeksY2)/5 + 10;
}
else{
    indeksY1 = (100 + indeksY1)/5 + 11;
    indeksY2 = (100 + indeksY2)/5 + 10;
}

//Går gjennom alle aktuelle MLC par fra og med Y1 til og med Y2. Y1-1 pga. første indeks starter som 0
for (int leafIndex = indeksY1-1; leafIndex < indeksY2; leafIndex++)
{
    float leafPositionLeft, leafPositionRight; //for å registrere venstre og høyre flanke for MLC parene

    //hvis lukket MLC par ([0,i]=[1,i]), finn eventuell flanke "over"
    if (beam.ControlPoints[i].LeafPositions[0,leafIndex] == beam.ControlPoints[i].LeafPositions[1,leafIndex])
    {
        if (beam.ControlPoints[i].LeafPositions[0,leafIndex+1] != beam.ControlPoints[i].LeafPositions[1,leafIndex+1])
        {
            if (beam.ControlPoints[i].LeafPositions[1,leafIndex+1] < beam.ControlPoints[i].LeafPositions[1,leafIndex])
            {
                flankeRight.Add(0); //høyre flanke
                leafPositionLeft = Math.Abs(beam.ControlPoints[i].LeafPositions[1,leafIndex+1] -
                beam.ControlPoints[i].LeafPositions[0,leafIndex+1]);
                flankeLeft.Add(leafPositionLeft); //venstre flanke
            }
            else if (beam.ControlPoints[i].LeafPositions[0,leafIndex+1] > beam.ControlPoints[i].LeafPositions[1,leafIndex])
            {
                flankeLeft.Add(0); //venstre flanke
                leafPositionRight = Math.Abs(beam.ControlPoints[i].LeafPositions[1,leafIndex+1] -
                beam.ControlPoints[i].LeafPositions[0,leafIndex+1]);
                flankeRight.Add(leafPositionRight); //høyre flanke
            }
            else
            {
                leafPositionRight = Math.Abs(beam.ControlPoints[i].LeafPositions[1,leafIndex] -
                beam.ControlPoints[i].LeafPositions[1,leafIndex+1]);
                flankeRight.Add(leafPositionRight); //høyre flanke
                leafPositionLeft = Math.Abs(beam.ControlPoints[i].LeafPositions[0,leafIndex] -
                beam.ControlPoints[i].LeafPositions[0,leafIndex+1]);
                flankeLeft.Add(leafPositionLeft); //venstre flanke
            }
        }
        else
        {
            flankeRight.Add(0);
            flankeLeft.Add(0);
        }
    }

    //hvis åpent felt ([0,i+1]<[1,i] & [0,i]<[1,i+1])
    else if (beam.ControlPoints[i].LeafPositions[0,leafIndex+1] < beam.ControlPoints[i].LeafPositions[1,leafIndex] &&
    beam.ControlPoints[i].LeafPositions[0,leafIndex] < beam.ControlPoints[i].LeafPositions[1,leafIndex+1])
    {
        leafPositionRight = Math.Abs(beam.ControlPoints[i].LeafPositions[1,leafIndex] -
        beam.ControlPoints[i].LeafPositions[1,leafIndex+1]);
        flankeRight.Add(leafPositionRight); //høyre flanke
        leafPositionLeft = Math.Abs(beam.ControlPoints[i].LeafPositions[0,leafIndex] -
        beam.ControlPoints[i].LeafPositions[0,leafIndex+1]);
        flankeLeft.Add(leafPositionLeft); //venstre flanke

        //siste MLC blad i feltet (i>Y2-1) & MLC paret ikke er lukket ([0,i] != [1,i]),
        //ELLER åpningen avsluttes pga lukket MLC par ([0,i+1] == [1,i+1])
        if (leafIndex >= indeksY2-1 && beam.ControlPoints[i].LeafPositions[0,leafIndex] !=
        beam.ControlPoints[i].LeafPositions[1,leafIndex] ||
        beam.ControlPoints[i].LeafPositions[0,leafIndex+1] == beam.ControlPoints[i].LeafPositions[1,leafIndex+1])
        {
                islands++;
        }
    }
```

```
//hvis overlapp ([0,i+1]<[1,i] & [0,i]>=[1,i+1])
else if (beam.ControlPoints[i].LeafPositions[0,leafIndex+1] < beam.ControlPoints[i].LeafPositions[1,leafIndex] &&
beam.ControlPoints[i].LeafPositions[0,leafIndex] >= beam.ControlPoints[i].LeafPositions[1,leafIndex+1])
{
    leafPositionRight = Math.Abs(beam.ControlPoints[i].LeafPositions[1,leafIndex] -
    beam.ControlPoints[i].LeafPositions[0,leafIndex]);
    flankeRight.Add(leafPositionRight);
    leafPositionLeft = Math.Abs(beam.ControlPoints[i].LeafPositions[1,leafIndex+1] -
    beam.ControlPoints[i].LeafPositions[0,leafIndex+1]);
    flankeLeft.Add(leafPositionLeft);

    //siste MLC blad i feltet (i>Y2-1) & MLC paret ikke er lukket ([0,i] != [1,i]) ELLER
    //åpningen avsluttes pga overlapp som følge av at [0,i]>=[1,i+1]
    if (leafIndex >= indeksY2-1 && beam.ControlPoints[i].LeafPositions[0,leafIndex] !=
    beam.ControlPoints[i].LeafPositions[1,leafIndex] ||
    beam.ControlPoints[i].LeafPositions[0,leafIndex+1] == beam.ControlPoints[i].LeafPositions[1,leafIndex+1] ||




            beam.ControlPoints[i].LeafPositions[0,leafIndex+1] != beam.ControlPoints[i].LeafPositions[1,leafIndex+1])
            {
                islands++;
            }
        }

        //hvis overlapp ([0,i+1]>=[1,i] & [0,i]<[1,i+1])
        else if (beam.ControlPoints[i].LeafPositions[0,leafIndex+1] >= beam.ControlPoints[i].LeafPositions[1,leafIndex] &&
        beam.ControlPoints[i].LeafPositions[0,leafIndex] < beam.ControlPoints[i].LeafPositions[1,leafIndex+1])
        {
            leafPositionLeft = Math.Abs(beam.ControlPoints[i].LeafPositions[1,leafIndex] -
            beam.ControlPoints[i].LeafPositions[0,leafIndex]);
            flankeLeft.Add(leafPositionLeft);
            leafPositionRight = Math.Abs(beam.ControlPoints[i].LeafPositions[1,leafIndex+1] -
            beam.ControlPoints[i].LeafPositions[0,leafIndex+1]);
            flankeRight.Add(leafPositionRight);

            //siste MLC blad i feltet (i>Y2-1) & MLC paret ikke er lukket ([0,i] != [1,i]) ELLER
            //åpningen avsluttes pga overlapp som følge av at [0,i+1]>=[1,i]
            if (leafIndex >= indeksY2-1 && beam.ControlPoints[i].LeafPositions[0,leafIndex] !=
            beam.ControlPoints[i].LeafPositions[1,leafIndex] ||
            beam.ControlPoints[i].LeafPositions[0,leafIndex+1] == beam.ControlPoints[i].LeafPositions[1,leafIndex+1] ||
            beam.ControlPoints[i].LeafPositions[0,leafIndex+1] != beam.ControlPoints[i].LeafPositions[1,leafIndex+1])
            {
                islands++;
            }

        }

        //plukker eventuelt opp feil/om noen MLC par ikke er blitt inkludert i noen av if-loopene over
        else
        {
            feil++;
        }
    }

    øyer.Add(islands);
}

//finner gjennomsnittet av MLC flankene og antall øyer for beam-ene
float averageFlankeLeft = flankeLeft.Average();




float averageFlankeRight = flankeRight.Average();
//float averageØyer = øyer/beam.ControlPoints.Count;

MessageBox.Show(string.Format("Beam no. {0} \n\nAverage MLC flank (per control point, per MLC leaf):" +
    "\nLeft leaf bank = {1} mm, " +
    "\nRight leaf bank = {2} mm. " +
    "\n\nTilsvarende MLC posisjon avgrenset av Y-kollimatorene: \nY1 = {3}, Y2 = {4}" +
```

```
                "\n\nTotalt antall øyer: {7} \nAntall kontrollpunkt = {8} \nAntall øyer per segment (gjennomsnitt av
                alle kontrollpunktene) = {5}" +
                "\n\n(Evt feil i scriptet: {6})", numBeams, averageFlankeLeft, averageFlankeRight,
                indeksY1, indeksY2, øyer.Average(),feil, øyer.Sum(), beam.ControlPoints.Count) );

            AllflankeLeft.Add(averageFlankeLeft);
            AllflankeRight.Add(averageFlankeRight);
            AllØyer.Add(øyer.Average());
            AllFlanke.Add(averageFlankeLeft);
            AllFlanke.Add(averageFlankeRight);
        }



    float averageAllflankeLeft = AllflankeLeft.Average();
    float averageAllflankeRight = AllflankeRight.Average();
    float averageAllFlanke = AllFlanke.Average();

    MessageBox.Show(string.Format("Plan {0} \n\nGjennomsnitt for alle felt:" +
                "\nLeft leaf bank = {1} mm, " +
                "\nRight leaf bank = {2} mm, " +
                "\nTotalt gj.nitt flanke for MLC bladene = {3} mm, " +
                "\n\nAntall øyer per segment (gjennomsnitt) = {4}",
                CurrentPlan.Id, averageAllflankeLeft, averageAllflankeRight, averageAllFlanke, AllØyer.Average() ), "MLC Flanke");

    }
  }
}
```

A.7.2 Average Opening

```
using System;
using System.Linq;
using System.Windows;
using System.Windows.Controls;
using System.Collections;
using System.Collections.Generic;
using VMS.TPS.Common.Model.Types;
using VMS.TPS.Common.Model.API;
using System.Text;

namespace VMS.TPS
{
  class Script
  {
    public Script()
    {
    }

    public void Execute(ScriptContext context /*, System.Windows.Window window*/)
    {
      if (context.Patient == null){
        MessageBox.Show("Please load a patient!");
        return;
      }

      int numBeams, numControlPts, numLeaves, indeksY1, indeksY2, x, y, xy;
      numBeams = numControlPts = numLeaves = indeksY1 = indeksY2 = x = y = xy = 0;

      //Liste for å registrere åpning mellom MLC bladene
      List<double> opening = new List<double>();

      //Liste for å registrere posisjonen til Y1 og Y2 kollimatorene (start og slutt posisjon til for løkken)
      List<int> startindeks = new List<int>();
      List<int> sluttindeks = new List<int>();

      // Display additional information. Use the active plan if available.
      PlanSetup CurrentPlan = context.PlanSetup != null ? context.PlanSetup : context.PlansInScope.ElementAt(0);

      foreach (var beam in CurrentPlan.Beams)
      {
        numBeams++;

        foreach (var controlPoint in beam.ControlPoints)
        {
            numControlPts++;

            float[,] lp = controlPoint.LeafPositions;

            indeksY1 = Convert.ToInt32(controlPoint.JawPositions.Y1);
            indeksY2 = Convert.ToInt32(controlPoint.JawPositions.Y2);

            // start and stop index to the for loop, iterating through relevante leaves
            if (indeksY1<-100 && indeksY2>100){
                indeksY1 = (200+indeksY1)/10 + 1;
                indeksY2 = (indeksY2-100)/10 + 50;
                xy++;
            }
            else if (indeksY1>-100 && indeksY2>100){
                indeksY1 = (100 + indeksY1)/5 + 11;
                indeksY2 = (indeksY2-100)/10 + 50;
                x++;
            }
            else if (indeksY1<-100 && indeksY2<100){
                indeksY1 = (200+indeksY1)/10 + 1;
                indeksY2 = (100 + indeksY2)/5 + 10;
                y++;
            }
            else{
                indeksY1 = (100 + indeksY1)/5 + 11;
```

```
            indeksY2 = (100 + indeksY2)/5 + 10;
        }

        for (int leafIndex = indeksY1-1; leafIndex < indeksY2; leafIndex++)
        {
            //numLeaves++;
            float leafPositionLeft = lp[0, leafIndex];
            float leafPositionRight = lp[1, leafIndex];
            double lpLeft;
            double lpRight;
            lpLeft = System.Convert.ToDouble(leafPositionLeft);
            lpRight = System.Convert.ToDouble(leafPositionRight);

                //if right leaf position is negative
                if (leafPositionRight < 0 && leafPositionRight < controlPoint.JawPositions.X2
                && leafPositionLeft > controlPoint.JawPositions.X1)
                {
                    double differanse = Math.Abs(lpLeft) - Math.Abs(leafPositionRight);
                    opening.Add(differanse);
                }
                else if (leafPositionRight < 0 && leafPositionRight < controlPoint.JawPositions.X2
                && leafPositionLeft < controlPoint.JawPositions.X1)
                {
                    double differanse = Math.Abs(controlPoint.JawPositions.X1) - Math.Abs(leafPositionRight);
                    opening.Add(differanse);
                }
                else if (leafPositionRight < 0 && leafPositionRight > controlPoint.JawPositions.X2
                && leafPositionLeft > controlPoint.JawPositions.X1)
                {
                    double differanse = Math.Abs(lpLeft) - Math.Abs(controlPoint.JawPositions.X2);
                    opening.Add(differanse);
                }
                // if the collimators limit the field
                else if (leafPositionRight > controlPoint.JawPositions.X2 && leafPositionLeft < controlPoint.JawPositions.X1)
                {
                    double differanse = Math.Abs(controlPoint.JawPositions.X1 - controlPoint.JawPositions.X2);
                    opening.Add(differanse);
                }
                // if right leaf position is positiv and left is negativ
                else if (leafPositionRight > controlPoint.JawPositions.X2 && leafPositionLeft > controlPoint.JawPositions.X1)
                {
                    double differanse = Math.Abs(controlPoint.JawPositions.X2 - lpLeft);
                    opening.Add(differanse);
                }
                else if (leafPositionRight < controlPoint.JawPositions.X2 && leafPositionLeft < controlPoint.JawPositions.X1)
                {
                    double differanse = Math.Abs(leafPositionRight - controlPoint.JawPositions.X1);
                    opening.Add(differanse);
                }
                // remaining; right leaf position is positiv, and both left and right leaf limits the field
                else
                {
                    double differanse = Math.Abs(leafPositionRight - lpLeft);
                    opening.Add(differanse);
                }
        }
    }

    startindeks.Add(indeksY1);
    sluttindeks.Add(indeksY2);
}

    StringBuilder builder1 = new StringBuilder();
    foreach (int safePrime in startindeks)
    {
        builder1.Append(safePrime).Append(", ");
    }
    string Y1list = builder1.ToString();

    StringBuilder builder2 = new StringBuilder();
    foreach (int safePrime in sluttindeks)
    {
        builder2.Append(safePrime).Append(", ");
    }
```

```
        string Y2list = builder2.ToString();


    MessageBox.Show(string.Format(" Startposisjoner (Y1 posisjon): {0} for hvert av felt(ene)." +
                                  "\n Sluttposisjoner (Y2 posisjon): {1} for hvert av felt(ene).", Y1list, Y2list) );
    MessageBox.Show(string.Format("Oversikt over området MLC bladene er åpne:" +
                                  "\nY1<-100 & Y2>100: {0}, \nY1>-100 & Y2>100: {1},\n" +
                                  "Y1<-100 & Y2<100: {2}", xy, x, y) );

    numLeaves = indeksY2-indeksY1+1;

    double averageOpening = opening.Average();

    MessageBox.Show(
        string.Format("The current plan {0} for patient {1} has {2} beam(s), " +
                      "{3} control points, and {4} relevante leaf positions. \n" +
                      "\nThe average MLC opening for the {5} beam(s) is {6} mm (per control point, per MLC leaf pair).",
           CurrentPlan, context.Patient.Name.ToString(), numBeams,
            numControlPts, numLeaves, numBeams, averageOpening),
         "MLC Opening");
    }
  }
}
```

A.7.3 Average Speed

```
using System;
using System.Linq;
using System.Windows;
using System.Windows.Controls;
using System.Collections;
using System.Collections.Generic;
using VMS.TPS.Common.Model.Types;
using VMS.TPS.Common.Model.API;
using System.Text;

namespace VMS.TPS
{
  class Script
  {
    public Script()
    {
    }

    public void Execute(ScriptContext context /*, System.Windows.Window window*/)
    {
      if (context.Patient == null){
        MessageBox.Show("Please load a patient!");
        return;
      }

      int numBeams, indeksY1, indeksY2; //, numControlPts, numLeaves;
      numBeams = indeksY1 = indeksY2 = 0; // = numControlPts = numLeaves;

      //Liste for å registrere differansen mellom MLC bladene i controll punkt [i] og [i+1]
      List<float> speedLeft = new List<float>();
      List<float> speedRight = new List<float>();

      List<float> speedGjennomsnitt = new List<float>();

      // Display additional information. Use the active plan if available.
      PlanSetup CurrentPlan = context.PlanSetup != null ? context.PlanSetup : context.PlansInScope.ElementAt(0);

      foreach (var beam in CurrentPlan.Beams)
      {
            numBeams++;

            for(int i=0; i<beam.ControlPoints.Count-1; i++)
            {
                indeksY1 = Convert.ToInt32(beam.ControlPoints[i].JawPositions.Y1);
                indeksY2 = Convert.ToInt32(beam.ControlPoints[i].JawPositions.Y2);

                if (indeksY1<-100 && indeksY2>100){
                    indeksY1 = (200+indeksY1)/10 + 1;
                    indeksY2 = (indeksY2-100)/10 + 50;
                }
                else if (indeksY1>-100 && indeksY2>100){
                    indeksY1 = (100 + indeksY1)/5 + 11;
                    indeksY2 = (indeksY2-100)/10 + 50;
                }
                else if (indeksY1<-100 && indeksY2<100){
                    indeksY1 = (200+indeksY1)/10 + 1;
                    indeksY2 = (100 + indeksY2)/5 + 10;
                }
                else{
                    indeksY1 = (100 + indeksY1)/5 + 11;
                    indeksY2 = (100 + indeksY2)/5 + 10;
                }

                for (int leafIndex = indeksY1-1; leafIndex < indeksY2; leafIndex++){
                    float leafPositionLeft, leafPositionRight;

                    leafPositionLeft = Math.Abs(beam.ControlPoints[i].LeafPositions[0,leafIndex] -
                    beam.ControlPoints[i+1].LeafPositions[0,leafIndex]);
                    speedLeft.Add(leafPositionLeft);
```

```
                leafPositionRight = Math.Abs(beam.ControlPoints[i].LeafPositions[1,leafIndex] -
                beam.ControlPoints[i+1].LeafPositions[1,leafIndex]);
                speedRight.Add(leafPositionRight);
            }
        }

        float averageSpeedLeft = speedLeft.Average();
        float averageSpeedRight = speedRight.Average();

        speedGjennomsnitt.Add(averageSpeedLeft);
        speedGjennomsnitt.Add(averageSpeedRight);

        MessageBox.Show(string.Format("Average MLC speed for beam no. {0}:" +
                        "\nLeft leaf bank = {1} mm" +
                        "\nRight leaf bank = {2} mm \n\n Lengde av liste: {3}, sum = {4}",
                        numBeams, averageSpeedLeft, averageSpeedRight, speedLeft.Count, speedLeft.Sum()) );
    }
    float averageSpeedGjennomsnitt = speedGjennomsnitt.Average();

    MessageBox.Show(string.Format("Average MLC speed for all {0} beam(s): {1} mm per control point.",
                        numBeams, averageSpeedGjennomsnitt), "MLC Speed" );

  }
 }
}
```

A.8 ØNH-cancer: Risikoorganer og toleransegrenser

Dokumentansvarlig: Kirsten Marienhagen
Dokumentnummer: PR23287
Godkjent av: Kirsten Marienhagen
Versjon: 3.2
Skrevet ut: 14.02.2017 09:46:48 Gyldig fra: 13.10.2016
Gyldig for: Stråleterapi UNN; Kreftavdelingen UNN
Toleransegrenser: ØNH

Doseringsvolum	ITV.
Dosekrav	D98, PTV $\leq$ 95% (helst). D98, PTV $\leq$ 90% kan aksepteres. Global maksimum dose: $\leq$ 105% (helst). Se også egen prosedyre i docmap.
Inntegning OAR	Se egen prosedyre i docmap. Stråleterapeut tegner inn: Medulla tegnes, gl. parotis, gl. submandibularis. Ved høye cancer (nasofarynxcancer/ sinonasale cancer) i tillegg Linser / fremre segment av øye og n. optikus, ev bakre segment av øyet/ retina (tegnes av stråleterapeut), videre chiasma, hjernestamme (i kontinuitet med medulla), evt. cerebellum, hypofyse og indre øret (tegnes av lege).
PRV-margin	Ved serielle risikoorganer som chiasma, medulla og n. optikus skal det genereres PRV = OAR + 3mm. Optic PRV = OAR+ 3 mm.
Hjelpevolum	X munnhule-PTV = Munnhule minus PTV52. Brukes til optimalisering. X larynx-PTV = Larynx minus PTV. Brukes til optimalisering.

Generelle kommentarer:
Risikoorganene bør spares så godt som mulig (ALARA-prinsipp:"As low as reasonable possible").
Serielle risikoorganer har høyest prioritet, deretter dekning av målvolum, så mindre kritisk normalvev.

Primær radikal strålebehandling: Totalt 68-70Gy. Postoperativ strålebehandling: Totalt 50-66Gy. Gis som regel konkomitant med ukentlige Cisplatinkurer. Gis som VMAT med integrert boost. For fraksjonering: Se her. Toleransegrenser tilsvarer Dahanca, bortsett fra medulla / medulla-PRV hvor vi aksepterer høyere max dose. Se også Dahanca stråleretningslinjer fra 2013 side 8-9.

Chiasma/-PRV	Dmax* $\leq$ 54Gy/60Gy. 55-60Gy til chiasma gir ang. 3-7% risiko for blindhet, og dose opptil 60Gy kan således vurderes i spesielle tilfeller.
N.opticus/-PRV	Dmax* $\leq$ 54Gy/60Gy
Hjernestamme/-PRV	Dmax** $\leq$ 54Gy/60Gy Hjernestamme ev opptil 57 Gy (individuell vurdering).
Medulla spinalis/-PRV	Dmax* $\leq$ 50Gy/52Gy
Øye bakre segment	Dmax $\leq$ 50Gy Helst $\leq$ 45Gy.
Øye fremre segment	Dmax $\leq$ 30Gy Vurderes opp mot dosedekning av målvolum.
Linse	Dmax $\leq$ 6-10Gy Vurderes opp mot dosedekning av målvolum.
Hypofyse	Dmax $\leq$ 54 Gy
Cerebellum	Dmax** $\leq$ 35 Gy
Cochlea	Dmax* $\leq$ 54Gy Vurderes opp mot dosedekning av målvolum.
Gl. parotis	Dmean $\leq$ 26Gy
Gl. submandibularis	Dmean $\leq$ 39Gy
Munnhule	Dmean $\leq$ 26Gy Tegnes som regel kun som hjelpevolum, for eksempel Munnhule – PTV52, brukes da hovedsakelig som constraint, dermed kan Dmean-verdien ikke vurderes direkte.
Tungebasis	Dmean $\leq$ 45Gy
Konstriktormuskel	Dmean $\leq$ 45Gy
Larynx	Dmean $\leq$ 45Gy

* Dmax tilsvarer volum $>$ 0.027cc og ikke bare et punkt.

**Dmax tilsvarer volum $>$ 0.5cc.

Palliativ strålebehandling: Aktuelle fraksjoneringer 3 Gy x (15-)18, 3 Gy x 10 (-13) og Quad shot regimet. For info se her. Som regel er medulladosen eneste begrensning. Obs Akutt toksisitet ved stort høydosevolum hos eldre pasienter i dårlig allmenntilstand (vurder pausedager eller å avslutte før tiden). Ev CTV-E gis ikke som SIB. Medulla Dmax* $\leq$ 45Gy Tilsvarer ca 54 Gy i 2 Gy‘s fraksjoner.

A.9 Retningslinjer ØNH, legedel

Dokumentansvarlig: Kirsten Marienhagen

Dokumentnummer: PR16248

Godkjent av: Kirsten Marienhagen

Versjon: 6.4

Gyldig for: Kreftavdelingen UNN; Stråleterapi UNN

Dette er kun en papirkopi. Gyldig versjon av dokumentet finnes i det elektroniske kvalitetssystemet.

1 Generelt

Prosedyren bygger på "Danish Head and neck Cancer Group" sine retningslinjer i DAHANCA stråleretningslinjer 2013, som beskriver standard behandlingsopplegg ved radikal bestråling av plateepitelkarsinomer i cavum oris, farynx og larynx, enten som primær radikal strålebehandling eller som postoperativ strålebehandling.

2 TNM-klassifikasjon

For TNM-klassifikasjon: Se NCCN sin klassifikasjon.

3 Utredning

For generelle opplysninger: Se docmap-prosedyre om pakkeforløp ØNH-kreft.
Anamnese inkludert røyking.
Klinisk undersøkelse (bruk gjerne skjematisk tegning). Ta foto om mulig, lagres i DIPS.
CT-collum. Vurder MR (ønskelig ved tungebasis-, tonsille- og nasofarynxcancer)
Vurder behov for PET/CT.
Metastaseutrending (rtg- eller CT-thorax, ultralyd eller CT-lever).
TNM-klassifikasjon og stadium.
Tannstatus: For tannsanering se docmap-prosedyre.
Nyrefunksjon: Kreatinin /eGFR før CT-doseplan, Cr-EDTA vurderes ved forhøyet kreatinin hos kjemoaktuelle pasienter.

4 Behandlingsopplegg kurativ strålebehandling

Anmerkning: For VMAT-behandling henvises til egne prosedyrer i docmap.
Det stråles hver dag mandag til fredag, i tillegg eventuelt lørdag. Pauser i strålebehandlingen bør unngås. For akseptabel behandlingstid: Se her.

4.1 Dosering og fraksjonering

Akselerert fraksjonering: 2.0 Gy / fraksjon, 6 fraksjoner / uke
Gis til alle med gjenværende makroskopisk eller mikroskopisk sykdom.
Gis om mulig på lørdag, ellers som en dobbelfraksjon.
Konvensjonell fraksjonering: 2.0 Gy / fraksjon, 5 fraksjoner / uke

4.2 Primær radikal strålebehandling
Makroskopisk sykdom
Uten konkomitant kjemoterapi: 70 Gy
Ved akselerering og konkomitant kjemoterapi: 68 Gy
Subklinisk sykdom: 60 Gy
Dosen til det elektive området har tradisjonelt vært 46 Gy. Ved overgang til VMAT med integrert boost må det kompenseres for forlenget behandlingstid. Grad av kompensasjon er avhengig av total behandlingstid (som avhenger av totaldose og hvorvidt det akselereres). Fraksjonering ved VMAT-behandling: Se her.

4.3 Postoperativ strålebehandling
Som hovedregel gis postoperativ bestråling. Unntak: Enkelte små, lavgradige tumores som er fjernet med god margin og små T1N0-cancere etter nøye vurdering. Se også avsnitt 5.
Makroskopisk radikaloperert?
R0 (mikroskopisk fritt): 60 Gy uten akselerering, ingen Naxogin, ingen kjemoterapi. UNNTAK: Ved stad. I/II gis 50 Gy, ellers som over.
R1 (mikroskopisk ufritt, makroskopisk fritt): 66 Gy med akselerering og Naxogin, ingen kjemoterapi.
NB: Yngre pasienter med (uttalt) N+ sykdom kan vurderes for konkomitant kjemoterapi.
Makroskopisk ufri (R2)
68 Gy med Naxogin, akselerering og eventuell kjemoterapi (70 Gy hvis ikke konkomitant kjemoterapi).
Dosen til det elektive området har tradisjonelt vært 46 Gy. Ved overgang til VMAT med integrert boost må det kompenseres for forlenget behandlingstid. Grad av kompensasjon er avhengig av total
behandlingstid (som avhenger av totaldose og hvorvidt det akselereres). Fraksjonering ved VMAT-behandling: Se her.

4.4 Konkomitant (samtidig) kjemoterapi
Gis generelt ved lokalavansert sykdom, dvs Stadium III/IV etter AJCC-klassifikasjonen.
Unntak: Nasofarynxcancere får kjemoterapi uansett T-stadium.

Alder < 70 år.
Forutsetter akseptabel nyrefunksjon (Kreatinin, evt. supplert med Cr-EDTA-clearance).
Det brukes rutinemessig ukentlig Cisplatin (Cisplatin 40 mg/m2 (± 5
1-dags kur, gis ukentlig (dvs. hver 7. dag, dette uansett pauser i strålebehandlingen). Kan justeres ± 1 dag ved behov. Totalt 6 (eventuelt 5) kurer.
Kurene skal optimalt gis 3-4 timer før strålebehandlingen.
Kur skal helst gis første stråledag, men senest torsdag den første uken slik at pasienten får minst to strålebehandlinger etter kur før helgepause / før siste behandlingsdag.
For dosejustering: Se kurbeskrivelse. Anmerkning: Ved god almenntilstand og fravær av infeksjonstegn kan kur likevel gis tross neutrofile på 0.9.
Postoperativ samtidig kjemoterapi vurderes nå til yngre pasienter med lokalavansert sykdom.

4.5 Neoadjuvant kjemoterapi.
Vurderes i spesielle tilfeller ved obstruerende lokalavansert kreft.
4 dagers CiFu-kur hver 3. uke, totalt 2-3 kurer. Klinisk OG radiologisk evaluering etter 2 kurer; dvs. CT, event. MR, tas like før innleggelse til 3.kur.
Ofte gis kur nr 3 i påvente av at strålebehandlingen blir ferdig planlagt.
CT doseplan tas oftest like før eventuell oppstart 3. kur, og kan av og til brukes som evalueringsbilder. Vurderes i hvert enkelt tilfelle.
Nøye vurdering av nyrefunksjon underveis. SKAL ha estimert kreatinin clearance ¿ 60. Husk at det er viktigere med cisplatin konkomitant, enn gitt neoadjuvant.
Tillegg av Taxan (såkalte TPF-kurer) kan vurderes.
Oppstart stråle 3 uker etter 1 dag av siste kur, som da gis konkomitant med ukentlig cisplatin.

4.6 Cetuximab
Foreløpig ingen indikasjon ved UNN.

4.7 Naxogin
Gis til alle pasienter med makro-/mikroskopisk sykdom (tumor eller glandel), som får kurativ behandling. Unntak: Larynxcancer T1: 66 Gy akselerert uten Naxogin
Gis 90 min før hver strålebehandling 1200 mg/m2. Ved ev fraksjon 2 gitt på samme dag gis redusert dose på 1 g uavhengig av kroppsoverflate. Blir strålebehandling utsatt til slutten av dagen (lang tid etter at Naxogin er gitt) kan man vurdere å gi ny dose, da på 1 g.
Kombineres med akselerert behandling.
Gis også til de som får kjemoterapi (ukentlig Cisplatin).
NB: Naxogin kan øke effekten av Marevan, følg INR nøye.

5 Kurativ strålebehandling: Unntak /spesielle anmerkninger

5.1 Larynx-cancer

Se også egen docmap-prosedyre.

T1N0: 66 Gy, akselerert men uten Naxogin

T2N0: 70 Gy, akselerert med Naxogin, tidl. 6 x 6-felt (ikke elektivt halsfelt). Stilles enten inn etter skjelettstrukturer (tidligere 6x6.felt) eller ved å tegne larynxmukosa som målvolum.

T3N0: 68 Gy, akselerert med Naxogin og konkomitant kjemoterapi (for økt larynxbevaring).

5.2 Munnhulecancer generelt

Se også Dahanca sine retningslinjer for munnhulecancer.

5.3 Tungecancer

Infiltrasjonsdybde > 3 mm, evt. infiltrasjon i lymfespalter og kar, samt margin (¿4-5mm) har betydning for om det skal gis postoperativ bestråling.

5.4 Ukjent origo

Se i DAHANCA stråleretningslinjer 2013.

Vurder behov for PET.

Makroskopisk tumor: 70 Gy.

Slimhinne i hele farynx: 50-60 Gy (kompenser for forlenget behandlingstid ved simultan integrert boost).

Elektivt halsfelt bilateralt: 52 Gy (ved simultan integrert boost).

Gis i utgangspunktet med akselerering og Naxogin. Kjemoterapi kan vurderes.

5.5 Spyttkjertelcancer

Se egne retningslinjer, blant annet Dahanca sine nasjonale retningslinjer fra 2012.

5.6 Sinonasal cancer

Se egne retningslinjer, blant annet Dahanca sine nasjonale retningslinjer fra 2009.

6 Rebestråling i potensiell kurativ hensikt

Aktuelle pasienter skal være vurdert for salvage-kirurgi. Rebestråling kan være aktuelt som konsolidering etter salvage-kirurgi, spesielt ved ufri margin eller gjenværende makroskopisk tumor.

Der kirurgi er uaktuelt kan rebestråling vurderes i spesielle situasjoner, hos velegnede pasien-

ter med noe tid fra primærbehandling.
Gis som regel hyperfraksjonert med 1.2 – 1.5 x 2 (5 dager i uken) opptil minimum 60 Gy, gjerne helt opptil 66 Gy om mulig. NB: Gis kontinuerlig uten tilsiktet pause, gjerne konkomitant med kjemoterapi (ukentlig cisplatin), og eventuelt også Naxogin (vurderes individuelt). Målvolum er makroskopisk tumor med 5-10 mm margin til CTV margin, som regel uten elektive halsfelt.

7 Palliativ strålebehandling

Palliativ strålebehandling kan benyttes for symptomlindring, både ved primært utbredt sykdom og ved tilbakefall. For generelle vurderinger se også Dahanca sine retningslinjer for behandling og pleie ved residiv eller primær fremskreden ØNH-cancer.

7.1 Som lokoregional primærbehandling

Ved UNN har vi tidligere mye brukt "split course-regimet" (hyperfraksjonert 1.5 Gy x 2 x 15, i to omganger med to ukers pause), et opplegg som både er krevende for pasienten og utfordrende logistisk. Vi har nå bestemt å gå bort fra hyperfraksjonering i palliativ setting. En rekke fraksjoneringsmønster har blitt benyttet nasjonalt og internasjonalt, alt fra engangsfraksjoner på 8-10 Gy, til 3 Gy x 15-18. Det er ikke evidens for å hevde at noen regimer er bedre enn andre. En må derfor velge fraksjonering basert på klinisk skjønn. Det er viktig at en ikke bruker unødvendig mye av pasientens tid.
Ved UNN foreslås primært følgende fraksjoneringsregimer
3 Gy x (15-)18: Vurderes ved pasienter som ikke finnes egnet for standard kurativ strålebehandling, men hvor en ønsker lengst mulig lokal kontroll. Som regel er målvolum makroskopisk tumor (både primærtumor og klart patologiske lymfeknuter), med 5 (-10) mm margin til CTV. I noen utvalgte tilfeller kan det være aktuelt å gi et elektivt halsfelt. DNR planlegger da 3 Gy x 14 = 42 Gy til CTV-E som tilsvarer rundt 45 Gy i 2 Gy ekvivalent med alfa/beta = 10 Gy. Behandlingen anbefales i så fall gitt som sekvensielt og IKKE simultant integrert (som SIB), dette fordi at behandlingen i blant må avsluttes før det er gitt 18 fraksjoner. Hovedproblemet ved denne fraksjoneringen er akutt toksisitet ved stort bestrålt volum (for eksempel ved bilateral hals hos eldre pasienter i dårlig allmenntilstand). Ved mye toxsisitet bør man vurdere å øke behandlingstiden ved å legge inn pausedager eller alternativt avslutte før tiden. En må være obs på medulladose siden behandlingen gis med 3 Gy's fraksjoner (max 45 Gy til medulla-PRV).
3 Gy x 10 (-13): Standard palliativ fraksjonering, vurderes ved eldre og / eller skrøpelige pasienter. Målvolum er primært makroskopisk tumor.
QUAD SHOT: 3.5 Gy x 2 daglig i 2 dager, 3-(4) ukers pause. Kan gjentas inntil 3 ganger.

Målvolum er kun makroskopisk tumor. Se The 'QUAD SHOT'—a phase II study of palliative radiotherapy for incurable head and neck cancer for bakgrunnsinfo.

7.2 Rebestråling gitt i palliativ setting

Kan være aktuelt ved lokoregional tilbakefall etter tidligere strålebehandling hos pasienter med kjent metastatisk sykdom, eller som ut fra en totalvurdering ikke er aktuell for kurativ intendert rebestråling. Fraksjonering må tas stilling til i hvert enkelt tilfelle, men få fraksjoner anbefales, gjerne engangsfraksjon, event. Quad shot.

7.3 Palliativ strålebehandling av fjernmetastaser

Følger vanlige retningslinjer for palliativ strålebehandling. Ved smertefulle skjelettmetastaser anbefales 8 Gy x 1 som standardbehandling. Unntak: Pasienter med truende tverrsnitt og forventet levetid på > 3 måneder.

8 CT-doseplan

Se prosedyre: CT-doseplan ØNH-cancer. Behandlingen gis vanligvis i ryggleie med pasient fiksert i maske, med armer ned. Tas med i.v.-kontrast (unntak larynxcancer T1-2N0), husk ny kreatinin før CT.

9 Målvolumdefinisjon ved kurativ strålebehandling

Bruk ØNH-skjema. For VMAT-fraksjonering se her.

9.1 Primær radikal strålebehandling

Mest brukte alternativer:

70 Gy akselerert uten kjemo. Dosetrinn 52 – 64 – 70 Gy

68 Gy akselerert med kjemoterapi. Dosetrinn 52 – 64 – 70 Gy

GTV-T	Primærtumor (tegnes i samråd med ØNH- og røntgenlege). Bruk MR og rekonstruerte CT-doseplanbilder (i IMPAX).
GTV-N	Patologiske lymfeknuter på hals (tegnes i samråd med røntgenlege). Bruk MR og rekonstruerte CT-doseplanbilder (i IMPAX).
CTV 0-68/70Gy	GTV-T + GTV-N uten margin (man antar at mikroskopisk sykdom utenfor GTV-T er eradikert etter 60 Gy
CTV 0-64Gy	GTV-T + 10mm + GTV-N + 5mm, justeres for kompartments/ naturlige begrensinger. CTV-T 0-64Gy og CTV-N 0-64Gy genereres hver for seg.
ITV 0-68/70Gy	CTV 0-68/70Gy (minimale interne bevegelser i ØNH-området),

	croppes med (1-) 3mm i forhold til hud (avhengig av om subcutis er affisert).
ITV 0-64Gy	CTV 0-64Gy (minimale interne bevegelser i ØNH-området), croppes med (1-) 3mm i forhold til hud (avhengig av om subcutis er affisert).
PTV 0-68/70Gy	ITV 0-68/70Gy + 5mm, croppes med 1mm i forhold til hud.
PTV 0-64Gy	ITV 0-64Gy + 5mm, croppes med 1mm i forhold til hud.

Elektivt halsfelt (CTV-E) (som regel CTV0-52Gy)

CTV-E	CTV 0-64Gy + CTV-E (tegnes i forhold til DAHANCA stråleretningslinjer 2013). Se også atlas og tabell.
ITV-E	CTV-E, croppes med 3mm i forhold til hud (obs: 1mm der hvor ITV-T/N er croppet med 1mm).
PTV-E	ITV-E + 5mm, croppes med 1mm i forhold til hud.

9.2 Postoperativ strålebehandling

Mest brukte alternativer:

R0-reseksjon: 60Gy ikke akselerert, ingen kjemo. Dosetrinn 52 – 60Gy.

R1-reseksjon: 66Gy akselerert, kjemo kan vurderes unntaksvis. Dosetrinn 52 – 63 – 66Gy.

GTV-T	Tumorseng (tegnes i samråd med ØNH- og røntgenlege). Bruk MR og rekonstruerte CT-doseplanbilder (i IMPAX).
GTV-N	Tumorseng på hals (tegnes i samråd med røntgenlege). Bruk MR og rekonstruerte CT-doseplanbilder (i IMPAX).

Ved R0-reseksjoner, dvs mikroskopisk fri rand

CTV-T 0-60Gy	GTV-T + 0-10mm (avhengig av hvor mye av marginen for mikroskopisk sykdom som allerede er med i "GTV"). Justeres for kompartments naturlige begrensinger.
CTV-N 0-60Gy	GTV-N + 0-5mm (avhengig av hvor mye av marginen for mikroskopisk sykdom som allerede er med i "GTV"). Justeres for kompartments naturlige begrensinger.
ITV 0-60Gy	CTV-T+N 0-60Gy (minimale interne bevegelser i ØNH-området), croppes med (1-)3mm i forhold til hud.
PTV 0-60Gy	ITV 0-60Gy + 5mm (setup-margin, relativ liten siden pasienten behandles i maske)

Ved R1-reseksjoner, dvs mikroskopisk ufri rand tegnes i tillegg CTV 60-66Gy:

CTV 0-66Gy	GTV-T uten margin (man antar at mikroskopsik sykdom utenfor GTV-T er eradikert etter 60 Gy)
ITV 0-66Gy	CTV 0-66Gy (minimale interne bevegelser i ØNH-området), croppes med (1-)3mm i forhold til hud.
PTV 0-66Gy	ITV 0-66Gy + 5mm, croppes med 1mm i forhold til hud.
CTV-T 0-63Gy	GTV-T + 0-10mm (avhengig av hvor mye av marginen for mikroskopisk sykdom som allerede er med i GTV). Justeres for kompartments naturlige begrensinger.
CTV-N 0-63Gy	GTV-N + 0-5mm (avhengig av hvor mye av marginen for mikroskopisk sykdom som allerede er med i GTV). Justeres for kompartments naturlige begrensinger.
ITV 0-63Gy	CTV-T+N 0-63Gy (minimale interne bevegelser i ØNH-området), croppes med (1-)3mm i forhold til hud (avhengig av om subcutis er affisert).
PTV 0-63Gy	ITV 0-63Gy + 5mm (setup-margin, relativ liten siden pasienten behandles i maske), croppes med 1mm i forhold til hud.

Elektivt halsfelt (CTV-E) (CTV0-52Gy eller CTV0-49Gy avhengig av opplegget – se fraksjonering ved VMAT-behandling her).

CTV-E	CTV 0-60Gy + CTV-E (tegnes i forhold til DAHANCA stråleretningslinjer 2013).
ITV-E	CTV-E, croppes med (1-)3mm i forhold til hud (obs: 1mm der hvor ITV-T/N er croppet med 1mm).
PTV-E	ITV-E + 5mm, croppes med 1mm i forhold til hud.

9.3 Elektivt halsfelt (CTV-E)

Hvilke glandelstasjoner som skal inkluderes og hvorvidt det skal gi unilateral eller bilateral elektiv bestråling er avhengig av lokalisasjon av primærtumor og TNM-klassifikasjon / stadium.

For nærmere info henvises til nyeste publikasjon Delineation of the neck node levels for head and neck tumors: a 2013 update. DAHANCA, EORTC, HKNPCSG, NCIC CTG, NCRI, RTOG, TROG consensus guidelines – se her og DAHANCA stråleretningslinjer 2013.

Bruk Dahanca/EORTC sin tabell og atlas.

Ved N0-sykdom: Sjekk konversjonsrate, dvs risiko for subklinisk sykdom ut fra lokalisasjon av primærtumor.

Elektiv halsfelt tegnes ved risiko for N+-sykdom > 15 %
Unilateralt eller bilateralt halsfelt? De aller fleste lokalisasjonene skal ha bilateralt halsfelt. Lateralisert orofarynx-Ca (for eks tonsille-Ca med tumor > 1cm fra midtlinjen) kan gis unilateral bestråling. Ved tonsillecancer T4 gis som regel bilateralt halsfelt.
Ved N+-sykdom: Som ved N0-hals, i tillegg involvert nivå + neste region kaudalt (minst 2 cm margin til makroskopisk tumor).

10 Risikoorgan og toleransegrenser
Risikoorganene bør spares så godt som mulig. Se prosedyre ØNH: Risikoorgan og toleransegrenser ved VMAT. Se også Quantec og DAHANCA stråleretningslinjer 2013, side 8.
Stråleterapeut tegner inn:
Medulla spinalis og medulla-PRV (medulla PRV = medulla + 3mm).
Gl. parotis, gl. submandibularis bilateralt.
Ved behov linser, retina og hjernestamme (avhengig av tumorlokalisasjon).
Lege sjekker risikoorgan stråleterapeut har tegnet, og tegner
Hjelpevolum: Z munnhule-PTV-E, Z larynx-PTV-E
Ved behov chiasma, n.opticus og hypofyse (avhengig av tumorlokalisasjon).

11 Bivirkninger / pasientinformasjon
Akutte bivirkninger vil variere med hvilket område som behandles. Det er viktig med god munnhygiene og god ernæringsstatus.
Mukositt / sårhet i munnen og svelget, spyttkjerteldysfunksjon / nedsatt spyttproduksjon med munntørrhet, seigt slim, smaksforstyrrelser, svelgvansker, ernæringsproblemer, stemmeforandringer, hudforandringer, smerter, soppinfeksjon, tretthet, kvalme
Senbivirkninger
Spyttkjerteldysfunksjon / nedsatt spyttproduksjon med munntørrhet, seigt slim, smaksforstyrrelser, karies / periodontal sykdom, svelgvansker, ernæringsproblemer, stemmeforandringer, osteo(radio)nekrose, trismus, unntaksvis myelopati
Se også pasientinformasjon i kreftlex. Her finner du også egen avsnitt om slimhinnereaksjoner.

12 Evaluering / kontroll / oppfølging
Evaluering under og etter avsluttet strålebehandling skjer i regi av ØNH-avdeling.
Palliativ kjemoterapi
Ukentlig Metotrexat.
Evt. Taxol/Xeloda palliativt.
Evt. CiFu palliativt eller ukentlig Cisplatin palliativt, alternativt palliativ Carboplatin/5-

FU.

14 Vedlegg

14.1 TNM-klassifikasjon

Se her (NCCN sin klassifikasjon).

14.2 Skjematisk tegning

Det er ønskelig at ØNH-lege tegner inn tumorutbredelse i skjematisk tegning som du finner her.

14.3 Anatomi-illustrasjon

14.4 Glandelstasjoner

Henviser til originalartikkelen – se her.